Subsurface Fracture Characterization based on Polarimetric Borehole Radar and its Application to Estimation of Hydraulic Properties

著者	Mansour Khamis Kabeel Ali
学位授与機関	Tohoku University
URL	http://hdl.handle.net/10097/54811

Subsurface Fracture Characterization based on Polarimetric Borehole Radar and its Application to Estimation of Hydraulic Properties

（ポーラリメトリック・ボアホールレーダによる地下き裂の性状評価と水理性推定への応用）

by

Khamis Kabeel Ali Mansour

The Thesis Presented in Partial Fulfillment of the requirements for the
degree of Doctor Philosophy in
Graduate School of Environmental Studies of

Tohoku University

Supervised by

Prof. Dr. Motoyuki Sato

Committee in Charge

Prof. Dr. Motoyuki Sato

Prof. Dr. Kunio Sawaya

Prof. Dr. Noriyoshi Tsuchiya

Prof. Dr. Tomochika Tokunaga

August 2012

Contents

Chapter 4. FDTD Electromagnetic Simulation………………………………. 42

Chapter 5. Subsurface Fractures Characterization…………..………… 66

List of Figures

List of Tables

Chapter 1
Introduction

1.1 Background and motivation

Understanding of fluid flow through natural fractures in rocks is important in many areas, such as in the hydrocarbon, geothermal energy extraction, water industries and particularly in the safe design of disposal sites for domestic, industrial and nuclear wastes. Fractures control the hydraulic conductivity of crystalline and tight sedimentary rock [1]. These effects arise from the fact that the surfaces composing a fracture are rough and mismatched at some scale. The shape, size, and number of contacts between the surfaces control the fracture mechanical properties. The fracture surfaces are propped apart by the contacting asperities and the opening space between the surfaces (or aperture) controls the transport properties. Hence, the surface roughness is important to quantify for the study of many fracture properties.

Borehole radar is a type of ground penetrating radar (GPR) for subsurface sensing, especially for the fractures in crystalline rocks. It can determine subsurface fracture location and orientation depending on the change of subsurface fracture properties and its filled materials. Yet, it has some limitations for measuring far objects due to high attenuation of the electromagnetic waves. Polarimetric analysis of electromagnetic waves has been showing significant role for analyzing geometrical properties of different scattered objects in radar remote sensing technology. For that reason, our group developed earlier full polarimetric borehole radar system which can be used to acquire a full polarimetric datasets [2]. The advantage of this system is that it overcomes the radar resolution by measuring full polarization states in the borehole. Also, a correlation was found between subsurface fracture properties and its polarimetric information analyses obtained from the measured borehole radar.

Subsurface fracture is not a regular shape or object like sphere or dihedral, For that reason, the electromagnetic scattering from its surface has a random scattering process. It is believed that the numerical simulation may be the key toward a deep understanding of the electromagnetic scattering from rock fractures and utilizing their scattering mechanisms to identify the hydraulic property of subsurface fractures. In this work, electromagnetic scattering from subsurface rough fracture was analyzed using a numerical model based on the finite difference time domain method (FDTD) [3]. Where, the fractional Brownian motion process was used to generate a band-limited rough fracture surface [4]. The reason to base fracture surface on a fractal framework is that fracture surface variations present a multi-scale structure and generally obey fractal statistics. Therefore, 3D models were generated to achieve this purpose.

The aim of this research work is to develop polarimetric analysis method for further use of the full polarimetric borehole radar system, which is equivalent to polarimetric analysis of PolSAR (Polarimetric Synthetic Aperture Radar) for characterizing subsurface targets. A field experiment at Mirror Lake fractured rock research site in New Hampshire, USA is described based on this radar system. Consequently, the eigenvector based decomposition method was performed, as an extension of the earlier approach with polarimetric analysis of the power scattering matrix [5], to recognize the scattering mechanism of the subsurface fractures. Therefore the results of fracture characterization have been interpreted and correlated with hydraulic fracture transmissivity tracer tests. The obtained polarimetric analysis results were validated by applying forward electromagnetic technique for generated fractal fracture models. In addition, numerical simulation results determine the reliability of using polarimertic analysis for the full polarimertic borehole radar dataset.

1.2 Literature review

The terms subsurface radar or Ground Penetrating Radar (GPR) refers to a wide range of electromagnetic techniques designed primarily to locate objects or interfaces buried beneath the earth's surface [6]. The pulsed radar has been developed extensively and systems where radar antennas are moved along the ground surface have many applications: e.g. in the determination of ice thickness in permafrost measurements [7], in civil engineering [8], in overburden characterization [9]. The range of the applications has been expanding steadily, and includes archaeology, road and rail bed quality assessment, location of voids, tunnels and landmines, as well as remote sensing by satellite. The term Borehole Radar (BHR) or Borehole Ground Penetrating Radar (BGPR) refers to a special subset of GPR, where the transmitters are placed into one or more boreholes to see the subsurface through the radar's eyes. BHR is a transient electromagnetic (EM) tool for detecting discontinuities in rock formation. Mainly pulsed radar systems have been used for borehole work for many years. In 1910, for example, Leimbach and Lowy [10] buried electromagnetic dipole antennas in an array of vertical boreholes and compared the magnitude of the low frequency signals when successive dipole pairs were used to transmit and receive. They proved that a crude shadow image could be formed within the array of an ore body, which absorbed electromagnetic radiation.

Cross-hole and single-hole experiments were made in diabase by Rubin et al [11]. A system for single-hole reflection measurements was developed by Wright and Watts [12] and used in a research related to radioactive waste [13]. Nickel et al [14] described a borehole radar system with antenna centre frequencies of 20MHz and 40MHz, designed for both reflection and cross-hole surveys, to determine the internal structure of salt domes. Reflections were obtained from targets that were at least 65m away. Thierbach [15] presented results showing reflections from over 180m away in salt and between 120m and 300m away in potash seams. Halleux et al [16] carried out both surface GPR and borehole radar surveys at the Borth salt mine in Germany. At 120MHz, the bottom of the surface, as well as structures within the underlying anhydrite, were clearly visible. At 80MHz, a layer of clay at 30m depth and the base of the anhydrite around 50m depth were delineated. Then, he deployed 60MHz RAMAC borehole radar probes in horizontal boreholes running ahead of the mine drift and he observed a refection from over 60m away, but with a single borehole and omni-directional antenna.

One of the important applications of borehole radar is to detect and map structures such as subsurface fractures [17] - [18], tunnels [19] and changes in lithology [20] in addition to other geophysical parameters, such as soil water content, fluid permeability, salinity and clay fraction within the vicinity of the probed region can be obtained from the radar data [21], [22] and [23].

Polarimetric Synthetic Aperture Radar inspired our group to develop the full polarimetric borehole radar system. As well as, the implementation of the polarimetric decomposition methods for the polarimetric synthetic aperture radar dataset have shown efficient and reliable information for classifying different nature or manmade objects on the earth's surface based on their electromagnetic scattering properties. The initial study for characterizing subsurface fracture using the polarimetric borehole radar dataset was begun with Zhao [24]. But his results cannot be validated also it used only two polarimetric parameters as characterization index for subsurface fractures.

1.3 Thesis structure

Chapter 1 gives an introduction to the research of the thesis and includes literature review. It also contains the motivation behind the research work. Chapter 2 contains description and configuration of the full polarimetric borehole radar system with its advantages compared to conventional borehole radar particularly for the application related to subsurface fracture characterization. Two measured full polarimetric borehole radar measurements are shown in this chapter including different fracture characteristics environments; one in Mirror Lake (USA) and the other in Kamaishi (Japan). The Mirror Lake measurements have been intensively shown hence the hydraulic tracer test is available for this site and it can be used for correlating the fracture characterization based on polarimetric analysis for the polarimetirc borehole datasets.

Chapter 3 is devoted for the process of fractal fracture generation and fractal fracture modeling for resembling the real subsurface fractures. In addition to that, I will examine in this chapter the variation property of fracture surface heights (roughness) according to controlling of the deterministic parameters for the generated fracture such as the proportional constant parameter, the fractal dimension and the highest and the lowest spatial frequency content of fracture surface.

Chapter 4 is introduction to the Finite Difference Time Domain (FDTD) technique that will be discussed in this chapter along with the usage of Maxwell equations for solving the numerical solution of discretized model objects. The using of fractal fracture model as simulated object will be shown where I have observed the electromagnetic scattering from it with respect to its surface roughness. These results will be discussed in details in this chapter where I have found a direct relationship between fracture roughness variation and the mean electromagnetic power scattered from fractures.

Chapter 5 describes the polarimetric analysis based on eigenvector decomposition (entropy, anisotropy and alpha) for the measured borehole radar data. That will be discussed in this chapter. Furthermore, the forward modeling of electromagnetic simulation results from a known determined fracture models will be also described in this chapter. The polarimetric analysis for the simulated data and the experimental results are applied where a comparison between the simulated and the measured results will be given in this chapter. The fracture characterization based on the eigenvector decomposition will be determined and the deduced hydraulic properties for each fracture zone have will be shown.

Chapter 6 shows a case study at southwest Lake Nasser in Egypt for the role of subsurface fracture systems, which are associated with fault trends, in linking the surface water to groundwater aquifers. Furthermore, the expected results that the polarimetric borehole radar provides in resolving the hydraulic property of each fracture zone related to certain tectonic trend. These results can be used to reveal the recharging mechanism of surface water from Lake Nasser to the adjacent Nubian aquifers to the lake. That expected results can be referred to the obtained fracture characterization at Mirror Lake site and the derivation of the hydraulic properties for fracture zones. These results can be estimated based on the polarimetric simulation approach for determined fracture properties which can be obtained from the field observations or rock core samples.

Chapter 7 summarizes all the results which I have achieved during the PhD research work with conclusions and outlook for further recommended work. Figure 1.1 shows the flow chart structure of the dissertation and the connection between each chapter.

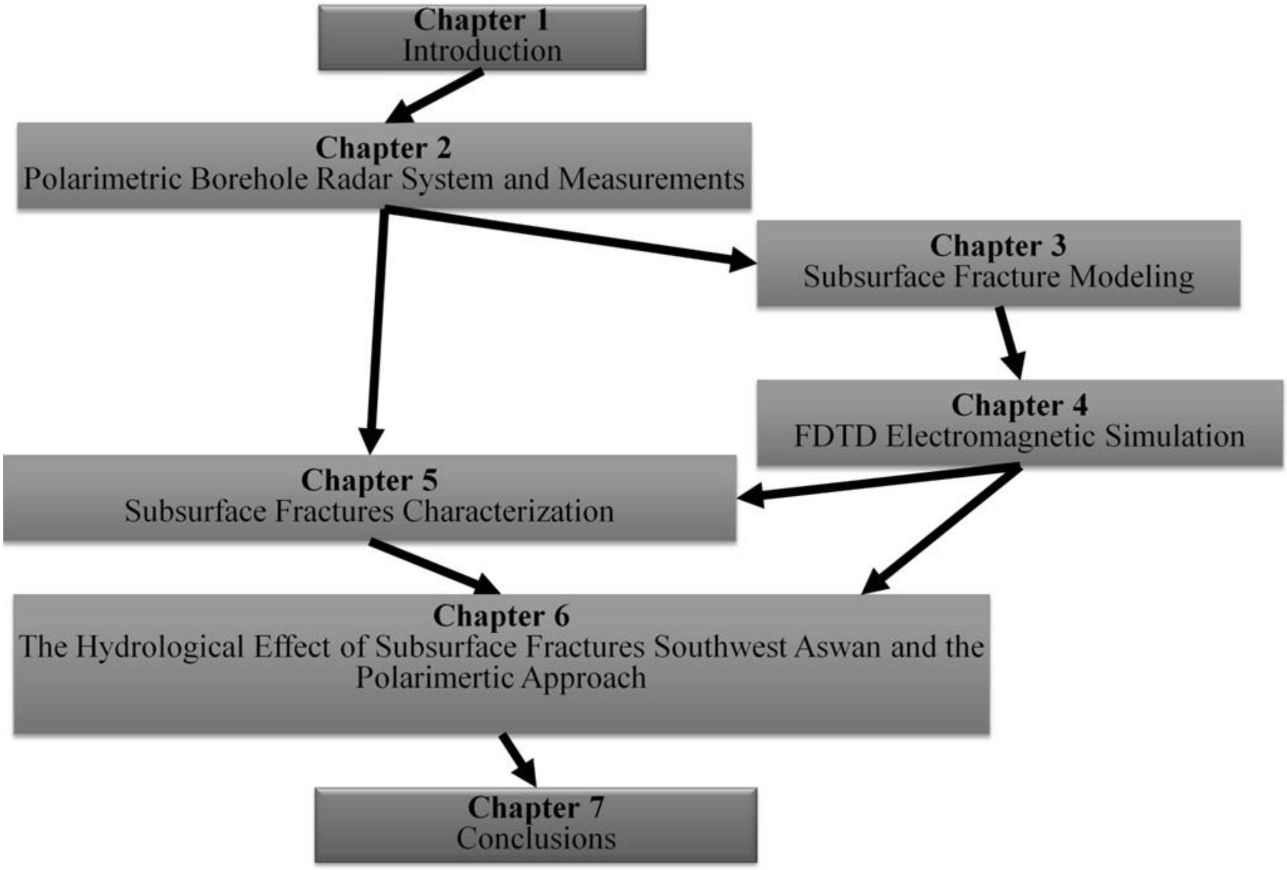

Fig. 1.1: The structure of the dissertation.

Chapter 2

Polarimetric Borehole Radar System of Measurements

2.1 Introduction

In Chapter 2, I will describe the borehole radar system generally and will give detailed explanation about the full polarimetric borehole radar system. In addition, its measurement configurations and the working theory with respect to radar polarimetry. On the other hand, I will describe the conventional borehole radar systems and highlight the radar acquisition mode of common offset. Furthermore, the directional borehole radar will be also shortly figured out as it is considered the appropriate tool for determining subsurface fracture azimuths and its results can be integrated with the polarimetric analysis of the polarimetric borehole radar data. Measured data for fracture test site will be shown in this chapter. Hence, full polarimetric radar dataset has been acquired at a borehole in Mirror Lake, New Hampshire, USA. Single borehole full polarimetric measured data will be provided as the evidence for the determination and detectability of fractures that cut the borehole axis and their extension away from the borehole.

The merit of the polarimetric borehole radar system, which was developed by our research group in Tohoku University, is that it overcomes the conventional borehole radar resolution limitation. As, it can be used to obtain the polarization information of the measured objects as well as from these data we can estimate the property of these targets depending on their electromagnetic scattering mechanisms. This is the meaning of the ability of polarimetric borehole radar system to be behind the resolution of radar signal. In addition, it provides not only the scattering properties of regular measured objects. But also, the irregular geometry objects such as subsurface rock fractures. This feature gives this radar system an advantage as subsurface sensing tool especially for subsurface fracture characterization and classification.

2.2 Radar data acquisition

There are four main modes of radar data acquisition, which namely: (1) common offset (reflection profiling), which is the borehole radar used for acquiring the measurements, (2) common source (wide-angle reflection), (3) common midpoint sounding and (4) Cross-hole radar tomography. I will briefly describe the acquisition of common offset mode where single-borehole measurements have similar layout.

In this mode of operation, the radar antenna (monostatic case: the offset is zero and both antenna are at same point; bistatic case: transmitter and receiver antenna are at a fixed distance) are moved over the surface simultaneously. The measured travel times to radar reflectors are displayed on the vertical axis, while the distance that the antenna has travelled is displayed along the horizontal axis in a radargram display. Most GPR surveys, mainly borehole radar surveys use a common offset survey mode. This mode of data acquisition can be used to improve the azimuth or plan resolution, where a long aperture is synthesized along the azimuth line. This type of operation, in the radar field, is called synthetic aperture radar image formation. Figure 2.1 shows a common offset bistatic data acquisition configuration. Thus, this mode of data acquisition is analogous to continuous seismic reflection profiling [1].

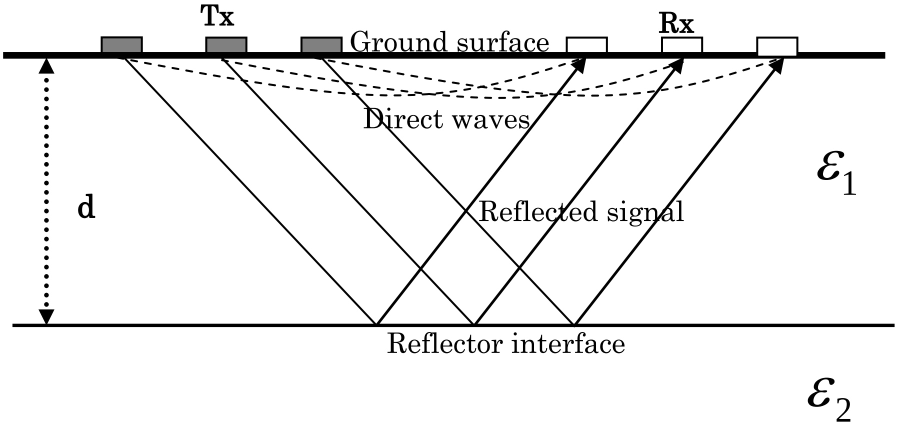

Fig. 2.1: Common offset mode data acquisition configuration in which the distance between transmitter and receiver antennas is fixed and the pair moves along a horizontal line.

2.3 Borehole Radar

Borehole radar is based on the same principles as ground penetrating radar systems for surface use, which means that it consists of a radar transmitter and receiver antennas. The antennas are connected via an optical cable to a control unit used for the signal generation and data acquisition. Borehole radar is a subsurface detection tool originally designed for imaging geological targets in resistive formations. As the formation becomes conductive, radar becomes ineffective for subsurface imaging because of the high attenuation of electromagnetic waves [2]. It determines subsurface fracture location and orientation depending on the change of electrical conductivity and dielectric permittivity of the subsurface fracture. In this part of this chapter, I will give a brief description about the conventional borehole radar systems and furthermore about a special kind of radar system which is direction borehole radar, where it has important role for determination of subsurface fracture azimuths, and finally a detailed explanation about our full polarimetric borehole radar system with respect to hardware components and its measurement configurations.

2.3.1 Conventional borehole radar system

Most conventional borehole radar systems use thin dipole antennas for both transmitting and receiving antennas arrangements, since the thin structure of dipole antennas is very suitable to be deployed into a waterproof borehole radar sonde. It is known that dipole antennas vertically deployed excite a vertically polarized electric field [3], which is parallel to the radar sonde axis. Conventional borehole radar systems use centre frequencies from 20 to 250 MHz mostly where radar waves are affected by soil and rock conductivity. If the conductivity of a medium is more than a certain level the reflectivity of the radar signal is difficult to occur due to high signal attenuation from that medium. For single-hole measurements, in high conductivity media the radar equation is not satisfied and very weak reflections will appear. In cross-hole and surface-to-borehole radar mode, measurements can be carried out in much higher conductivity areas because no reflections are needed and in this case important information concerning the local geologic conditions is evaluated from the amplitude of the first arrival and the arrival time of the transmitted wave only, not a reflected component.

2.3.2 Directional borehole radar

Directional borehole radar is able to determine the position of targets in three dimensions (3-D). For example, the fracture azimuth is one of the essential objects that can be estimated with this borehole radar system. Subsurface fracture characteristics can be provided with the full polarimetric borehole radar which I will discuss in chapter5. Furthermore, the integration of polarimetric borehole radar results with fracture azimuth information which estimated by directional borehole radar led to deep understanding of the fluid flow movement mechanisms through the rock fractures. For that reason, I will shortly introduce this radar system in this part of chapter2. Tohoku University has developed array type directional borehole radar system. This system is a vector network analyzer (VNA) based stepped-frequency continuous wave radar system. The transmission antenna is a dipole antenna having a length of 90cm. An RF analogue optical link (5dBm output, DC – 1000MHz bandwidth) is used to feed the transmitting antenna from the VNA. Four optical electric field sensors for the receiving antenna are set around a plastic pipe casing of 6cm in diameter as shown in Figure 2.2 90cm dipole antenna element is connected to the each optical electric field sensor. A YAG laser diode outputs four-channel optical waves transmitted through optical fibers to the receiver sensors. The modulated signals from the sensors are transmitted to a photo detector which outputs four-channel RF signals. One of the RF output signals is selected by a RF switch circuit and is sent to a receiver port of the VNA. A 2-axis magnetic sensor (for vertical boreholes) and a 3-axis accelerometer (for horizontal boreholes) are mounted on the array receiver to measure the rotation angle of the radar sonde in borehole. The receiving antenna array and the transmitting antenna are installed into a waterproof downhole sonde of 90mm in diameter and 4m in total length [4].

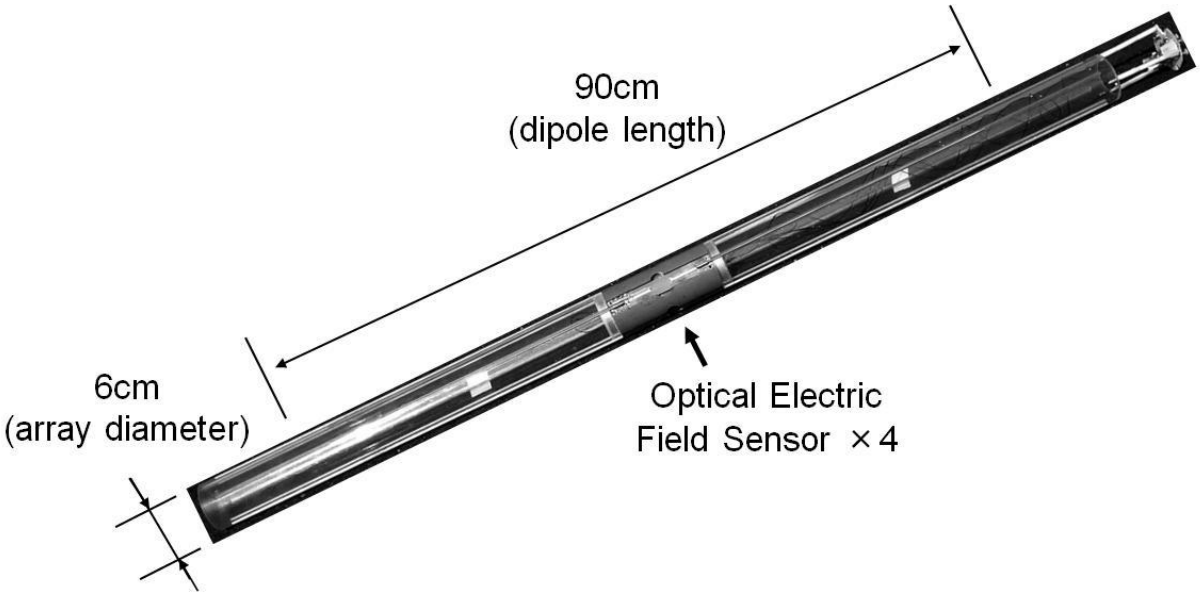

Fig.2.2: Receiving circular antenna array. Four dipoles (90cm length) are evenly placed on a circular of 6cm diameter. Each dipole is terminated by an optical electric field sensor.

2.3.3 Full polarimetric borehole radar system

The full polarimetric borehole radar system is a stepped frequency radar system based on a Vector Network Analyzer (VNA). We selected the stepped frequency radar system [5] - [8] because it can be constructed simply by using a VNA. On the other hand, an advantage of the usage of VNA is that it can be used for broadband frequencies without changing any components [6] - [8]. Figure 2.3 shows the diagram of the developed full polarimetric borehole radar system. An oscillator and a receiver are built into a network analyzer. Therefore, a radar system can be constructed if a transmitting antenna and a receiving antenna are connected to the transmitter and receiver ports, respectively. In practical measurements with a borehole radar we have to place the antennas in a down-hole sonde and, as a result, the connection between a network analyzer and antenna via coaxial cables becomes problematic. This is because coaxial cables are susceptible to electric and magnetic disturbances, existing universally during a measurement. Instead of coaxial cables, an analog optical link system is used for the signal transmission between a network analyzer on the ground surface and the antenna in the subsurface. The analog optical link system is composed of commercial components, RF amplifiers and optical transducers. For the signal transmission from ground surface into subsurface, we employ a downlink system, which consists of R/O (RF signal to Optical signal) and O/R (Optical signal to RF signal) converters, and whereas a uplink system with O/R and R/O converters is used for the signal transmission from the subsurface to the ground surface. In the real measurement performance, The RF output of the network analyzer is converted to optical signals and is transmitted to the down-hole sonde. The optical signals from the network analyzer are converted to RF signals and amplified by a power amplifier and fed to the transmitting antenna. Similarly, the received radar signal is amplified by a built-in amplifier firstly, and converted to the optical signal in the receiver sonde to be finally acquired by the network analyzer. The optical link has a frequency range from 2 MHz to 500 MHz, and a dynamic range of more than 70 dB.

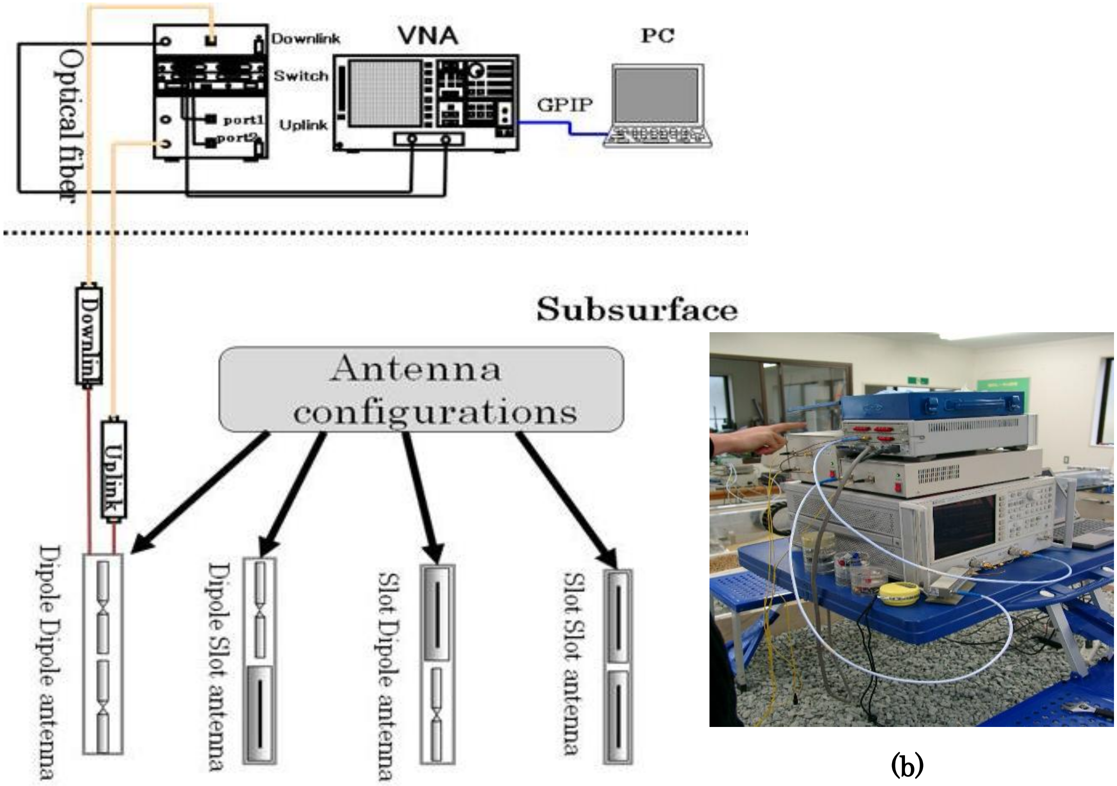

(b)

(a)

Fig. 2.3: The full polarimetric borehole radar system. (a) The system configuration, (b) Vertical Network Analyzer (VNA).

2.3.3.1 Antenna configuration

For the acquisition of full polarimetric dataset, we combine two types of antennas which are dipole and slot antennas. The slot antenna is necessary to generate the orthogonal electrical field to the radar sonde axis. We produced an axial slot antenna on a conducting cylinder [9], [10]. This type of axial slot antenna on a conducting cylinder is considered a variation of a one-turn loop antenna, thus it can be approximated as a vertical magnetic dipole in a vertical borehole, and to radiate horizontally polarized electric field. On the other hand, a dipole antenna radiating a vertically polarized electric field that has the same polarization direction parallel to the radar sonde axis.

Therefore, the combination of dipole and slot antennas enables the acquisition of full polarimetric datasets. Figure 2.4(a) is an image of both dipole and slot antennas, and Figure 2.4(b) provides a description of the polarizations of dipole and slot antennas as the dipole antenna produces vertically electric polarized electromagnetic signal while the slot antenna generates horizontally electric polarized electromagnetic one. In order to acquire full polarimetric signals, we repeat the measurement four times in a same borehole with four antenna combinations shown in Figure 2.8(a).Thus, there are two antennas in each measurement, one transmitter and one receiver with the same polarization or orthogonal one.

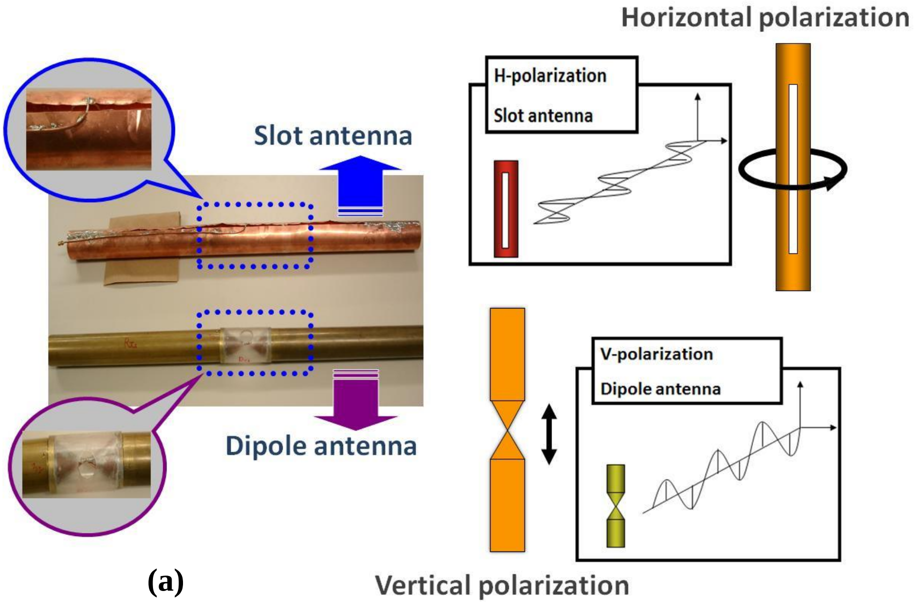

(a)

(b)

Fig.2.4: The antenna configurations of the full polarimertic borehole radar. (a) an image of the dipole and slot antennas, (b) polarization characteristics for each antenna.

2.4 Hydraulic tracer test measurements

Hydrologic properties of a fracture or fracture zone are determined using hydraulic tracer testing. Because fracture systems are complex, unique models of ground-water flow and solute transport are difficult to obtain from hydraulic or tracer tests alone. Other information is needed to accurately describe the flow geometry, boundaries, and heterogeneity [11, 12].

Researchers in U. S. Geological survey have carried out a variety of methods to characterize fractured rock systems at Mirror Lake site. In 1995, a tracer testing was measured for verifying the results of geophysical measurements [13]. The transmissive zone is isolated in a borehole using specially constructed polyvinylchloride packers. During the tracer test, the lower hydraulically conductive zone between FSE-1 and FSE-4 was isolated using straddle packers. The packed-off interval in FSE-4 was pumped at about 9L/min (liter per minute) while a NaCl solution with concentrations of 20 to 28 g/L (grams per liter) was injected into the packed-off interval in FSE-1 at about L/min. The experiment involved the repeated, near-continuous injection of NaCl tracer during the collection of borehole-radar data. Radar data were collected before and during tracer injection to establish the `background' conditions and to measure any changes resulting from the presence of the tracer.

The tracer testing revealed two hydraulically conductive zones connect the boreholes in FSE site as shown in Figure 2.5. The upper zone is near the bottom of casing and has hydraulic conductivities from 10^{-7} to 10^{-6} m/s. The lower zone is approximately 40 m below the top of casing and has hydraulic conductivities from 10^{-6} to 10^{-5} m/s [13]. Tracer testing results are displayed in the Table 2.1 of FSE1 borehole. These results will be used for verification of the polarimetric analysis of borehole radar in chapter5.

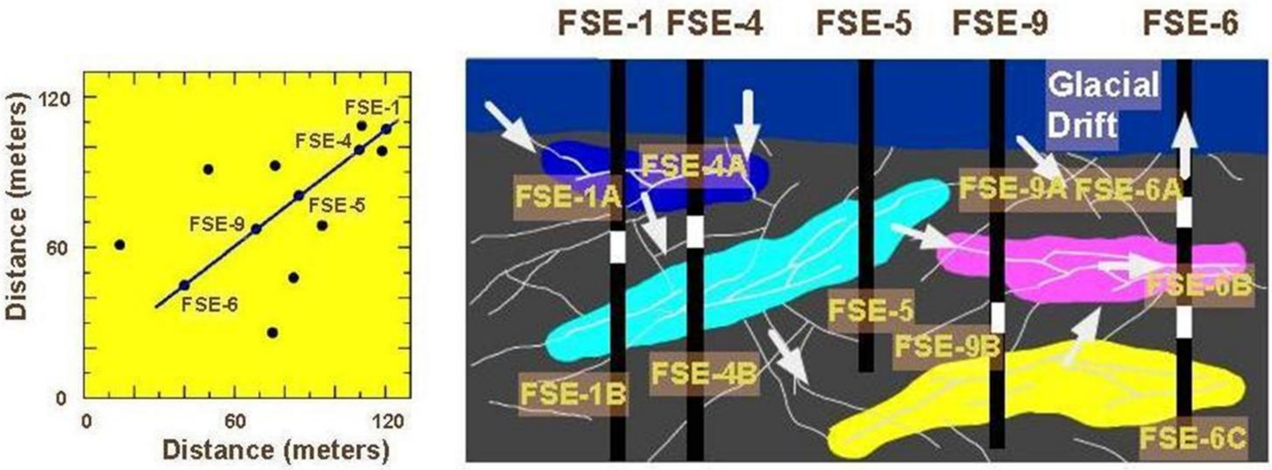

Fig. 2.5: The conceptual model of high transmissive zones in the FSE6-FSE1 cross section (after Hsieh et al., 1999).

Table 2.1: Hydraulic tracer testing of borehole FSE1 (provided by USGS)

Interval top (ft)	Interval bottom (ft)	Interval top (m)	Interval bottom (m)	Time at Start	Time at Steady State	Upper (ft)	Head Increase Mid. (ft)	Lower (ft)	INJECT. RATE gpm	Inject. Rate, Q (l/min)	Note*	Head Increase Mid., h (m)	Q/h (m**2/s)	Trans-missivity (m**2/s)
55.0	65.0	16.8	19.8	10:18	10:45	0.0	-1.9	0.7	-0.300	-1.137	2	-0.6	3.3E-05	3.3E-05
75.0	95.0	22.9	29.0	11:26	11:34	0.0	37.1	0.0	0.446	1.690		11.3	2.5E-06	2.5E-06
95.0	115.0	29.0	35.1	15:58	16:15	0.0	111.0	0.1	0.002	0.007		33.8	3.4E-09	3.4E-09
110.0	130.0	33.6	39.7	14:43	14:55	-0.1	118.0	0.0	0.006	0.022		36.0	1.0E-08	1.0E-08
120.0	140.0	36.6	42.7	10:47	11:05	-0.1	107.0	0.1	0.056	0.212		32.6	1.1E-07	1.1E-07
138.0	158.0	42.1	48.2	14:17	14:45	-0.1	-1.0	-0.7	-0.273	-1.032	2	-0.3	5.6E-05	5.6E-05
160.0	180.0	48.8	54.9						0.000	0.000			0.0E+00	0.0E+00
175.0	195.0	53.4	59.5						0.000	0.000			0.0E+00	0.0E+00
210.0	230.0	64.1	70.2						0.000	0.000			0.0E+00	0.0E+00
240.0	260.0	73.2	79.3						0.000	0.000			0.0E+00	0.0E+00

2.5 Full polarimetric borehole radar measurement

The full polarimetric borehole radar system has been applied for measuring the full polarimetric dataset of subsurface fractures in different sites such as in Mirror Lake - USA, Korea and Kamaishi-Japan. In this research work, we are going to show two measurement cases which are at Mirror Lake site, USA and Kamaishi field, Japan. We will concentrate on the polarimetric measurements at Mirror Lake test site because fracture hydraulic tracer tests have been carried out in this site. Those results can be used to correlate with the full polarimetric data analysis that will be discussed in chapter 5.

2.5.1 Measurements at Mirror Lake, USA

Mirror Lake lies at the lower end of the Hubbard Brook valley in the southern White Mountains of New Hampshire. The surface area that drains into Mirror Lake occupies 0.85 km^2 of mountainous terrain, which varies in altitude from 213 m at the lakes surface to 481 m at the top of the drainage divide. The bedrock is a sillimanite-grade schist extensively intruded by granite, pegmatite, and lesser amounts of lamprophyre [14]. It is covered by 0 to 55 m of glacial drift. Outcrops are few; the largest exposure of bedrock occurs where a highway cuts through a small hill. The “pavement method” was used by Barton [15] on a glaciated surface and four highway road cuts near Mirror Lake. Exposures on highway road cuts exhibit a high degree of lithologic and structural variability. Four subvertical surfaces, exposed by road construction, and one subhorizontal surface, cleared by glaciation, provide approximately 8,000 m^2 of exposed rock for mapping and studying fractures and geology. The roadcut shows a complex distribution of rock types. The schist is multiply folded. The granitic intrusions occur as dikes, irregular pods, and anastomosing fingers, ranging in width from centimeters to meters. Pegmatite and basalt dikes cross-cut both the schist and granite.

The predominant lithology of the Mirror Lake area is the Silurian Rangeley Formation. The lower part of this formation is a metapelite, and the upper part is a pelitic schist of sillimanite-grade metamorphism [14]. The strike of foliation ranges from N25E to 45E, and it dips predominantly 60 to 67NW and 40 to 80SE. Folding, faulting, metamorphism, and igneous intrusions associated with the Acadian orogeny (and possibly the Alleghanian orogeny) have resulted in a complex distribution of lithology and fractures.

Since 1990, the Toxic Substances Hydrology Program of the U.S. Geological Survey (USGS) has been supporting investigations of bedrock in the Mirror Lake watershed. The aim is to address the Nation’s need for accurate and efficient methods of evaluating ground-water resources in fractured rock, and for determining ground-water pollution. About 25 research scientists from the USGS, from universities, and research institutes engaged in collaborative studies at the Mirror Lake site, and the broad spectrum of techniques being applied at the Mirror Lake site includes geologic, geochemical, geophysical, and hydrologic methods. The joint research group of Tohoku University and USGS also carried out field measurements at the Mirror Lake site, which are analyzed here.

Figure 2.6 shows the Mirror Lake fractured-rock hydrology research site. The Mirror Lake drainage basin lies partly within the Hubbard Brook Experimental Forest, which is an ecosystem research site operated by the U.S. Forest Service. Fractures at land surface might not be representative of fractures underground, so boreholes have been drilled at two locations with differing densities for two scales of investigations. The local scale investigations focus on two experimental plots, which are referred to as the “FSE” and the “CO” borehole fields; each occupies a 100-by-100- meter area, where boreholes are spaced from 10 to 40 meters apart. By the end of 1994, 13 boreholes had been completed in bedrock in the FSE borehole field, nine in the CO borehole field, and 14 at other locations throughout the drainage basin. Figure 2.6 shows the location of FSE boreholes and the conceptual model for the subsurface transmissive fracture zones a cross FSE1 and FSE6 boreholes.

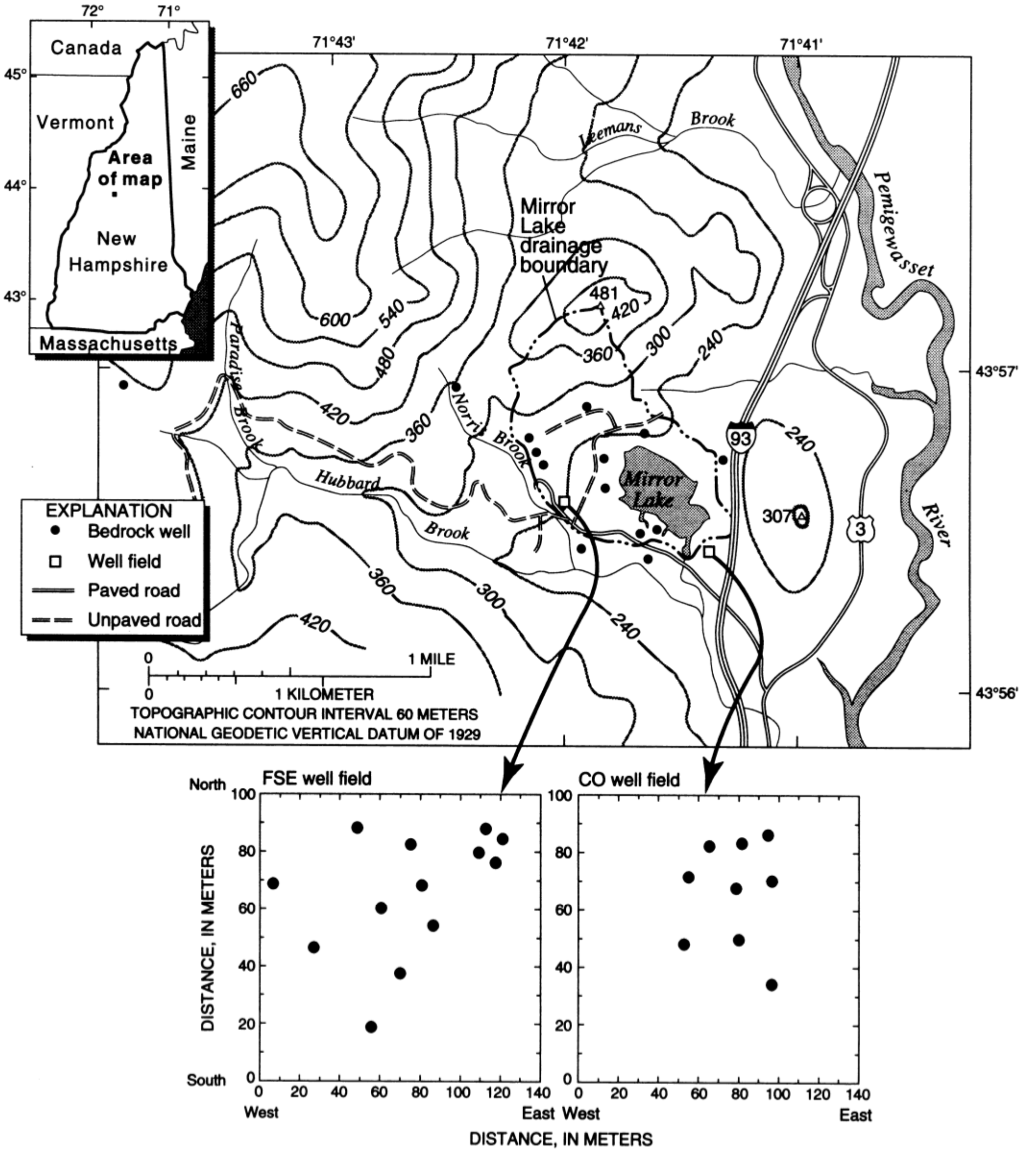

Fig. 2.6: Mirror Lake rock fractured research site that is located in Grafton Country, New Hampshire, USA.

Using our full polarimetric borehole radar system, single-hole reflection measurements and cross-hole transmission measurements were carried out at this test site. Figure 2.7 shows the borehole cluster which we used for measurements. The single-hole reflection measurements were conducted at FSE-1, with an antenna separation of 1.6 m in all antenna arrangements. The cross-hole measurement was carried out between FSE-1 and FSE-3 for all combinations of dipole and slot antennas.

The separation of the FSE-1 and FSE-3 was 9 m. In all the measurements, frequency domain datasets were acquired between 2 - 402 MHz with a 2 MHz frequency interval.

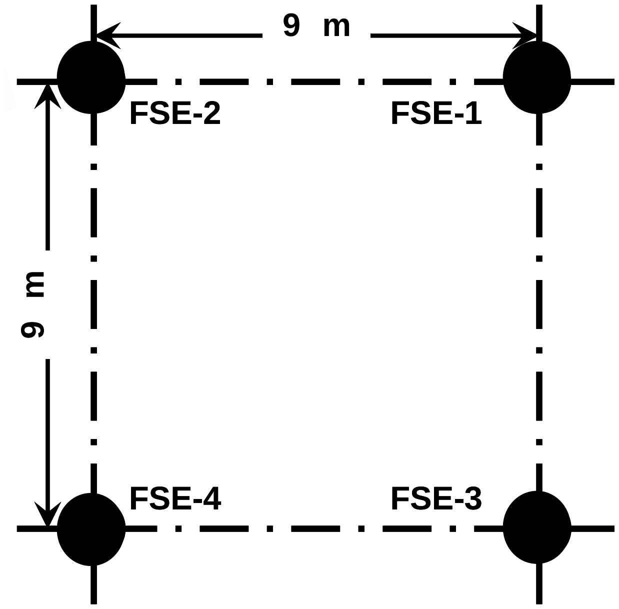

Fig. 2.7: Plan view of borehole: FSE-1, -2, -3, and -4 of the Mirror Lake test site.

According to the accumulated USGS geological data, the host rock at Mirror Lake is granite and quite homogeneous except for fractures. The dielectric constant of the host rock is about 8, and the conductivity is less than 0.001 S/m within the frequency band of 1 – 500 MHz. To accurately determine the velocity of the medium, we calculated two velocity tomograms by using cross-hole measurement with dipole-dipole and slot-slot antenna combinations [16], [17]. The velocity tomography results based on an algebraic reconstruction method and the two average velocities were calculated to be 0.1309 m/ns and 0.1331 m/ns with the two antenna combinations, respectively. We used a velocity value 0.13 m/ns as a constant velocity of electromagnetic propagation in the subsurface medium at the Mirror Lake test site.

The full polarimetric borehole radar profiles in borehole FSE-1 are shown in Figure 2.8 for every polarization state after signal processing for the raw data and antenna compensation [18]. The detectability for subsurface fractures can be observed at every polarization state, especially for Co-polarization (VV and HH) and about nine fractures zones can be determined from this data.

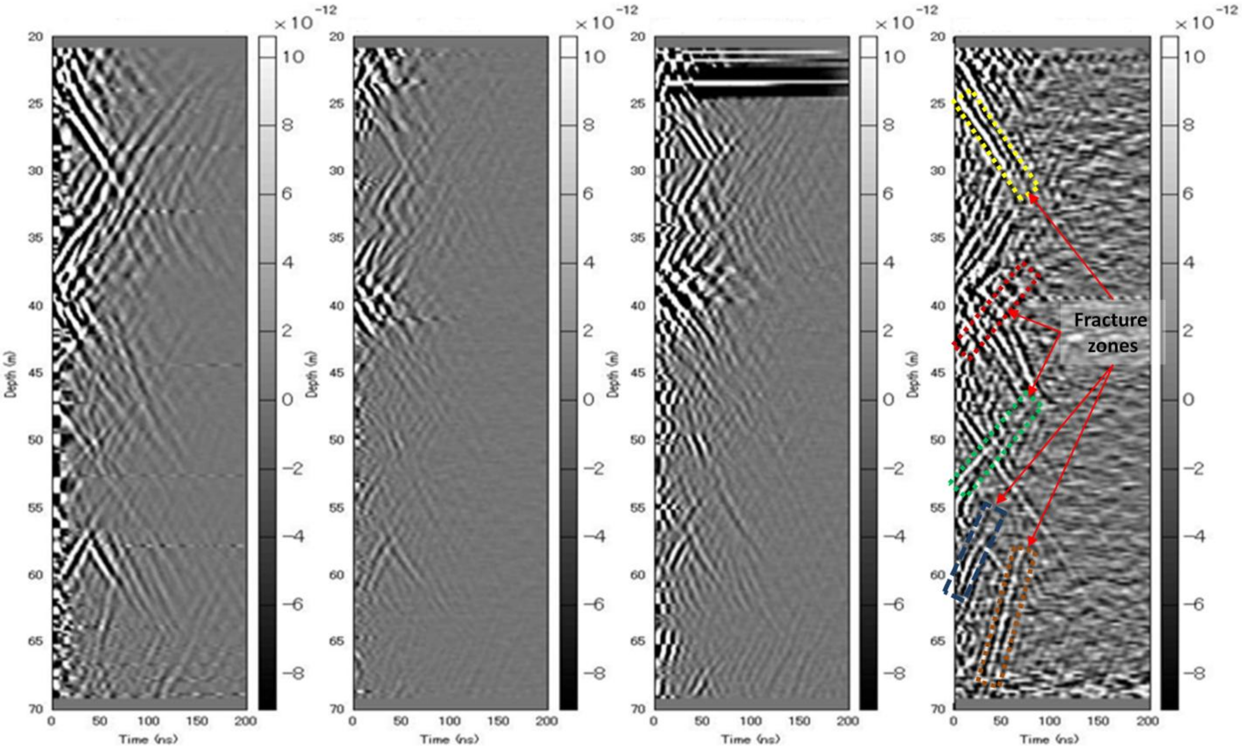

(VV) (VH) (HV) (HH)

Fig. 2.8: Full polarimetric borehole radar dataset at FSE1 borehole at Mirror Lake- USA. (VV) vertical-vertical polarization, (VH) vertical-horizontal polarization, (HV) horizontal-vertical polarization and (HH) horizontal-horizontal polarization measurement, respectively.

2.5.2 Measurements at Kamaishi, Japan

The Kamaishi mine began operating in 1857 in the skarn ore deposit at the southern end of the Kurihashi granodiorite, Iwate Prefecture, northeastern Japan. The main period of mining activity was around the 1940s in the southern part of the granitic bodies. It was therefore decided to select the northern-most part of the granitic body for detailed investigations as it was expected that this part would be less disturbed by previous mining activities [19]. The Kamaishi in situ studies were conducted in an existing drift 550 m above sea level, and in a drift 250 m above sea level, which had been excavated 25 years ago for exploration purposes. The geology in Kamaishi area consists of Paleozoic and Cretaceous sedimentary rocks and two igneous complexes, Kurihashi granodiorite and Ganidake granodiorite [20]. During the last two decades, the mine has been diversifying from mining into underground research sites for developing new methods of geological and geophysical studies and for rock mechanics, hydrology, and so forth.

The field measurement was carried out at the Kamaishi mine test site in Japan as a sketch map for the borehole locations can be seen in Figure 2.9. This site characterized by the presences of many permeable and water filled fractures caused by tectonic activities. Also, the host rock is invaded by multiple veins. These boreholes are located in a tunnel dug for mining. The polarimetric single-hole data was acquired for well KR-2 and Figure 2.10 shows the full polarization states radar profiles with an antenna separation of 1.6 m.

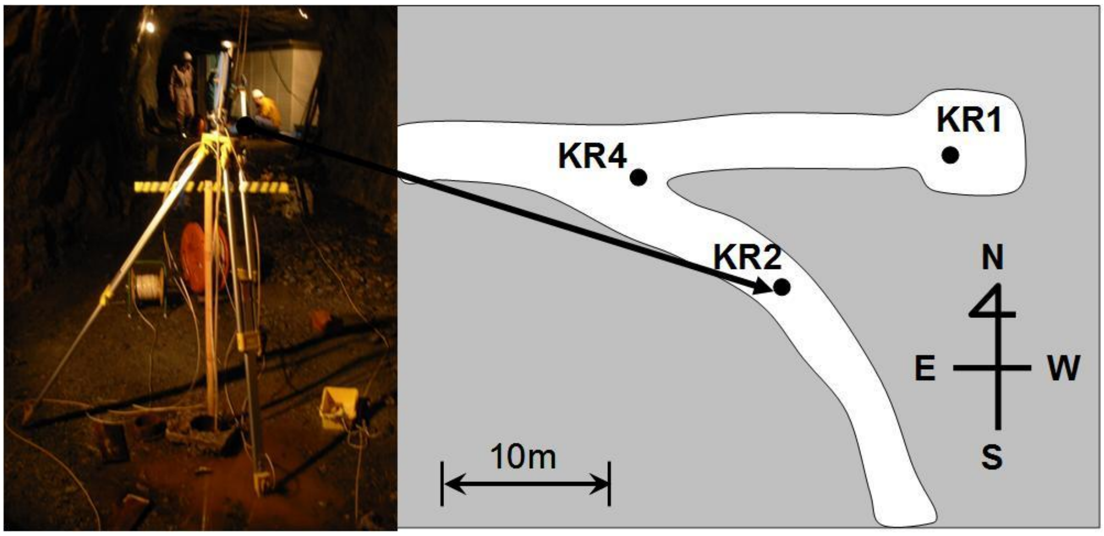

Fig. 2.9: The sketch of the borehole locations inside Kamaishi mine, Japan.

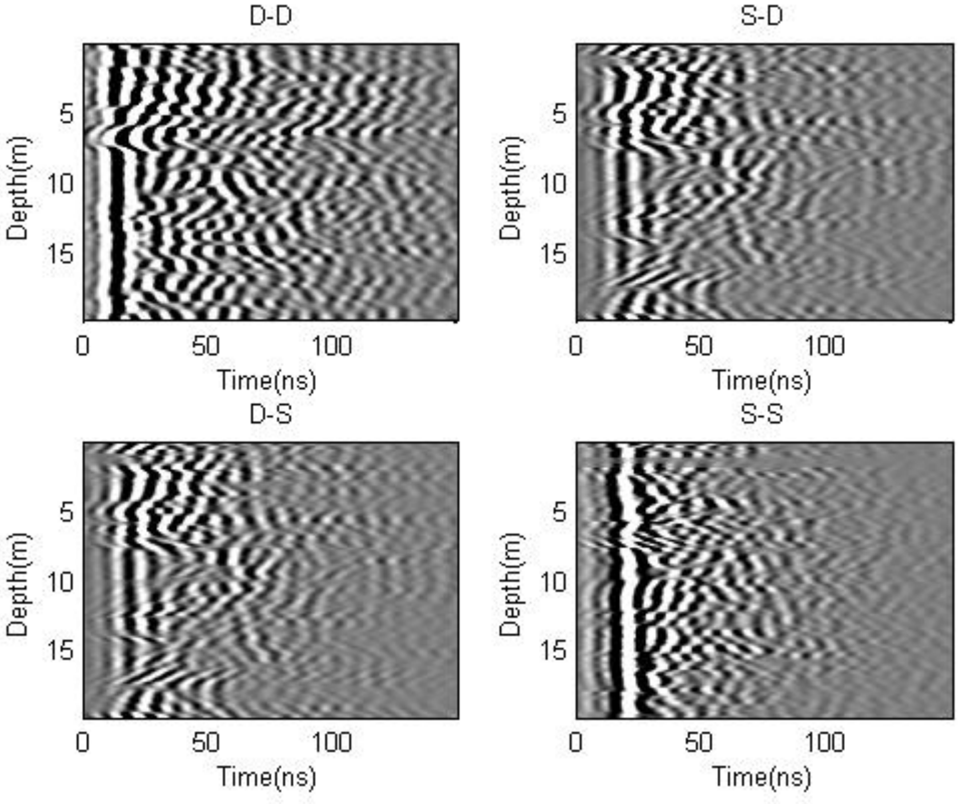

Fig. 2.10: The full polarization states radar profiles for KR-2 borehole at Kamaishi site, Japan.

2.6 Summary

In Chapter 2, different borehole radar systems have been introduced in this chapter as we showed three kinds of borehole radar systems. Which are the conventional borehole radar system, the directional borehole radar system and the full polarimetric borehole radar system. I have described briefly the function of the first and second borehole radar systems and I introduced the structure of the full polarimetric borehole radar system and its antenna configurations. Furthermore, the polarization properties of dipole antenna and slot antennas have been figured out. It was shown how these two antenna combinations can acquire the full polarimetric radar dataset which can be used to estimate scattering properties of the measured object and especially that has irregular shape such as subsurface fractures.

Two field studies for the measurement of the polarimetric borehole radar system have been clarified for subsurface fracture examination. The first one was for fracture test site in Mirror Lake, USA and the other one was in Kamaishi, Japan. The measurements in Mirror Lake field have an important role for the evolution of our polarimetric borehole radar system because the hydraulic tracer tests of fractures have been acquired for that site. This can be used for correlating our polarimetric borehole radar analysis while it is not available for Kamaishi test field.

Chapter 3

Subsurface Fracture Modeling

3.1 Introduction

To build predictive models and understand the behavior of complex fracture systems it is necessary to understand the property of a single fracture where fracture aperture represents the key parameter in determining the flow and transport characteristics of fractured surface media. In natural fractures there is usually a large distribution of fracture apertures even within a single fracture. The distribution is controlled by a number of factors. The flaws and inclusions in the material and the history of mechanical, thermal and chemical stresses on the material, from before it fractured, through the primary fracturing process and the subsequent fracturing episodes on to its current state [1]. A sudden release of the confining pressure may result in a widening of the fractures. Fracture spacing, which may be a result of both material strength and stress history, also affects the fracture aperture distribution.

The prediction of the fracture aperture distribution given the material properties and stress history (even if it could be somehow precisely determined over millions of years) is next to impossible, since the material is likely to fail at flaws or inclusions in the matrix, which cannot be captured in the averaged material properties. Field determination of the fracture aperture distribution, or even simply mean aperture, is currently an area of active research. Several direct techniques for detecting and imaging fractures are under development. Small-scale features can be imaged using video imaging inside a well [2] and [3] which of course only provides an image of the fracture aperture in the immediate vicinity of the well as can be seen in Figure 3.1, where the aperture of the fractures is most likely affected by the well boring process. For larger scales, geophysical imaging techniques include (1) seismic reflection, where seismic waves are generated at one location and measured at several points for 3D imaging, measuring the reflection of the seismic energy at discontinuities; (2) electrical methods, which rely on the fact that water-filled fractures have a higher conductivity than unfractured rock and can mobilize ions in solution; and (3) ground-penetrating radar, in which electromagnetic radiation is applied in a similar manner as with seismic imaging but at much higher frequencies (10 to 1000 MHz), with propagation of the radar signal depending on the dielectric constant and electrical conductivity of the materials and reflection of the signal at discontinuous boundaries.

Indirect techniques of measuring the statistics of the fracture distribution and its hydraulic properties include pumping and tracer injection tests. These are currently the most known accurate means of assessing fracture and its distribution in the field. At the laboratory scale, much higher resolution can be attained in the determination of the fracture aperture distribution. The higher resolution can be used to increase our understanding of the controlling mechanisms and key parameters for flow and transport in fractured media.

Several techniques have been applied to determine fracture aperture in the laboratory. The two surfaces of an open fracture can be scanned using a surface profiler [4] and [5] providing a map of the surface roughness at a theoretical resolution of 10 μm for surface features and these two halves of the fracture are then closed using a precise guidance mechanism to measure the change of fracture surfaces property, from fixed reference plane, with others mechanical forces such as shear effect.

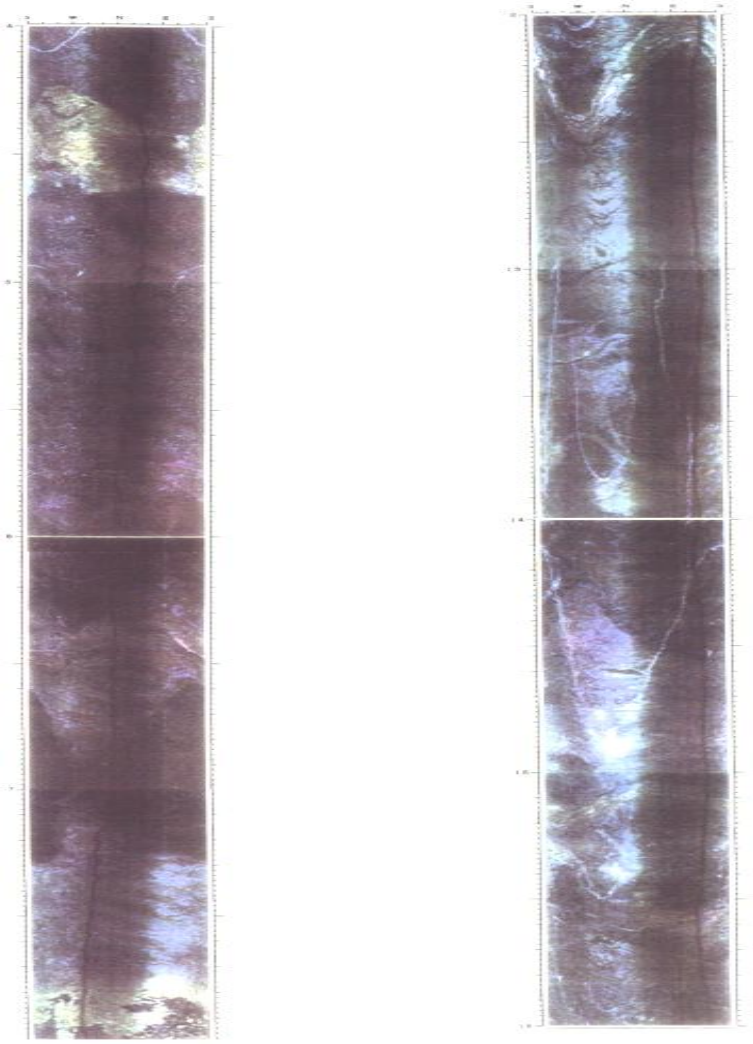

(a) (b)

Fig. 3.1: Borehole TV images between (a) 4 to 8 m and (b) 12 to 16 m at Kamaishi, Japan.

3.2 Fracture surface measurements

Rock samples to be used for fracture surface characterization may be very limited in size. Unlike outcrop samples or fault zones where large amounts of data can be collected and processed, core samples from deep boreholes are much smaller, at the order of centimetres. However, characterizing these fracture surfaces is needed to understand the fluid flow inside them. In addition, modeling of these fractures is important for different fields of engineering.

A fracture consists of two surfaces that determine the properties of the fracture aperture and we can obtain the surface features by laser scanning on those surfaces. Figure 3.2 shows a laser profiling apparatus for acquiring the topography of fracture surfaces.

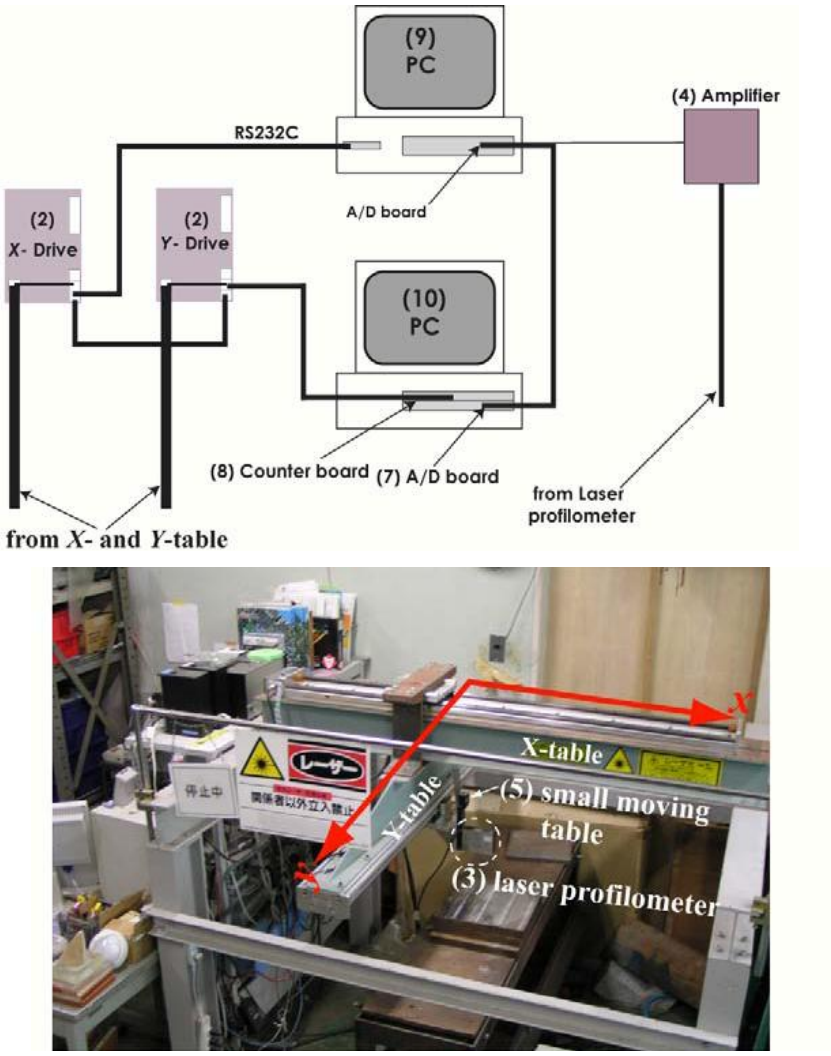

Fig. 3.2: System used to measure surface heights of a fracture using a laser profilometer.

3.2.1 Measurement surface height

For mapping the surface roughness, a computer-controlled surface scanning device was used as shown in Figure 3.3. The scanning is accomplished by a needle that can displace vertically. The needle is fixed at a known distance over the sample and calibrated based on this distance. The needle is moved down by means of step motor. Once the needle touches the fracture surface, the number of step motor rounds is counted and converted to the distance using a calibration constant to calculate the traveled distance from the initial point. Then, the needle moves to next pixel which is 1 mm away by means of step motor. The elevation values on the surface plane are measured to the resolution of 1/10 mm in the vertical axis (z) and 1 mm in the horizontal axes (x and y).

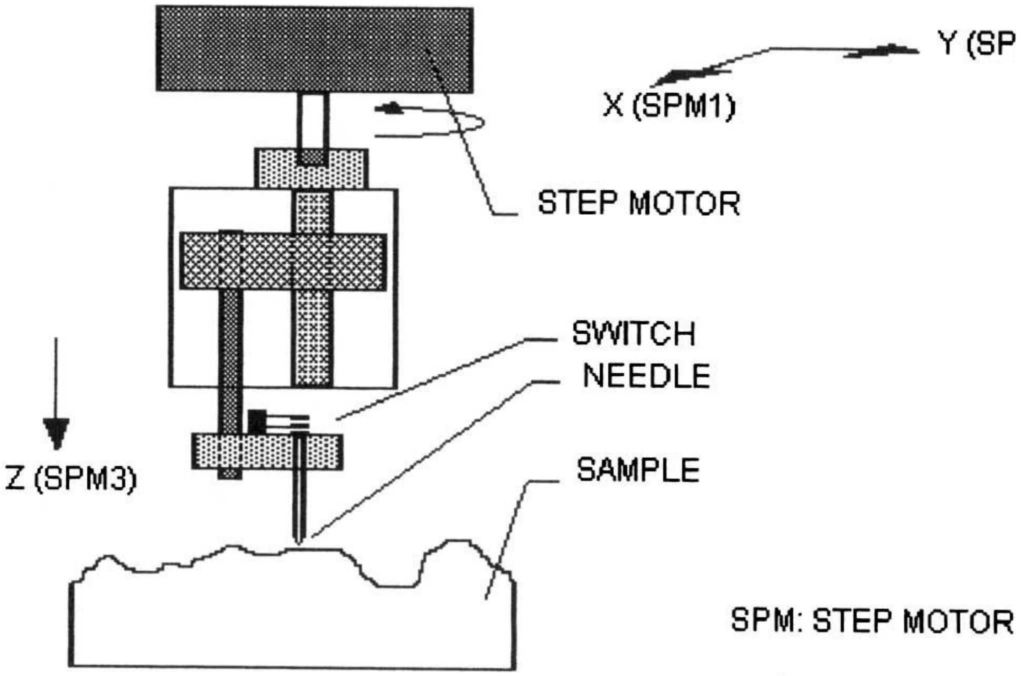

Fig. 3.3: Sketch of scanning device used to measure the surface roughness.

3.2.2 Imaging and 3D representation of fracture

Various techniques have been used to characterize fracture geometry and the most known techniques are: (1) those that use measurements of the roughness of the two surfaces composing the fracture and (2) those that involve filling the void space with a casting material. In the first category one method is to sum the surface roughness heights from both sides of the fracture to generate a "composite topography." Specifically, if the heights of the surfaces on opposing walls of the fracture are $h_1(x,y)$ and $h_2(x,y)$, measured relative to the mean level of each surface with positive values increasing outward from the surface, the composite topography is defined as $h_c(x,y) = h_1(x,y) + h_2(x,y)$. The composite topography contains only the mismatched parts of the surface roughness and represents the distribution of local apertures [6]. For precise and accurate fracture surface data measurement, the laser profilometer can fulfill this property. Thus, this measuring tool is widely used these days. Figure 3.4 represents the geometrical image of one of fracture surfaces after measured it with a laser profilometer.

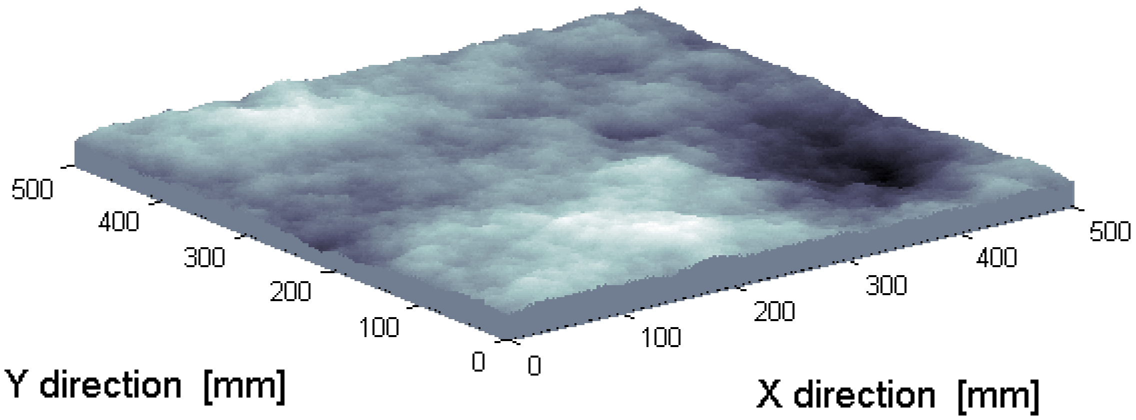

Fig. 3.4: 3D image of the fracture surface measured with a laser profilometer.

The second category is method that involves filling the void space with different materials such as epoxy or Wood's metal and other casting techniques. Epoxy castings provide good estimates of local aperture geometry, but some techniques require the sample to be sliced and consequently destroyed. Estimates of the areal distribution of void space can be obtained accurately by using Wood's metal, but it is difficult to obtain local aperture geometry.

3.3 Fracture surface generation based on Power spectral method

Brown and Scholz (1985) and Power et al. (1987) [7]-[8] computed the power spectral density, $G(k_x)$, for various rock surfaces, natural joint surfaces in crystalline and sedimentary rocks, a bedding-plane surface, and frictional wear surfaces. Their results show that there is remarkable similarity among these surfaces. Profiles of these widely different surfaces yield power law spectra of the form

$$G(k_x) = C\, k_x^{-\alpha} \qquad (3.1)$$

where k_x is the wavenumber related to the wavelength λ of surface roughness according to $k_x = 2\pi/\lambda$. The exponent α has a fairly limited range (typically between 2 and 3) and C is the proportionality constant. The power spectrum (and therefore the roughness) can be described to first approximation by two parameters: (1) the exponent α (i.e., the slope of the power spectrum on a log-log plot) and (2) the proportionality constant parameter C.

This power law form of the power spectrum indicates that fracture surface topography can be represented in terms of fractal geometry where the fractal dimension of the surface, D, is related to the power spectrum exponent as

$$D = \frac{7-\alpha}{2} \qquad (3.2)$$

where this relationship is true only if the phase spectrum is random and the topographic heights have a normal distribution.

Figure 3.5 illustrates the superimposing of several single frequency waves to form 1D rough fracture surface. The fractal dimension describes the proportion of high frequency to low frequency roughness elements and is a measure of surface texture. For natural fracture surfaces, D falls in the range of 2 to 3, with small values representing smoother surfaces. Variations in α over different measurement scales indicate, however, that it may be unrealistic to extrapolate the power spectrum outside the range of measured wavelengths.

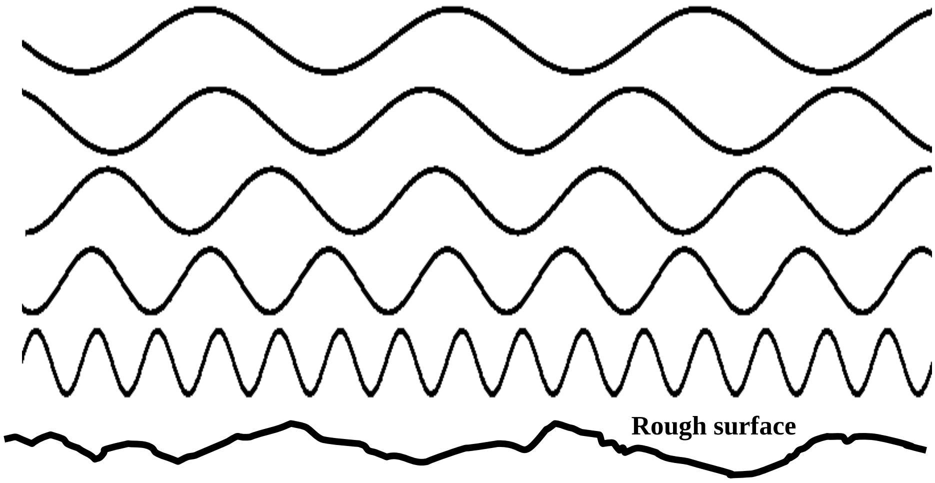

Fig. 3.5: Sketch showing the superimpose of several single frequency wave components to form 1D rough surface.

3.4 Fractal fracture model

All the fractures modeled in this thesis research work have the same fractal representation of rough fracture surfaces. Fractal surfaces are composed of a sum of Fourier harmonics where the intensity decays gradually as a power of the wave-number, with phases that are random. After generation of the Fourier spectrum, an Inverse Fast Fourier Transform (IFFT) is applied in order to obtain the topography of fracture surfaces. This method of generating a fractal surface is called power spectral for synthesizing fracture surface. The discrete inverse Fourier transform to create an isotropic fracture surface h(x, y) of size X x Y with N x N points is given by the following equation

$$h(x,y)=\sum_{k=0}^{N-1}\sum_{l=0}^{N-1}G_1(k_x,k_y)\,e^{2\pi j\left(\left(\frac{k\Delta x}{X}+\frac{l\Delta y}{Y}\right)/N\right)} \qquad (3.3)$$

where $G_1(k_x,k_y)$ is a complex Fourier component of the surface for the spatial frequencies *k/X* and *l/Y* in the X- and Y-directions, respectively.

3.4.1 Model of the lower fractal fracture surface

Lower fracture surface can be generated according to Equation 3.3; hence we can determine the lowest and the highest spatial frequency of the generated surface model depending on the minimum grid spacing and its maximum size. Linear regression of the full power spectrum density (PSD) for the surfaces, and the linear short wavelength portion of the aperture, allow the fractal dimensions of the surfaces and aperture to be calculated. Let us note that the fractal dimension represents a measure of the scaling behavior of the surface and will contain information regarding the relative positions of profile heights of different sizes. Figure 3.6 illustrates the power spectral density profiles for different fractal fracture surface models. These models shared the same properties such as the slope of its power spectral density for their surface heights α (fractal dimension); and the lowest and the highest spatial frequency limits. However, they show different roughness properties when using different proportionality constant variable. Thus, the rough fracture surface model is created with the larger proportionality constant values according to Equations 3.1 and Equations 3.3. Furthermore, the slope of power spectral density profile α and the fractal dimension D is derived according to the relation of Equation 3.2.

Fractal dimension (D) 2.297 was used for the generated models with the longest wavelength 6000 mm. That represents the maximum size of the model. In addition the shortest wavelength is 5.86 mm. We also note that the wavenumber contents (i.e., spatial frequency band limit), the fractal dimension and the proportionality constant determine the characteristics of the fracture model. This is because they control the fracture surface roughness property where they cause and determine the scattering behavior of the electromagnetic waves from it.

3.4.2 Model of the upper fractal fracture surface

The two surfaces which bound the fracture (i.e., the lower and the upper surfaces) are not exactly the same, and they are not completely independent. So the random phases of Fourier harmonics of these surfaces should be partially correlated.

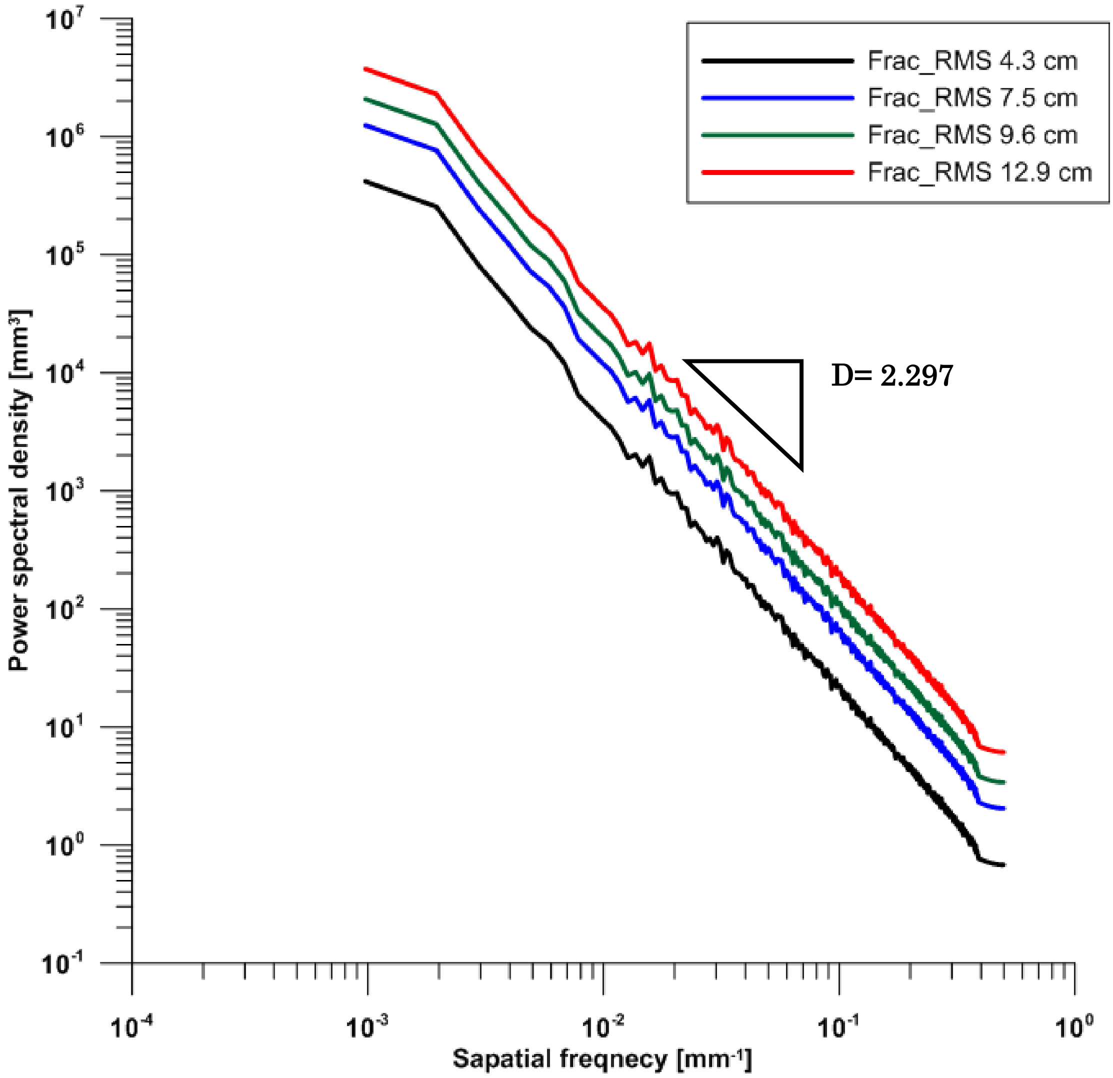

Fig. 3.6: Power spectrm density for diffrent generated fractal surfaces have the same fractal dimension and different proportional constant C.

Brown (1995) [9] proposed that harmonics having wavelength greater than some mismatch length λ_c are perfectly correlated while harmonics with shorter wavelength are independent. The upper surface of fracture can be represented by Fourier components with the same amplitude as the lower surface but a different relative phase. Thus, $G_2(k_x, k_y)$ of the upper surface can be represented by

$$G_2(k_x, k_y) \propto (k_x^2, k_y^2)^{-(4-D)/2}\, e^{j(2\pi\phi_1 + 2\pi\gamma(f)\phi_2)} \qquad (3.4)$$

where, ϕ_1 and ϕ_2 are series of random numbers which are independent. Also, $\gamma(f)$ is incoherence function of the spatial frequency f which is equal to or less than 1. Thus, $\gamma(f)$ =1 when $f \geq f_c$ and it will be less than 1 when $f < f_c$. where f_c is the inverse of mismatch length scale (=1/λ_c) and the aperture of fracture is determined based on matedness between the two surfaces for wavelengths greater than mismatch length scale (λ_c). Fracture aperture was synthesized from the lower and the upper surfaces and its thickness varies from zero up to several centimeters where the zero thickness means that these two fracture surface fall to each other (i.e., the lower and the upper surfaces are matched perfectly) while when they are less matched, an aperture will have certain value. Here, we are mainly concerned with the fracture surface roughness and the effect of this roughness on the electromagnetic scattering as well as the variations of fracture size. For simplification, I proposed the fracture aperture to be homogenous water filled which can be approximated as a fracture zone. This fracture zone in reality can be filled with water, rock fragments, rock matrix and air. In addition, I used 3cm fracture size for some simulated models based on a field study at Mirror lake area showed that subsurface fracture zones have sometimes width of 5 or 6 cm [10]. The illustration of a full fracture model can be seen in Figure 3.7.

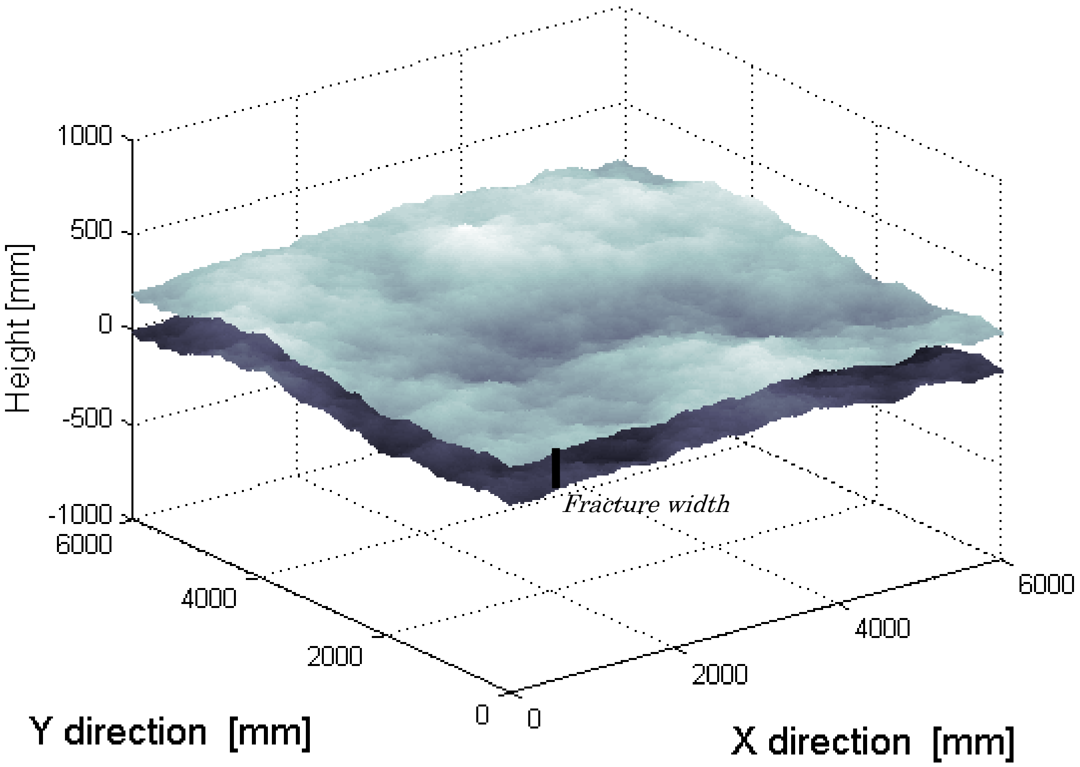

Fig. 3.7: Fracture model shows fracture surfaces with 43 (mm) RMS height and a constant fracture width.

3.5 Fracture roughness

Creation of synthesized fractal fracture depends on three important factors which are 1) the fractal dimension of the power spectrum, 2) the proportional constant parameter (*C*) as shown in Equation 3.1 and finally 3) the spatial frequency contents of the fracture surface which can be determined according to the maximum length of the generated fracture surface (low spatial frequency) and the discretized grid spacing (high spatial frequency).

3.5.1 Fractal dimension

A surface is called fractal if the height and spatial frequency contents of the surface do not vary over the frequency of measurement. This property has the principal advantage that the roughness of a fracture surface can be determined by its fractal dimension [11]. We have used this concept for generating successively rough fractal fracture surfaces with different fractal dimension as appeared in Figure 3.8, where the roughness of synthesized fractal fracture surface is increasing with high fractal dimension parameter as in Figure 3.8(e) which has fractal dimension 2.8 and the smoothest created surface is for Figure 3.8(a) with 2.0 fractal dimension parameter. The generated fracture surfaces have fractal dimension between 2 and 3 and the fracture surfaces can be modeled according to Equations 3.1-3.2 and 3.4. The variation of the fractal dimension led to the change of the fracture roughness but also it changes the correlation length of the obtained fracture models. In this research, we are interesting in observing the electromagnetic scattering from rough fracture surfaces with the same correlation length and the variations of fracture size property. For that, this condition can be fulfilled by adjusting the proportional constant factor that will be explained in next part.

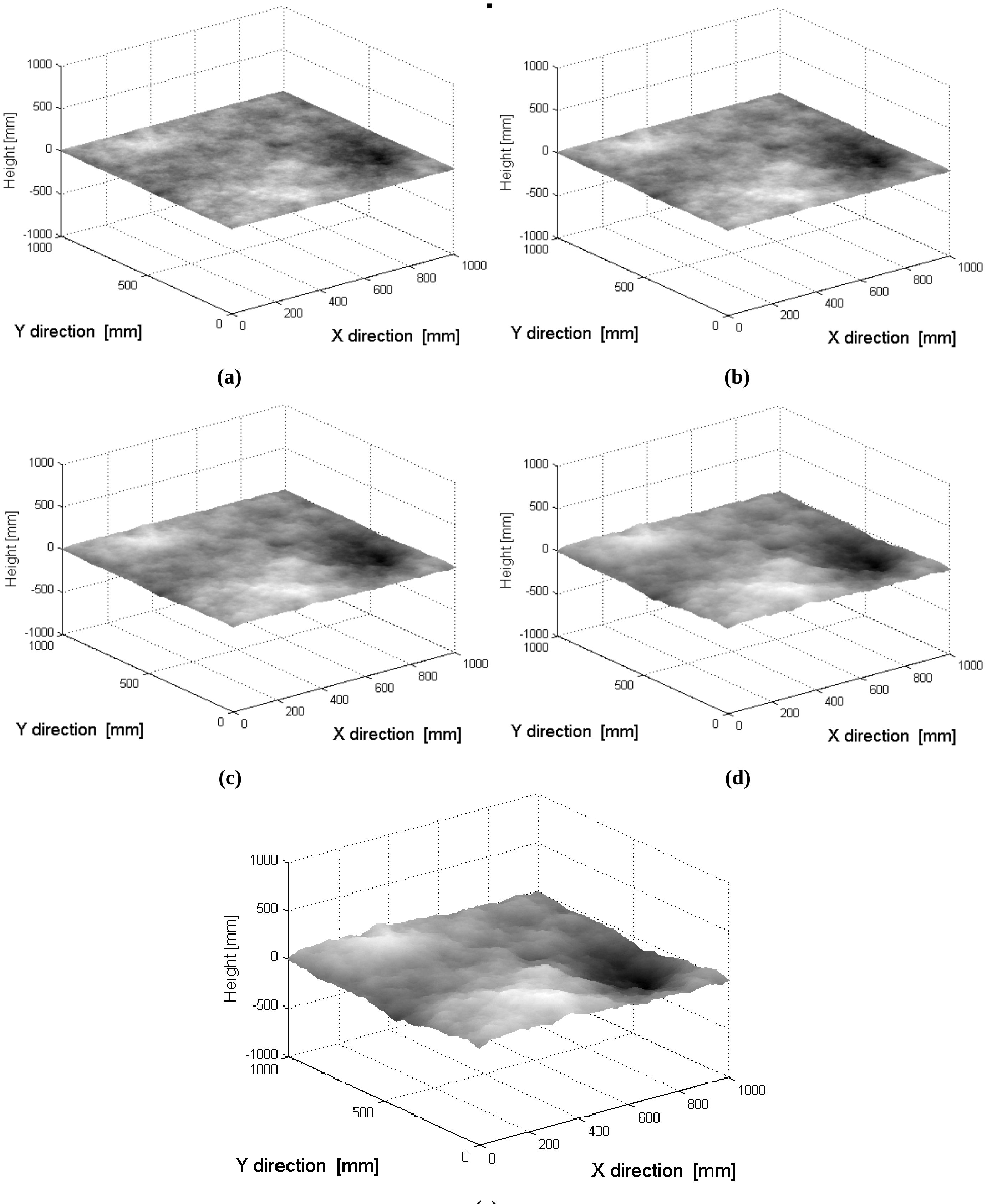

(a)

(b)

(c)

(d)

(e)

Fig. 3.8: Generated fracture surfaces with different fractal dimension (a) 2.0, (b) 2.2, (c) 2.4, (d) 2.6 and (e) 2.8 successively.

3.5.2 Proportional constant parameter

In this research work, we consider that proportional constant parameter (*C*) as shown in Equations 3.1 is the key for defining the fracture roughness property. Thus, to examine the electromagnetic scattering from rough fracture, which we will discuss in next chapter, we should keep in mind that the correlation length of the generated fracture surface has to be constant while only the RMS height should be varied. This condition can be fulfilled by changing the proportional constant and not the fractal dimension parameter.

Figure 3.9 shows six fracture surface models with different roughness property (RMS heights). We maintained the fractal dimension for this synthesized surface to be 2.297 which is a real fractal dimension value obtained from scanned fracture surfaces [12]. The proportional constant was selected between C=50 and C=1000 and the resulting RMS heights were 10 mm for the smoothest fracture surface and 43 mm for the roughest one. The length of the fracture is 1 meter and the minimum discretized grid spacing is 4 mm.

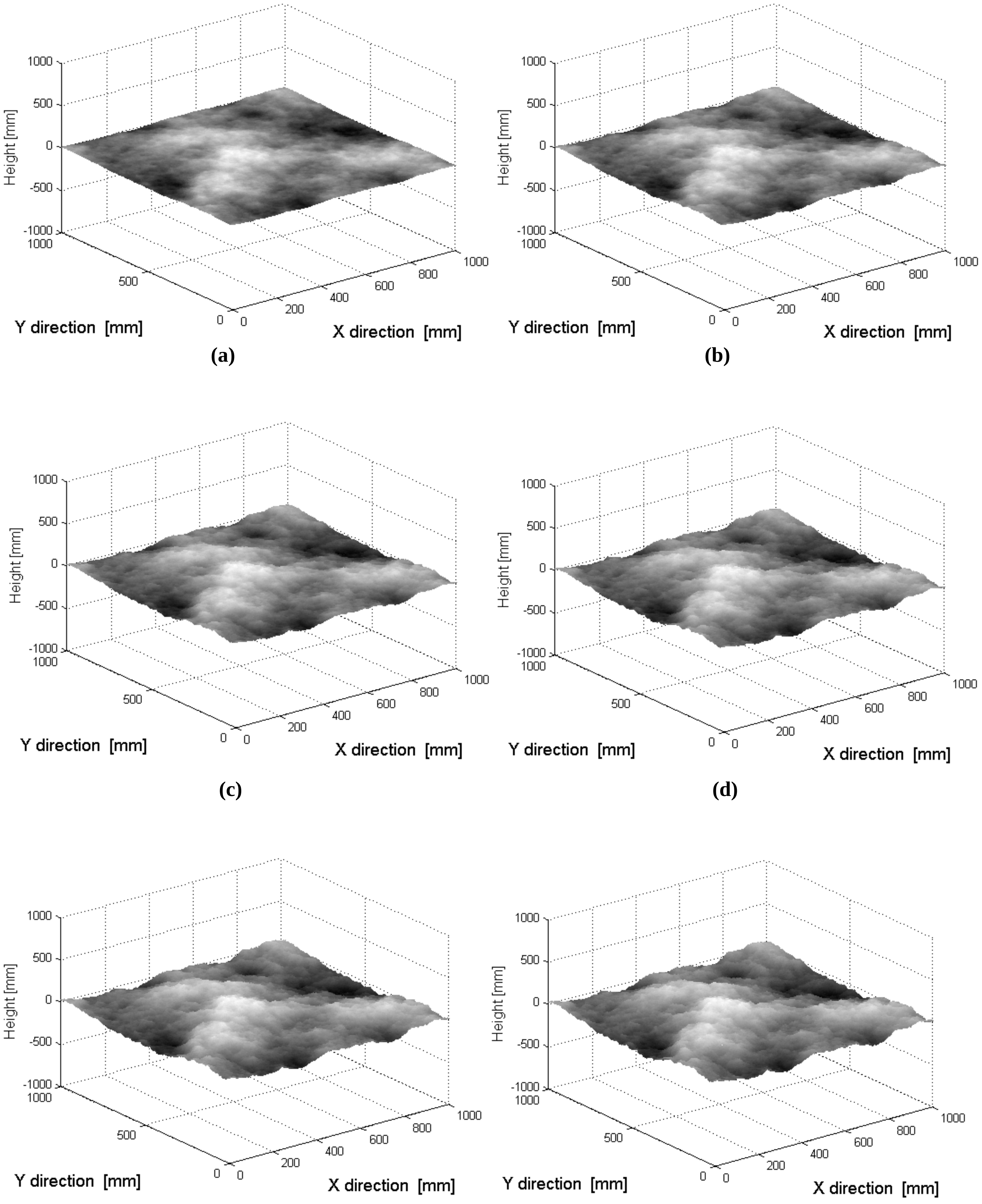

(a) (b) (c) (d) (e) (f)

Fig. 3.9: Synthesized fracture surfaces having different roughness property RMS height of (a)10mm, (b)21mm, (c)29mm, (d)36mm, (e)41mm and (f)43mm.

3.6 Summary

In this chapter, I have summarized how the rock fracture can be scanned and I explained the mechanism for acquiring the image of the fracture surface by using profilometer. In addition, I briefly figured out the theory for this scanning device. The importance of using power spectral method for the generation of the fracture model has been reviewed according to several fracture properties observation for different rock types. It was shown that most of the fractures in nature are obeying power exponent law. I effectively can generate fractal fracture model by using this technique and the fracture roughness property can be controlled depending on these three factors which are the fractal dimension, fracture spatial frequency contents and the proportional constant parameter (C). The relation between both fracture surfaces (lower and upper) has been cleared and fracture aperture as a result was produced.

In this research work, we are interesting in the fracture roughness property and its effect upon electromagnetic scattering as well as the change of fracture size. For that, the proportional constant parameter (C) is considered the key to define the fracture roughness property. I proposed the fracture for some models to be homogenous material content with water filled as simplification for representing the fracture zone in reality. That is the case for examining the electromagnetic scattering from rough fracture. On the other hand, the examinations of electromagnetic scattering from varied fracture apertures were implemented using the same roughness property and changeable aperture size as will be described in chptaer5.

Chapter 4

FDTD Electromagnetic Simulation

4.1 Introduction

FDTD simulation for fracture models will be introduced in this chapter. That FDTD method was derived from Maxwell's equations. The electric and magnetic fields are vector quantities that have both magnitude and direction. The relation and variation of electric and magnetic fields, charges, and currents associated with electromagnetic waves are governed by a physical law which is known as Maxwell's equations. These equations, as I have indicated, were arrived at mostly through various experiments carried out by different investigators, but they were put in their final form by James Clerk Maxwell, a Scottish physicist and mathematician. These equations can be written either in differential or integration forms [1]. The differential form in the time-domain are given by

$$\nabla \times E = -\frac{\partial B}{\partial t} \qquad (4.1)$$

$$\nabla \times H = \frac{\partial D}{\partial t} + J \qquad (4.2)$$

$$\nabla \cdot D = \rho_v \qquad (4.3)$$

$$\nabla \cdot B = 0 \qquad (4.4)$$

where, *E* is the intensity of the electric field in volts per meter, *D* is the electric flux density in coulombs per square meters, *H* is the intensity of the magnetic field in amperes per metre, *B* is the magnetic flux density in webers per square meter, *J* is the electric current density vector in amperes per square metres, *t* is the time in seconds and ρ_v is the volume electric charge density in coulombs per cubic metres.

The wave field quantities *E*, *B*, *H*, *D* and *J* in Maxwell's equations are related to each other with four supplementary relations known as the constitutive relations. These relations connect the aforementioned wave field quantities to the macroscopic electromagnetic properties of media, also known as the constitutive parameters, and which are the electric permittivity in farads per metre, the magnetic permeability in henries per metre, the electric conductivity in siemens per metre and an equivalent magnetic resistivity in ohms per metre. The constitutive relations are given by

$$B = \mu H \qquad (4.5)$$

$$D = \varepsilon E \qquad (4.6)$$

The constitutive parameters can be functions of the field directions (i.e., anisotropic media), functions of space position (i.e., inhomogeneous media), functions of frequency (i.e., dispersive media) and functions of strength of the field (i.e., nonlinear media). In this work, all the media are considered to be linear and isotropic and therefore, the tensors of μ , ε , σ and ρ reduce to scalar quantities. Where μ is the magnetic permeability of the media, ε is the electric permittivity, σ is the electric conductivity and ρ is the electric current density.

4.2 FDTD technique

In order to better understand the hydraulic property of subsurface fractures by polarimetric borehole radar as an assessment method, there is a need for experimentation. However, the presence of field sites with available hydraulic information about subsurface fracture is not available as the case of Kamaishi test site and to conduct hydraulic measurement for subsurface fractures, it is time consuming and costly. For that, a series of experiments were conducted by means of numerical modeling. Therefore, the theory of numerical modeling of GPR is presented. In this chapter, the numerical solution of the GPR forward problem using the FDTD method is discussed also in this part of the chapter I will describe the basic principles of the FDTD method as well as its model excitation.

The FDTD method was introduced by Yee (1966) and is also known as the Yee scheme. In this explicit scheme, the electric and magnetic fields are sampled at discrete points in time and in space. The building block of this discretised FDTD grid is the Yee cell [2] and it is illustrated for the 3D case in Figure 4.1. In order to simulate the subsurface numerically, a number of Yee cells are used to create the computational domain. Then, each of those cells is assigned with individual medium properties represented by the material's constitutive parameters (i.e., its permittivity, conductivity and permeability).

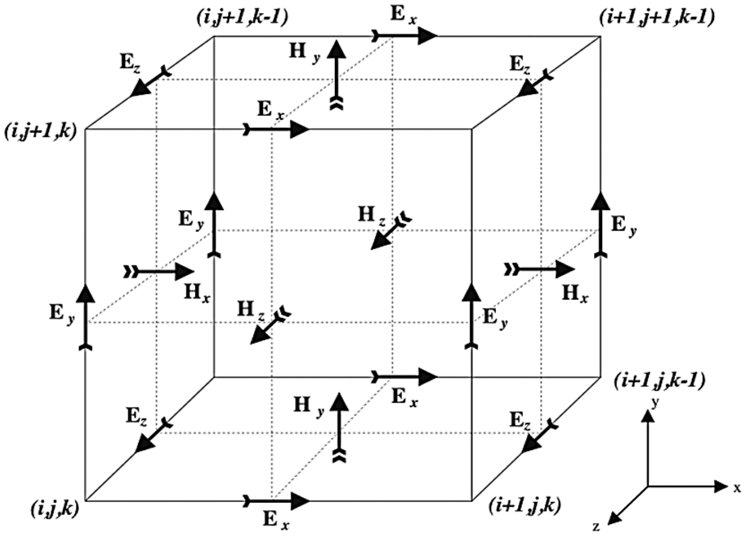

Fig.4.1: The 3D FDTD Yee cell. *Ex*, *Ey*, and *Ez* are the electric field components and *Hx*, *Hy*, and *Hz* are the magnetic field components at the *x*, *y* and *z* directions, respectively. The indices *i*, *j*, *k* denote the position of the cell in the computational grid.

4.2.1 Excitation of 3D FDTD model

Research interested in this thesis is involving for the electromagnetic scattering from rough fracture and various fracture aperture sizes. For that reason, implementation of electromagnetic plane wave is appropriate incident field type. The incident plane wave as electromagnetic field type is an advantage for scattering field formulation. Hence, using the incident field as a Gaussian pulse plane wave provides a smooth roll off in frequency content and is simple to implement and provision for arbitrary incidence angle direction [3].

The plane wave source provides the opportunity to simulate an incident wave from a source, located a large distance from the observed object which is the fracture plane in our case, in combination with farfield monitors. For the FDTD numerical simulation, exciting the model with a plane wave source needs several conditions to be satisfied such as the surrounding space should consist of a homogenous material distribution, boundary conditions must be defined at the direction of incidence and other excitation ports must not be located on boundary conditions [4].

The dominant frequency for our polarimetric borehole radar system is 1 MHz up to 200 MHz [5]. This frequency range was used in all FDTD numerical simulations which we will discuss in the following part of this chapter. A Gaussian pulse was used for FDTD simulation. The time waveform of incident plane wave can be observed in Figure 4.2(a) and its frequency spectrum in Figure 4.2(b).

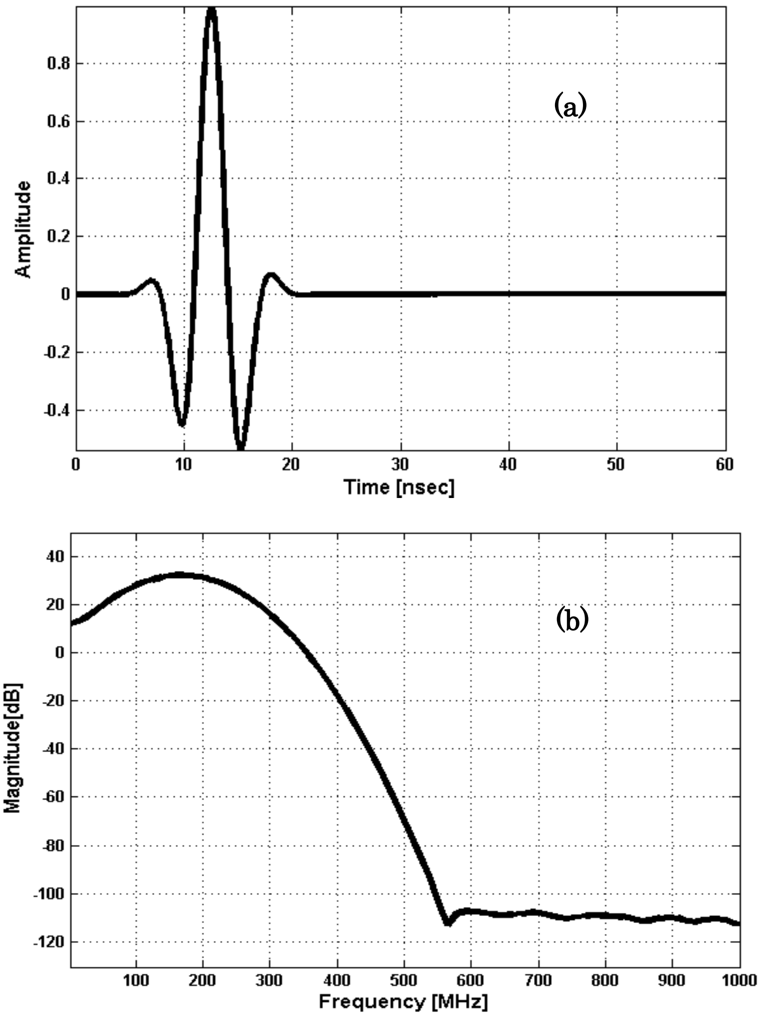

Fig. 4.2: (a) The Gaussian pulse as the source of FDTD (b) Its frequency spectrum.

4.3 Fracture zone description

Fracture zone is a used terminology to describe some discontinuities in the rock. Defining the fracture as a zone is standing for a wide space fracture property and it can be occur as combinations of many tiny aligned fractures. The forms of fracture zone depend on different factors one of them is the rock type. For example, the shearing stress on crystalline rocks cases the presence of tinny discrete fracture sets as shown in Figure (4.3a). These sets have the same direction propagation as the shearing stress and they increase with the load shear stress. The shearing increases the propagation as well as the connectivity of produced tinny fracture sets. The occurrence of the fracture zone in nature has close configuration to the form in Figure (4.3d) and Figure (4.3f) which consists of main fracture pass and it has many tiny associated fracture sets. For the sedimentary rocks, the fracture zone is filled with rock fragments, rock matrix, water and air as shown in Figure (4.4b) and it is called heterogeneous fracture zone. For the electromagnetic point of view and the used frequency range of the polarimetric borehole radar, a fracture zone is observed as one object. The electromagnetic reflectivity from the heterogeneous fracture zone has a complicated process due to the filled materials and as the electromagnetic signals cannot propagate through such fractures as well as the backscattered signals from that fracture zone have no frequency dependency. Based on this, the effect of the fracture zone surface is expected to be the main parameter for characterizing that fractures and the fracture width has no effect in this case. However, I proposed the fracture zone in the FDTD simulations as homogenous water filled fracture. The electromagnetic reflectivity from homogenous fracture models shows frequency dependency process and both the fracture roughness and width parameters will affect the backscattered electromagnetic signals.

The configuration of the fracture zone in Figure (4.3f) shows a tiny associated fracture set distributions to the main fracture pass. These tiny associated fractures are distributed either parallel or having a certain angle to the main fracture pass and the fluctuation of distributions for that tiny fracture sets is an index for the hydraulic connectivity of the fracture. The distribution variations are observed with the electromagnetic signals as surface variations or in other words surface roughness change. For that reason, I proposed the change of the fracture roughness to be indirect index for define the fracture hydraulic property and this feature can be measured with the polarimetirc borehole radar system as I explained it in chapter2.

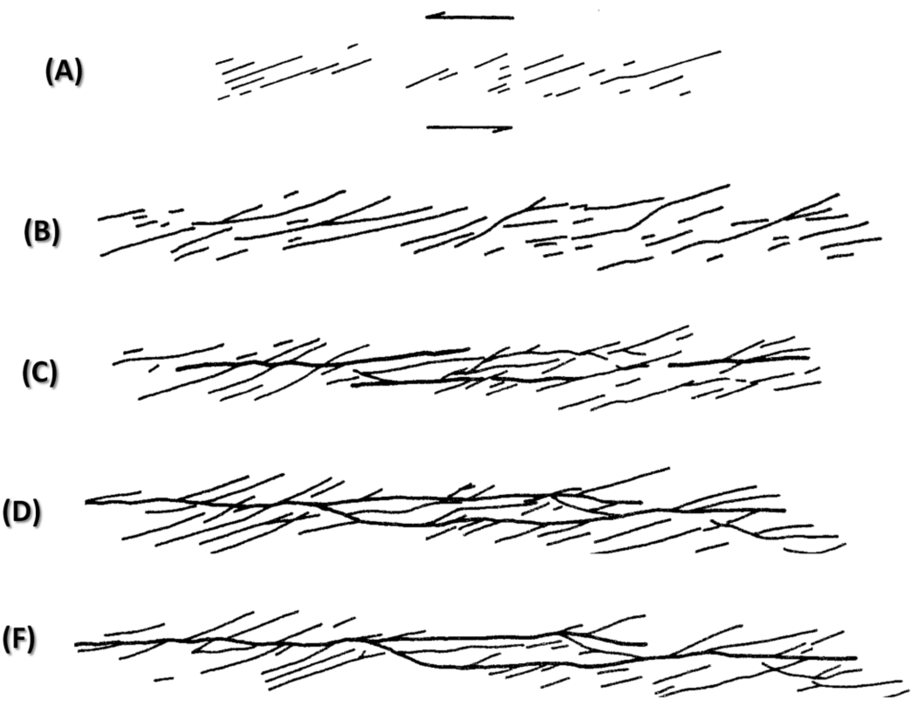

Fig. 4.3: The creation of fracture zone due to shearing stress: (A), (B), (C), (D) and (F) the progress stages successively.

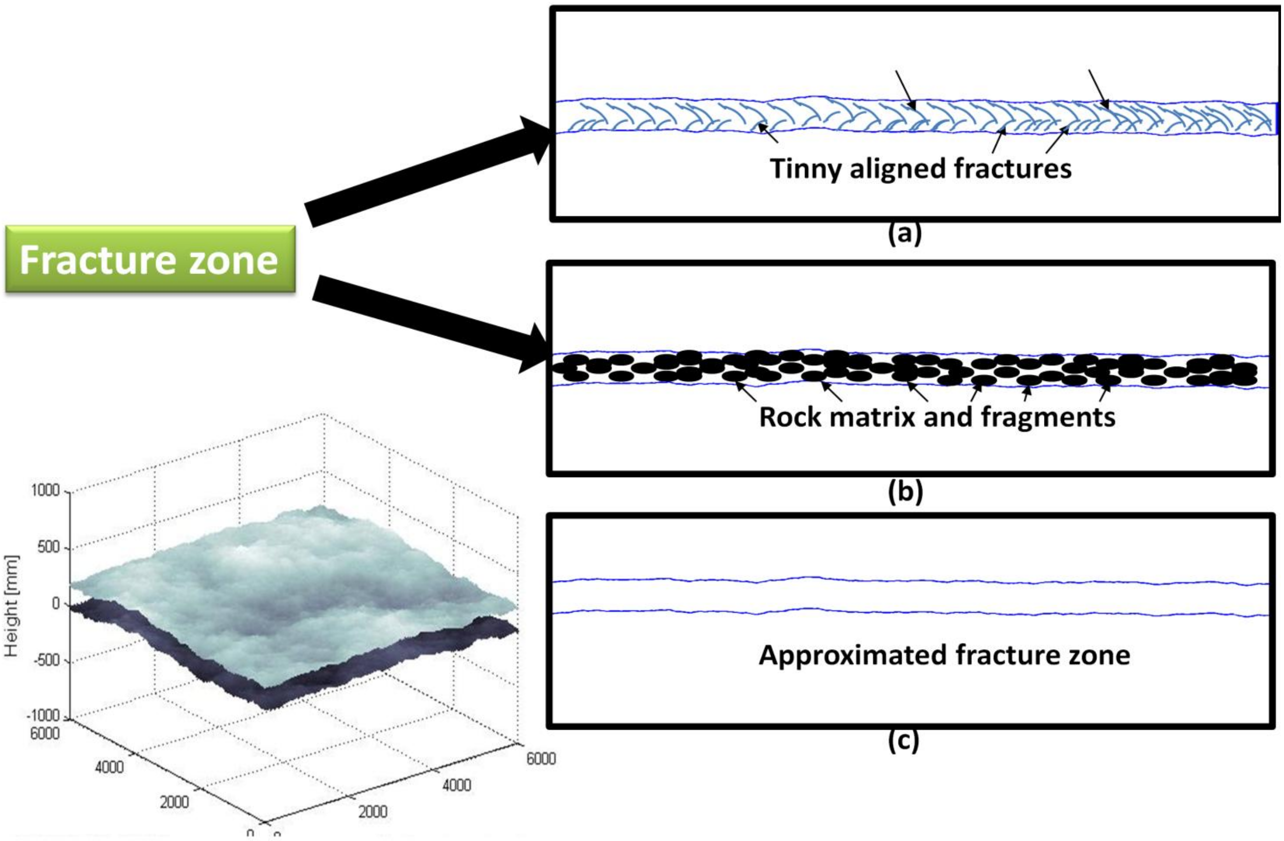

Fig. 4.4: (a) and (b) the representation of fracture zones in reality. (c) Fracture zone approximation.

4.4 FDTD numerical simulation of fracture model

A commercial software CST MICROWAVE STUDIO® was used as FDTD simulator for observing the electromagnetic scattering from a determined fractal fracture. Table 4.1 shows the numerical simulation parameters for a 6-meter fracture model with Gaussian pulse as electromagnetic source. This model was simulated with operating frequency from 1 MHz up to 200 MHz; we also considered the model to have two materials. The first one has relative permittivity 9 that represents the rock material while the second one has permittivity 81 (since we considered the fracture as fracture zone with water filled). The electromagnetic scattering occurs related to fracture roughness parameter and the fracture model is shown in Figure 4.5. In addition, this figure illustrates a generated fracture for the FDTD modeling of calculated different fracture models.

Table 4.1: FDTD numerical simulation parameters

Model size	6mx6mx6m
Source	Gaussian pulse
EM incident type	Plane wave
Frequency range	1 MHz – 200 MHz
Permittivity of mediums	Rock medium 9 Fracture medium 81
Absorbing boundary condition	PML

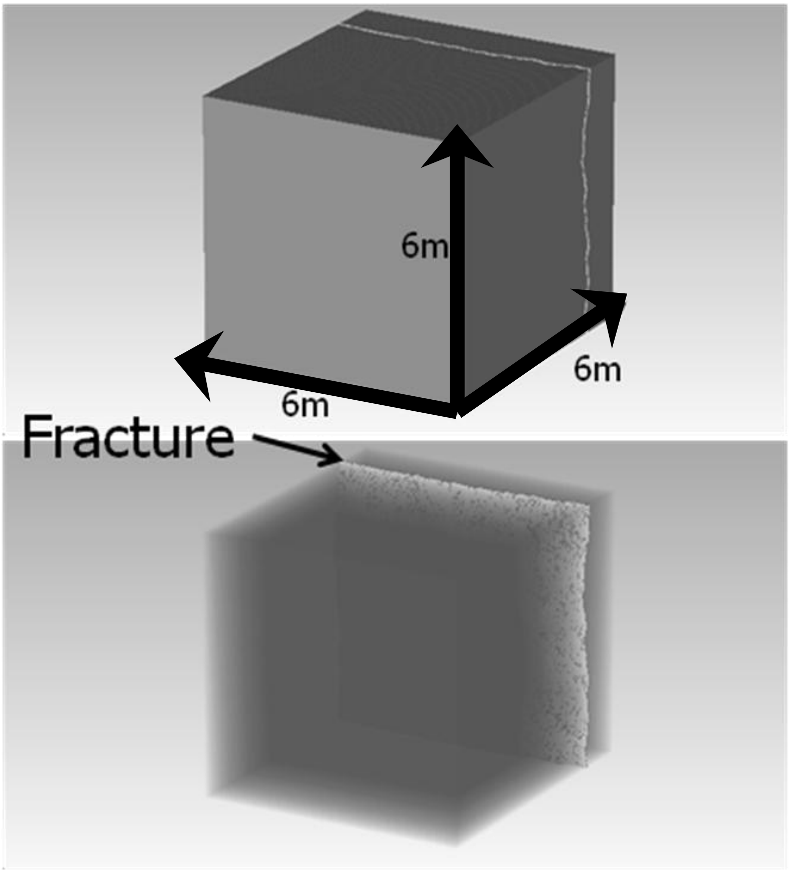

Fig. 4.5: 6x6x6 meters FDTD model of a homogenous and water filled fracture.

4.4.1 Fracture roughness parameter

The study of fracture roughness effect on electromagnetic waves was done in this research and I examined the electromagnetic backscattering from different rough fracture models. The fracture roughness was varied according to previously mentioned parameter in Chapter 3, which is the proportional constant parameter (*C*) in the Equations 3.1 and 3.3. Furthermore, I modeled the fracture to be filled with one phase fluid and the surrounding materials as crystalline rock with dielectric constant of 9 as shown in Figure 4.6. The power spectral density of these generated models can be seen in Figure 4.7.

The observed backscattered EM signals from rough fractures include high amplitude component in the waveform. It is related to the direct-wave between the incident plane wave (transmitted antenna as for borehole radar case) and the observing probes (receiving antenna). The highest backscattered amplitude is due to the reflection from the closest point of the upper fracture plane to the observing probe. Besides, the reflection from the lower fracture plane surface, these two reflections are superimposed on each other to form a composite signal. The detailed electromagnetic reflectivity process from the flat fracture is described in Appendix A. The scattering from farther points of the upper fracture plane has low amplitude component compared to the direct scattering from the nearest part of fracture surface. This process is continuing for observing the reflection from the whole fracture surface until signal is completely decayed as shown for the time waveform in Figure 4.8. The direct wave

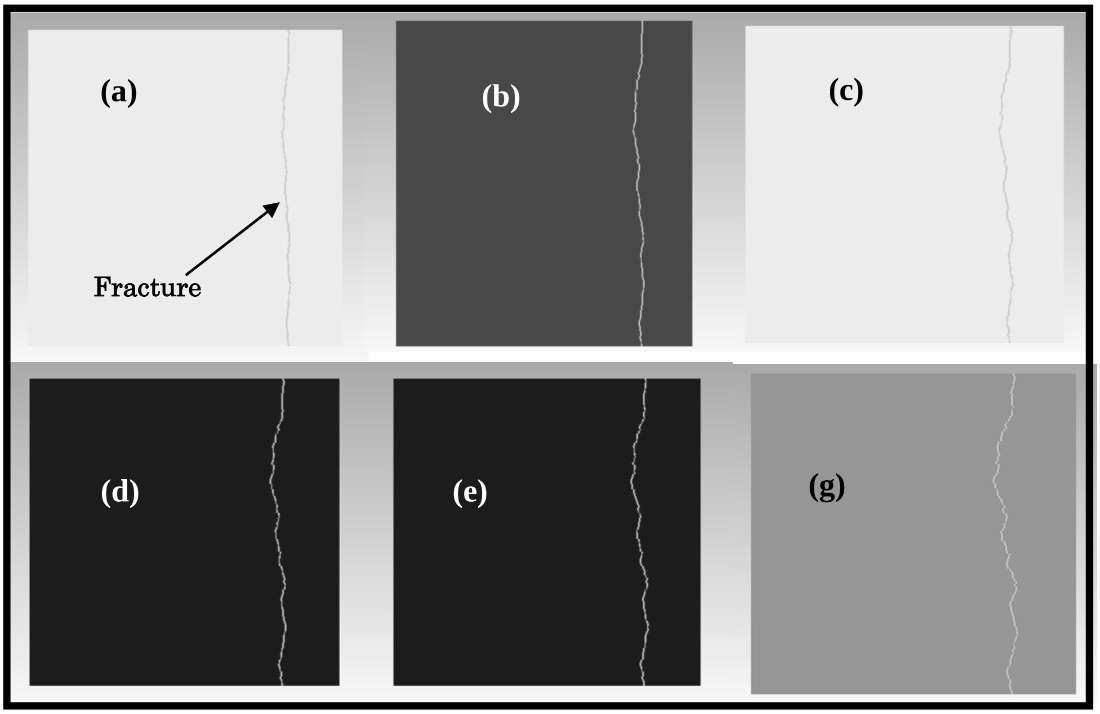

Fig. 4.6: FDTD modeling of different fracture roughness (a) 43, (b) 61, (c) 75, (d) 86, (e) 96 and (g) 129 mm RMS heights. respectively.

is removed by applying time gating and only scattering from rough fracture is kept.

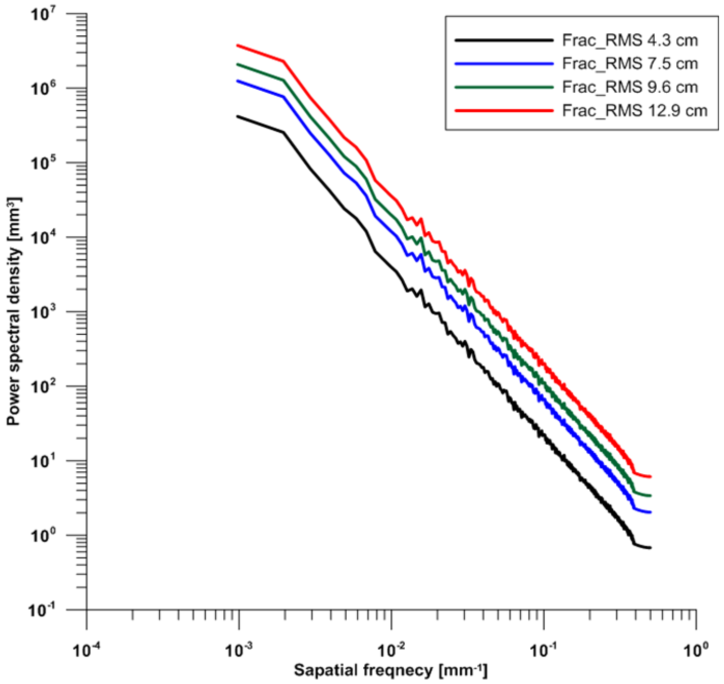

Fig. 4.7: Power spectral density for simulated fracture models.

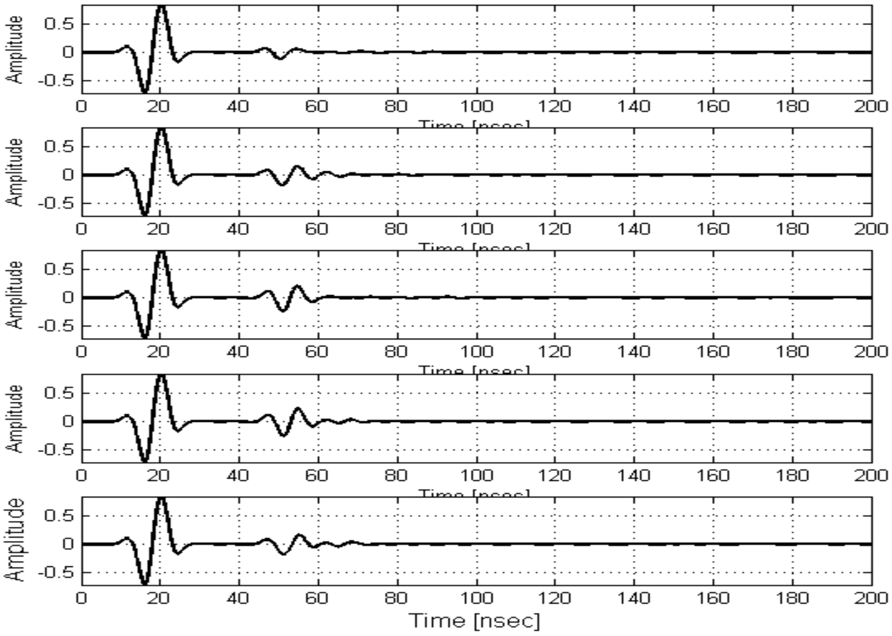

Fig. 4.8: Backscattered EM signals from rough fracture model with 96 mm RMS height at different aligned observing points parallel to it.

4.4.2 Fracture content

The content of fracture is one of the important factors that the backscattered radar signal depends on. Fractures can have one phase fluid such as air, oil and water or sometimes it has two-phase composites such as air- water, which can be the case for groundwater presence beneath fractured rocks, water-oil and air-oil. In this research work, I focused on the study of one phase fluid which is water type only. On the other hand, an air and oil filled fracture was briefly examined their effect on the electromagnetic reflectivity.

Modeled fractures were assumed to be fracture zones that in real case contain inhomogeneous materials. For simplification, a homogeneous filled material fractures were used. The dielectric permittivity ratio for air filled fracture will be 9:1. But for the water filled fracture it is 9:81 and for the oil filled fracture it will be 9:5. The reflection from the same geometry of rough fracture is highly affected by the fracture fluid content as it can be seen in Figure 4.9. The highest backscattered signal is from the water filled fracture. On the other hand, the lowest backscattered signal is from oil filled fracture. These results occur because the reflection coefficient for the filled water fracture is the highest among the air and oil filled fractures.

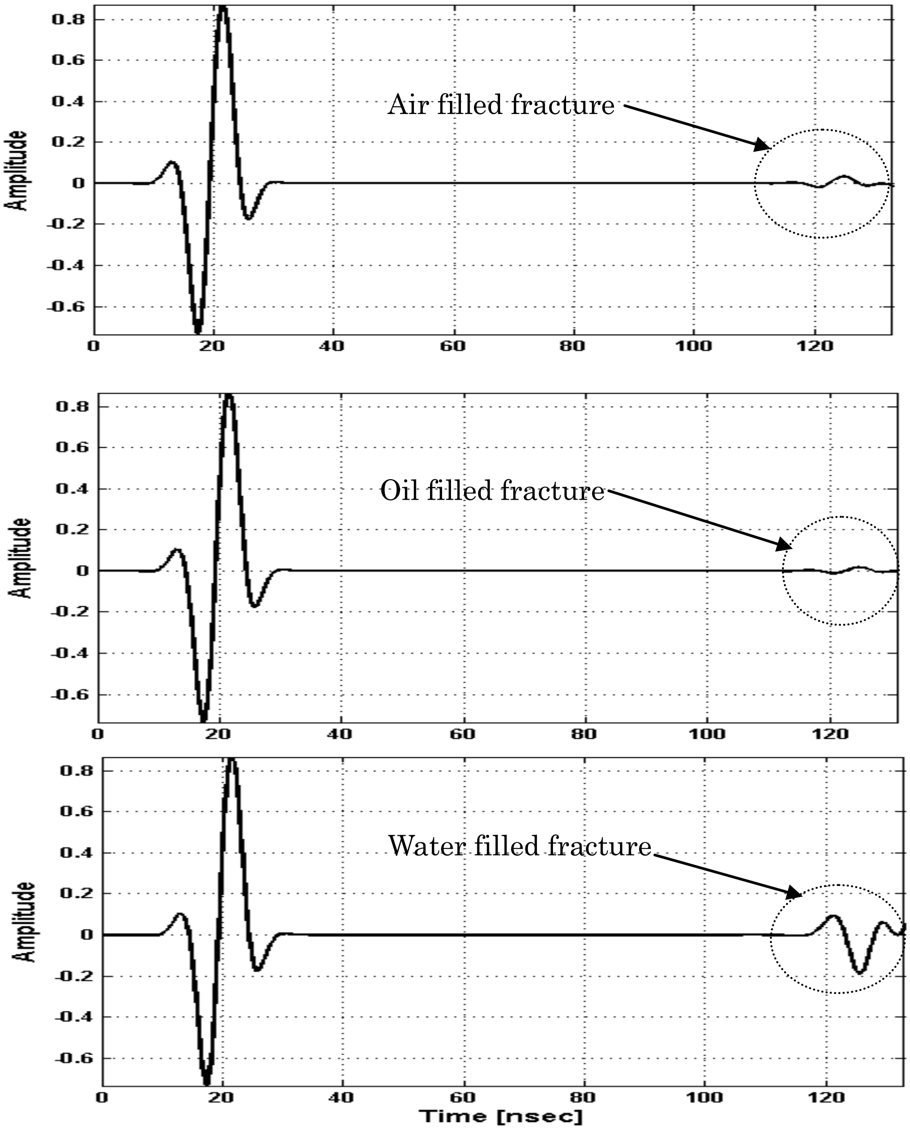

Fig.4.9: EM reflectivity from the same rough fracture with different fracture content (air or oil or water).

4.5 Full polarimetric EM Simulation with a rough fracture

The study of the scattering of electromagnetic waves for characterizing and examining the geometry of objects was initiated in the radar remote sensing field. Hence, a lot of information about the illuminated targets by radar waves can be obtained depending on the depolarization of backscattered EM signals. For full polarimetric borehole radar, we use the advantage of full polarization EM measurements in order to obtain more information about irregular geometric targets such as subsurface fractures. We have already obtained good results by using full polarimetric borehole radar system [6]. But, these results need the validation and to evaluate its reliability. This urged us to use the polarimetric approach for the full polarimtery FDTD modeling technique of known fractal fractures, which we have discussed in chapter 3.

Table 4.2 pointed out the simulation parameters that were used for the numerical simulations. The plane wave was used as the source type and we could obtain the full polarization states (VV, VH, HH and HV). VV stands for the vertically polarized transmitted plane wave and the measured vertically polarized electrical field. That is implementing the incident plane wave to be vertically linear polarized electric field and horizontal one enable us to measure the vertical polarized scattered (VV, HV) fields and horizontal ones (VH, HH) according to the polarization states of the electric field. Figure 4.10 shows the configuration of these polarization states.

Table 4.2: Full polarimetry EM FDTD simulation of fracture models

Model size	6mx6mx6m
EM Source and Source type	Gaussian pulse -Plane wave
Frequency range	1 MHz – 200 MHz
Polarization states	VV-VH-HH-HV
Mediums permittivity	first medium 9 second medium 81
Fracture roughness	43-61-75-86-96 and 129 mm

I calculated reflected signals for fracture with various roughness (43 mm, 61 mm, 75 mm, 86 mm, 96 mm and 129 mm) and I observed that the cross polarization components are sensitive to the roughness change of the fracture models. This conclusion has important meaning related the ability of polarimetric information to determine subsurface fractures characteristics. Hence, the cross polarized (VH and HV) backscattered EM signals strength is increasing with fracture roughness property. Comparing these results of rough fracture model with flat one having the same width showed the cross polarization components (VH and HV) of flat fracture are zero as can be seen in Figure 4.11. This conclusion shows how effect the electromagnetic polarization information can differentiate various fractures in subsurface qualitatively related to electromagnetic backscattering from rough fractures.

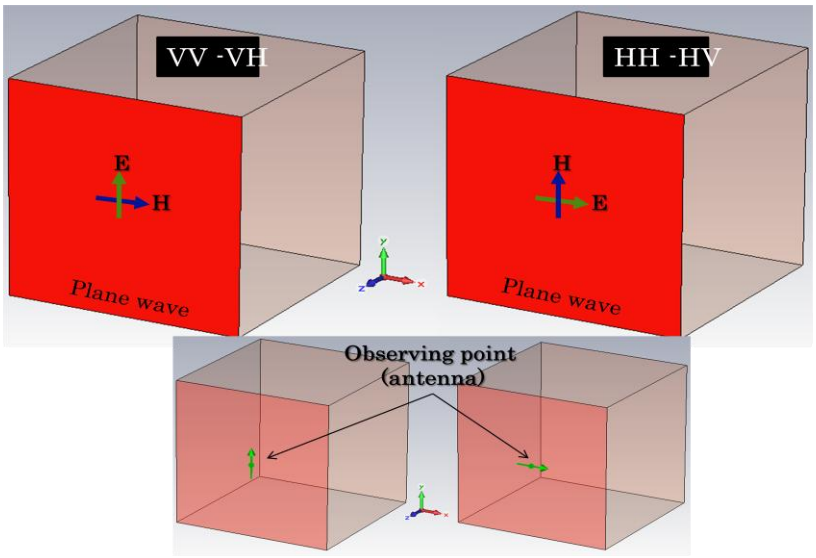

Fig.4.10: Configuration of polarization states VV, HH, VH and HV of incidence plane waves and observing points.

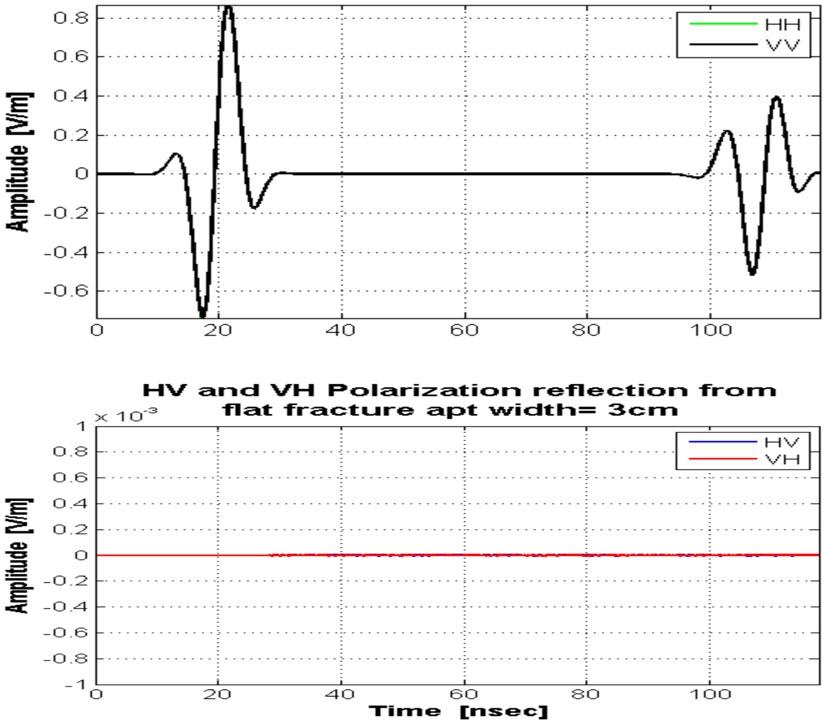

Fig.4.11: Polarization reflection states of VV, HH, VH and HV components from a flat fracture calculated by FDTD.

4.6 EM mean power scattering from fracture

4.6.1 Mean power scattering from fracture zone

The mean power scattering matrix approach was proposed for subsurface fracture characterization and classification with the full polarimetric borehole radar by Sato et al [7], [8] and [9]. This approach, as one of the first radar polarimetric analysis techniques, produced very straightforward qualitative fracture characterization and classification. The mean power scattering matrix is obtained by taking the power summation of each element of full polarimetric component in the time domain signal as shown in Equation 4.7.

$$P=\begin{pmatrix} P_{HH} & P_{HV} \\ P_{VH} & P_{VV} \end{pmatrix}=\begin{pmatrix} \int_{l1}^{l2}\int_{t1}^{t2} S_{HH}^{2}\,dtdl & \int_{l1}^{l2}\int_{t1}^{t2} S_{HV}^{2}\,dtdl \\ \int_{l1}^{l2}\int_{t1}^{t2} S_{VH}^{2}\,dtdl & \int_{l1}^{l2}\int_{t1}^{t2} S_{VV}^{2}\,dtdl \end{pmatrix} \tag{4.7}$$

In Equation 4.7, the terms S_{HH}, S_{HV}, S_{VH} and S_{VV} denote amplitude intensities of four different polarization states, which we have discussed in the previous part, in the time domain. The integration of power is taken in a window of the time-depth domain, which shows the isolated reflection signals corresponding to different subsurface fractures. By applying the frequency-wave number (F-K) filter, we can separate the upper part and the lower part of the V-shaped train of a reflected signal corresponding to some specific fractures.

Figure 4.12 shows the mean power scattering matrices for the studied nine fractures for FSE1 borehole in Mirror Lake, New Hampshire, USA. The EM backscattered signals from rough fractures were obtained in time domain after removing the direct wave between the source and receiver by using time gating. The summation of the power of EM scattering for every polarization states is calculated to estimate the mean power scattering matrix for a certain fracture. We can observe that the fractures at 42, 40.25, and 47.8 m have much stronger cross-polarized components than all other fractures, while the fractures at 24.75, 28.5, and 60m have weaker cross-polarized components. Different roughness of fracture surfaces is conjectured to cause the difference between co-polarized and cross-polarized scattering power: relatively smooth fracture surfaces produce strong co-polarized power and thinner apertures, while rough fractures as well as thicker ones produce strong cross-polarized power.

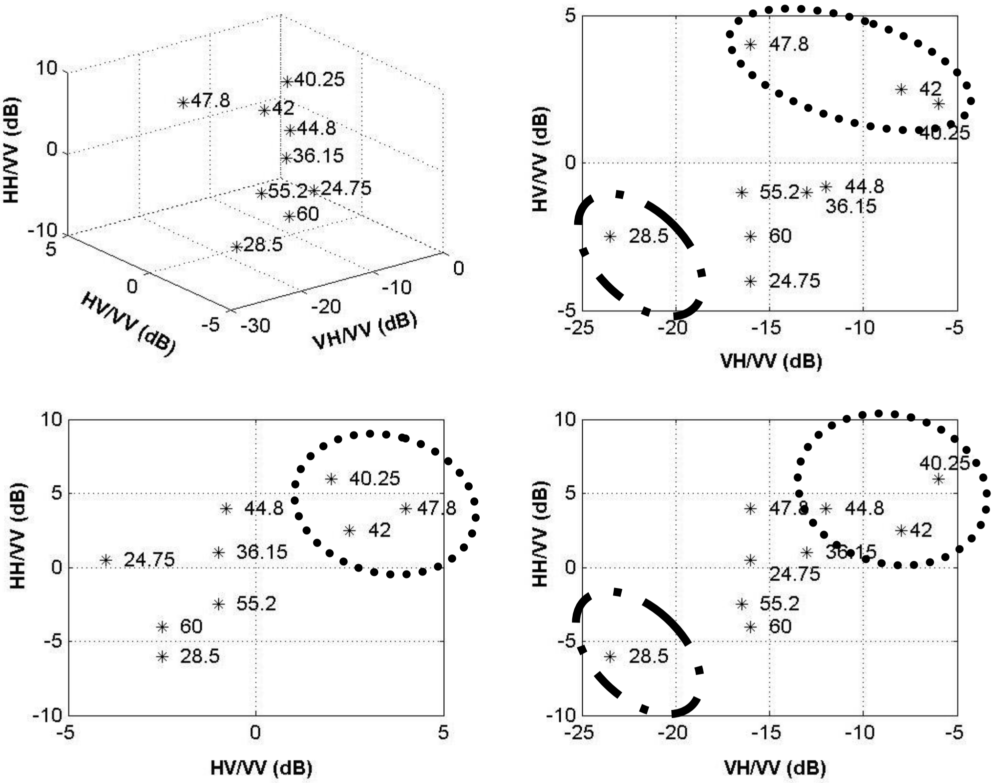

Fig. 4.12: Mean power scattering matrices of subsurface fractures, FSE1 borehole, Mirror Lake, USA. The numbers indicate the fracture zone depth.

This conclusion for the measured full polarimetric dataset and its explanation related to the meaning of mean power scattering matrix for fracture classification should be validated by using a forward model. For that reason, I have analyzed the full polarimetric simulated data for created different rough fracture model as shown before in Table 4.2. I kept all generated fracture models to be homogenous water filled fractures. Borehole TV logging for some boreholes at Mirror Lake fracture test site have shown that the fracture zones, which intersect the borehole axis, have various widths [10]. Hence, this real fracture information can be used as guidance for defining the fracture zone width for the simulated fracture models.

The mean power scattering matrix of simulation result for 4.3 cm, 6.1 cm, 7.5 cm, 8.6 cm, 9.6 cm and 12.9 cm fracture roughness models can be seen in Figure 4.13. The cross polarization component (VH and HV) show significant change with respect to fracture roughness parameter, they show almost linear relationship between the fracture roughness changing and the obtained cross-polarization components as illustrated in Figure 4.14. The possible reason for those results and its liner variation of cross polarization with fracture roughness increasing is that the depolarization of backscattered signal is increasing with fracture roughness property. On the other hand, the co-polarization component (VV and HH) have no variation at all with the increase of fracture roughness. These FDTD simulation results validated and confirmed the proposed analysis of measured data for FSE1 borehole dataset and demonstrated the ability of full polarimetric borehole radar system as subsurface sensing tool for characterizing subsurface fractures. More concrete polarimetric analysis will be further examined and shown in the next chapter based on the eigenvector decomposition.

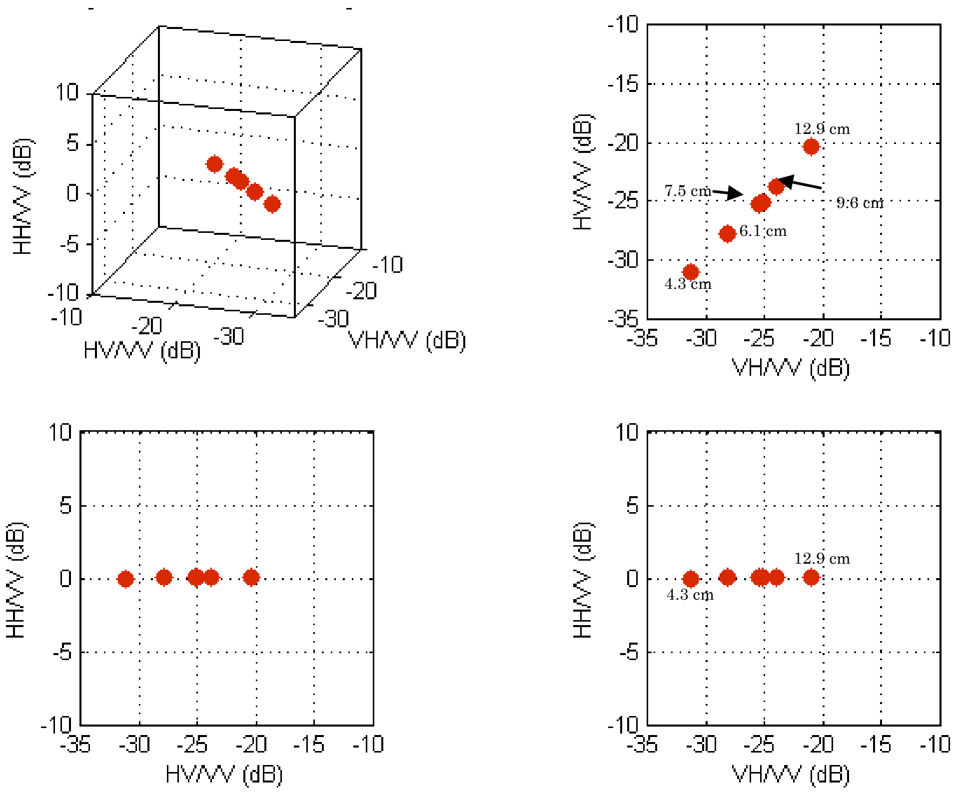

Fig.4. 13: Mean power scattering matrix for simulated different rough fracture models (43,61, 75,86, 96 and 129 mm) rms.

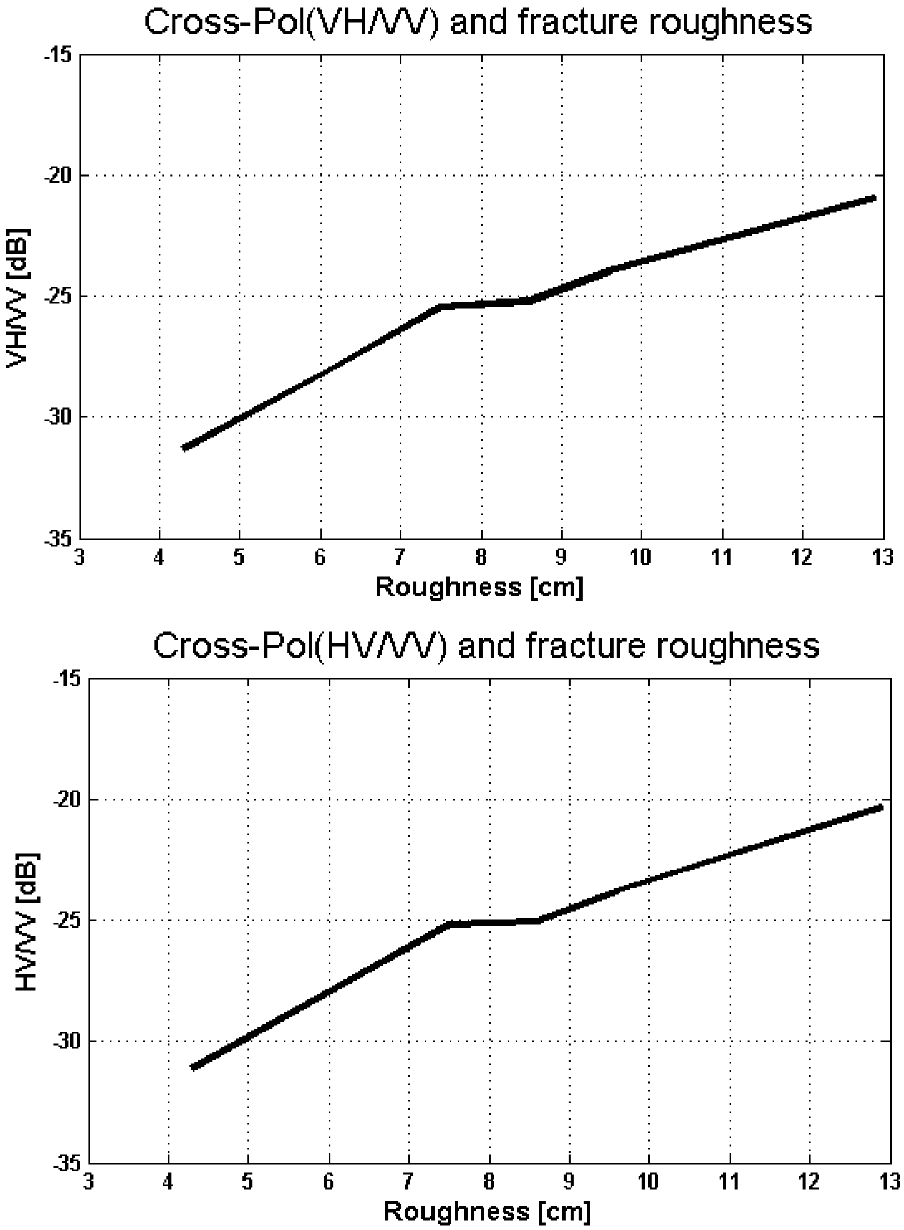

Fig.4. 14: The variation of cross-polarization components (VH and HV) with fracture roughness.

4.6.2 Mean power scattering from thin fracture

To generalize the reliability of using the mean power scattering approach for determining subsurface fracture characterization, I simulated the electromagnetic scattering from a different fracture aperture sizes with varied roughness (7mm, 15mm, 20mm and 33mm RMS heights) having a thin fracture thickness compare to fracture zone that described in section 4.6.1. The variation of fracture roughness for these thin fractures generate different mean aperture sizes and it is related to the roughness change between upper and lower fracture surfaces as described in chapter 3. The mean aperture of thin fracture model is controlled by the fracture roughness where for very smooth thin fracture the mean aperture has almost zero width (close fracture) up to 1mm. However, for the rough thin fracture the mean aperture has meaningful aperture width (higher than zero aperture width up to 5mm aperture). Figure 4.15 represents various fracture models having different roughness which generate different mean aperture models and their aperture varies from 0 up to 5mm.

I observed the full polarized electromagnetic backscattering from thin fracture models. The mean power scattering matrix was estimated for these thin fractures and the results can be seen in Figure 4.16. The results that I obtained from thin fracture models and their mean power scattering analysis showed the same conclusion as for the fracture zone. The cross polarization components vary also proportionally with fracture roughness increasing of thin fractures. But, the powers of backscattered signals of the thin fractures are low compare to the ones of fracture zones. For the smooth thin fracture case, 7mm RMS fracture model, the aperture varies between 0 thickness (close fracture) to open aperture with around 1mm aperture width and the backscattered from this fracture is not strong compare to the rougher one with 33 mm RMS height.

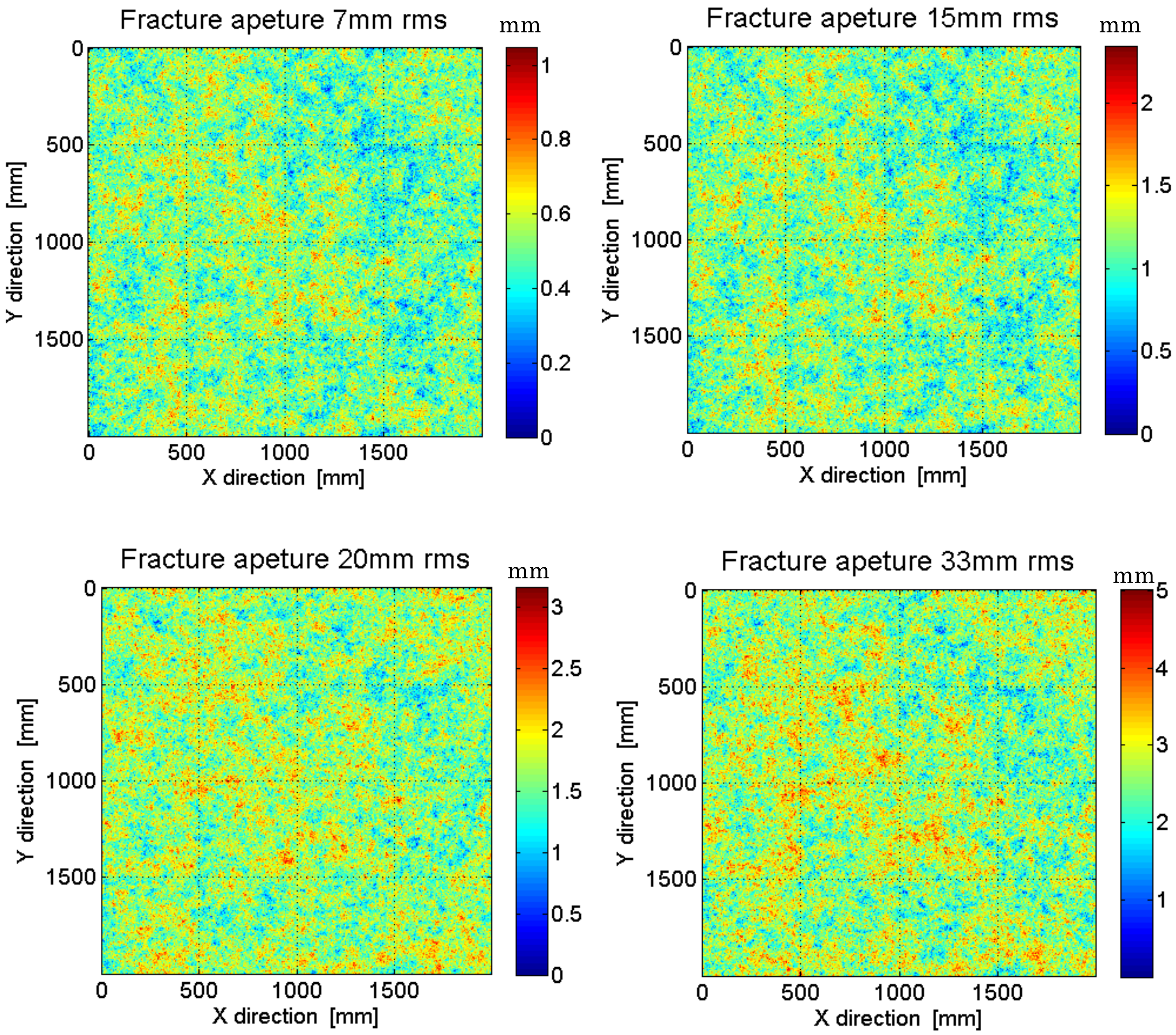

Fig.4.15: The fracture aperture distributions for various rough fracture models (7mm, 15mm, 20mm and 33mm RMS heights).

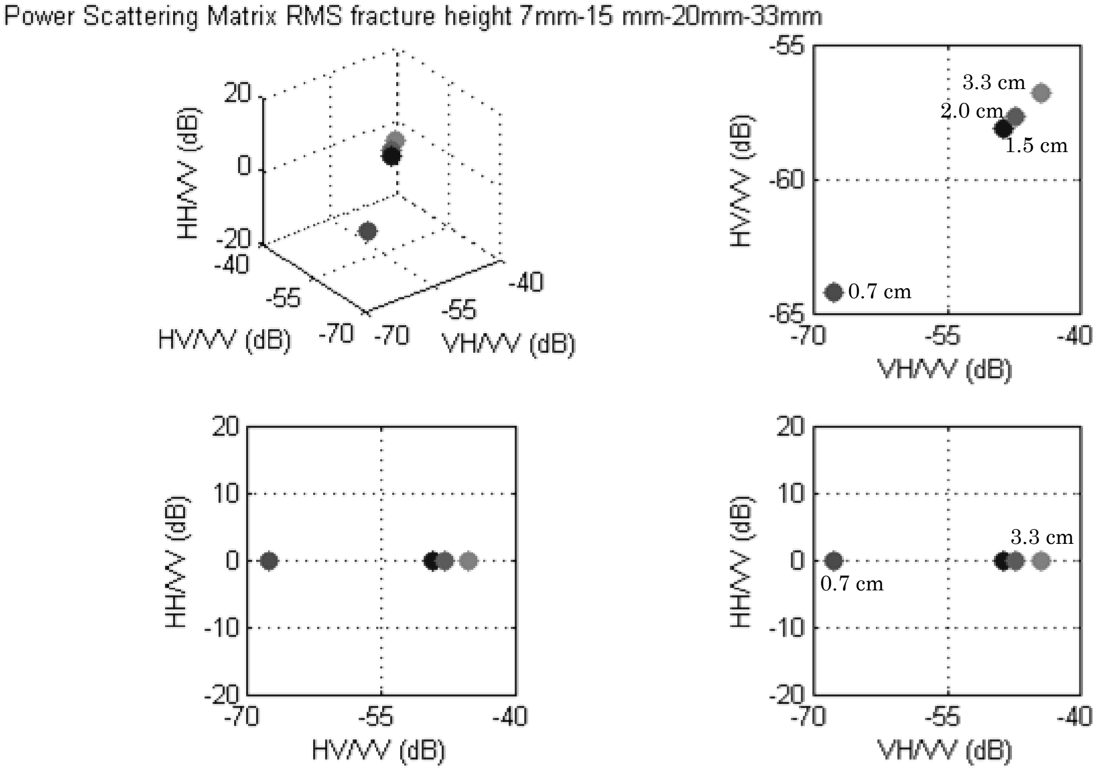

Fig.4. 16: Mean power scattering matrix for simulated various thin rough fracture models with 7, 15, 20 and 33 mm RMS heights.

4.7 Summary

In this chapter, I have shown FDTD simulation method and role of the Maxwell’s equations for addressing out the numerical solutions. In addition to that, I explained the excitation of FDTD fracture models.

The use of the rough fracture model as a target in an FDTD simulator was done and I demonstrated the effect of fracture roughness upon the backscattered electromagnetic waves. The fracture material contents were examined when it contains water or air or oil. In each case, I observed the behavior of reflected signals and how far the fracture content varies the electromagnetic scattering. The full polarimetric FDTD simulation data have been calculated for different rough fracture models and the validation of the measured data and its mean power scattering matrix analysis for FSE1 borehole has been done. Thus, the full polarimetric backscattered electromagnetic wave shows proportional change in amplitude of cross polarization (VH and HV) components depending on the fracture roughness. To emphasize the polarimertic analysis of the mean power scattering matrix approach, various thin fracture models have been simulated with varied fracture apertures. The variation of the cross polarization components of varied fracture aperture models showed the same conclusion as fracture zone case. With the mean power scattering matrix, the full polarimetric borehole radar dataset can be used to estimate the subsurface fracture characteristics qualitatively while quantitative analysis will be described in next chapter.

Chapter 5

Subsurface Fractures Characterization

5.1 Introduction

In Chapter 4, the role of mean power scattering matrix estimation for deriving qualitatively subsurface characterizations of the measured full polarimertic borehole datasets was shown. In addition to this, the reliability of fracture characterization technique has been validated based on forward modeling of FDTD simulation of rough fractures. Further descriptors of fracture characterization are still required which can be more concrete methods and verified in simulation test studies. Synthetic Aperture Radar (SAR) remote sensing introduced us this connection.

In Chapter 5, I use an alternative method which is the eigenvector based decomposition or *H*-*A*-alpha decomposition method of Shine Cloude and Eric Pottier [1], [2]. Nowadays almost classical polarimetric decomposition method, the eigenvector based decomposition approach has been increasingly employed for characterizing the scattering properties of reciprocal media, symmetric scattering matrix scenarios [3].The entropy-anisotropy-alpha decomposition is based on the Kennaugh matrix or equivalently the covariance matrix approaches. Three important physical features can be derived from this decomposition are entropy, anisotropy and alpha. Where, the entropy estimates the randomness of the scattering process. The anisotropy defines the relation between the second and the third eigenvalues, and is a measure for the difference of the secondary scattering mechanisms. The anisotropy provides complementary information to the entropy and facilitates the interpretation of the surface scatterer. The great advantage of these two parameters arises from the invariance of the eigenvalue problem under unitary transformations: the same surface leads to the same eigenvalues and consequently to the same entropy and anisotropy values independently on the basis used to measure the corresponding scattering matrix [4]. The third one is the alpha parameter, which is a continuous angle between 0 and 90 degrees describing various canonical scattering mechanisms. Therefore, the entropy-anisotropy and alpha parameters are expected to be a powerful classification technique for the full polarimetric borehole radar dataset.

In this chapter, the eigenvector based polarimetric target decomposition developed by Cloude and Pottier will be introduced, and then I will show the simulation results of electromagnetic scattering for varied rough fracture models in addition to different fracture widths, and then I will estimate the three eigenvector based polarimetric parameters for the simulated models. After, constructing the same SAR configuration for the FDTD simulated models. I will apply the same polarimetric decomposition to the measured full polarimetric borehole radar data for providing and recognizing different scattering mechanisms from different subsurface fractures. Describing the expected subsurface characteristics for the measured data based on the electromagnetic forward simulation of determined fracture models. Correlating subsurface fracture characterizations based on polarimetric analysis with subsurface fractures tracer test results.

5.2 Polarimetric analysis of simulated data

5.2.1 H-A-alpha description

The three eigenvector based parameters (entropy H, anisotropy A and alpha α) can be estimated from the coherency matrix $\boldsymbol{T_3}$. Where, this matrix can cover a wide range of scattering mechanisms. It was introduced by Shane Cloude and Eric Pottier. Where, the coherency matrix $\boldsymbol{T_3}$ is a hermitian, positive, and semi-definite matrix, it can always be diagonalized using unitary similarity transformations. As a result, the coherency matrix $\boldsymbol{T_3}$ can be rewritten as

$$T_3 = [U_3][\Sigma][U_3]^{-1} = [U_3]\begin{bmatrix} \lambda_1 & 0 & 0 \\ 0 & \lambda_2 & 0 \\ 0 & 0 & \lambda_3 \end{bmatrix}[U_3]^{-1} \qquad (5.1)$$

$$[U_3] = [\boldsymbol{e_1}, \boldsymbol{e_2}, \boldsymbol{e_3}]^{\mathrm{T}} \qquad (5.2)$$

where $[\Sigma]$ is the diagonal eigenvalues matrix of $\boldsymbol{T_3}$ with $\lambda_1 \geq \lambda_2 \geq \lambda_3 \geq 0$ and it is the real nonnegative values, and $[U_3]$ is a unitary matrix whose elements correspond to the orthonormal eigenvectors $\boldsymbol{e_1}, \boldsymbol{e_2}, \boldsymbol{e_3}$ of the coherency matrix $\boldsymbol{T_3}$.

By this way, the three orthonormal eigenvectors $\boldsymbol{e_1}, \boldsymbol{e_2}, \boldsymbol{e_3}$ of the coherency matrix $\boldsymbol{T_3}$ can be expressed as

$$\begin{aligned} e_1 &= e^{j\theta_1}[\cos\alpha_1 \quad \sin\alpha_1\cos\beta_1 e^{j\delta_1} \quad \sin\alpha_1\sin\beta_1 e^{j\gamma_1}]^T \\ e_2 &= e^{j\theta_2}[\cos\alpha_2 \quad \sin\alpha_2\cos\beta_2 e^{j\delta_2} \quad \sin\alpha_2\sin\beta_2 e^{j\gamma_2}]^T \\ e_3 &= e^{j\theta_3}[\cos\alpha_3 \quad \sin\alpha_3\cos\beta_3 e^{j\delta_3} \quad \sin\alpha_3\sin\beta_3 e^{j\gamma_3}]^T \end{aligned} \qquad (5.3)$$

There are three important physical features arising directly from this decomposition: the first one is the entropy H. This is defined as

$$H = \sum_{i=1}^{3} P_i(-\log_3 P_i), \qquad P_i = \frac{\lambda_i}{\lambda_1 + \lambda_2 + \lambda_3} \qquad (5.4)$$

As for the physical meaning of the entropy H, this parameter provides information about the number of involved scattering processes. If $H = 0$, that denotes a pure deterministic scattering process. The scattering in such pixels ($H = 0$) is dominated by one pure scattering process. In the other extreme case, if $H = 1$, the scattering process corresponds to a pure incoherent random scattering, and it means that all different scattering processes contribute in the same way to the scattering process. The second feature, introduced by Shane Cloude and Eric Pottier is the polarimetric anisotropy *A*, which is defined as

$$A = \frac{\lambda_2 - \lambda_3}{\lambda_2 + \lambda_3} \qquad (5.5)$$

The parameter anisotropy *A* yields the normalized relation between the two minor eigenvalues, namely, the information between the two less dominant scattering mechanisms. For the two extremes of $H = 1$ or $H = 0$, the anisotropy yields no additional information. On the other hand, in the case of low or medium entropy ($\lambda_1 > \lambda_2$, λ_3), the parameter entropy *H* yields no information about the relationship between the two minor eigenvalues λ_2 and λ_3. In that case, the anisotropy *A* contains additional information. A medium entropy means that more than one scattering mechanism contribute to the scattering process, and in this case a high anisotropy states that only the second scattering mechanism is important, while a low anisotropy yields that the third scattering mechanism plays a role expect for the second one.

The third parameter is the polarimetric alpha, and the average alpha $\overline{\alpha}$ which can be calculated as

$$\overline{\alpha} = \sum_{i=1}^{3} P_i \alpha_i \, , \qquad (5.6)$$

The alpha parameter is a continuous angle ranging from 0^o to 90^o, and it represents an internal degree of freedom of the target and can be used to describe the type of scattering mechanism. This parameter can be used to represent a wide variety of different scatters. At $\overline{\alpha} = 0^o$, we obtain an isotropic surface. However, as $\overline{\alpha}$ increases, the surface becomes anisotropic. At $\overline{\alpha} = 45^o$ we have a dipole. If $\overline{\alpha} > 45^o$, then an anisotropic dihedral can be inferred. In the other extreme case of $\overline{\alpha} = 90^o$, the scattering mechanism can be characterized by isotropic even bounce scattering. However, it should be remembered that entropy-anisotropy-alpha decomposition was derived for the open propagation, surface scattering for air space remote sensing and not for the closed polarimetric borehole radar fracture scattering description. For that reason, I used EM simulation to determine the reliability of this technique to be used for analyzing the full polarimetric borehole radar data and this represents the significance of this research work.

5.2.2 Eigenvector based decomposition

In this section, I will discuss the polarimetric analysis for electromagnetic simulation of generated varies rough fractures and different fracture widths. 2D very dense observation plane has been proposed for deriving the three polarimetric parameters (entropy, anisotropy and alpha) for these fracture models. For the obtained data in FDTD simulation, we use normal incidence plane wave with a proposed 2D very dense observation points. The observed EM backscattered at each observation point can be represented as $f(x', y')$. That $x'y'$ is the observation plane.

From the obtained backscattered $f(x', y')$, that represents the measured EM scattered field at each observing point of very dense observation plane for the simulated fracture model, We can extract the scattering matrix [S] as in Equation 5.7 for every cluster data points of the observation plane at each single frequency

$$[S] = \begin{bmatrix} S_{HH} & S_{HV} \\ S_{VH} & S_{VV} \end{bmatrix} \qquad (5.7)$$

Window size was used to derive the coherency matrix T_3 from the cluster observing points. This window can be selected as 3x3, 5x5 or 7x7 and it was moved averaging to estimate the coherency matrix T_3 successively as shown in Figure 5.1.

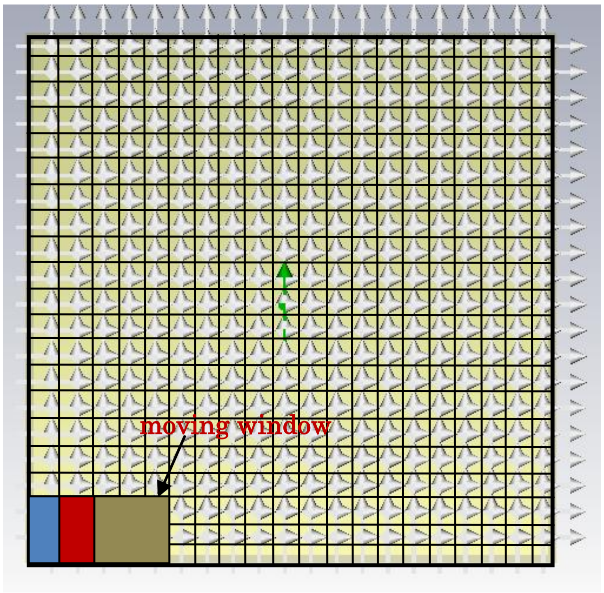

Fig.5.1: Proposed very dense obervation plane of points shows the moving window over to estimate the cohernace matrix.

For detailed explanation about deriving coherency matrix, in frequency domain data we can extract the scattering matrix for every cluster data points at each single frequency. For example at observing point located in the center of the observing plane where X' and Y' positions are $\frac{x'}{2}, \frac{y'}{2}$ coordinates we have $S_{hh}(\frac{x'}{2}, \frac{y'}{2})$ and $S_{hv}(\frac{x'}{2}, \frac{y'}{2})$ for horizontally polarized incident plane wave and $S_{vv}(\frac{x'}{2}, \frac{y'}{2})$ and $S_{vh}(\frac{x'}{2}, \frac{y'}{2})$ for vertically polarized incident plane wave at single frequency. By using 3x3 window size we include the scattering matrixes of the observing points $\sum_{l=0}^{L}\sum_{k=0}^{K} f\,(\frac{x'}{2}+l, \frac{y'}{2}+k)$ and L, K are determining the selected window size (3, 5 or 7). From this window we can estimate the coherency matrix $\boldsymbol{T_3}$ at the center of the observation plane. By repeating this process for every cluster points of the dense grid observing points (over observation plane) we can extract all the scattering matrices and determine the coherency matrix $\boldsymbol{T_3}$. Furthermore, alpha and entropy distributions are derived from coherency matrix $\boldsymbol{T_3}$ as seen in Figure 5.2.

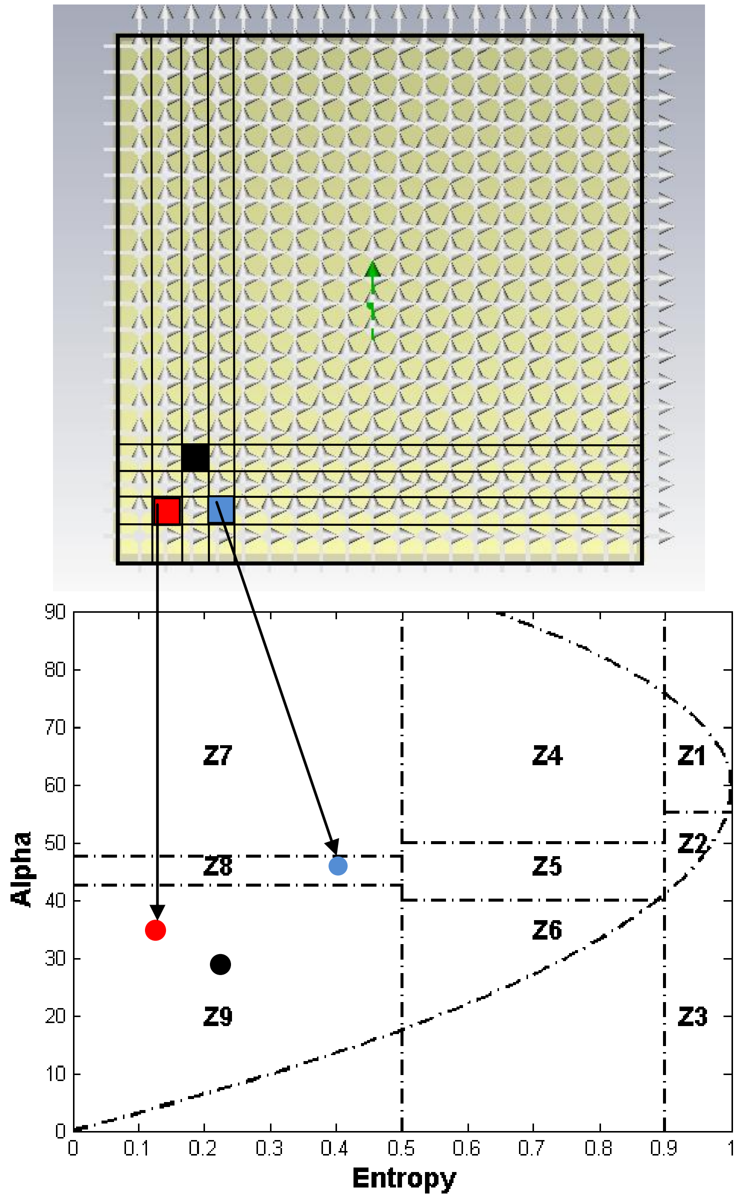

Fig.5.2: Alpha and entropy estimation from FDTD simulation data.

Firstly, the electromagnetic scattering was examined for different fracture surface heights (9.6cm; 12.9cm; 19.2cm and 23.6cm) and the fracture in this case was assumed as a fracture zone. The fracture is proposed to have electrical permittivity 81(we consider the fracture is homogenous and water filled type). The normal incidence plane wave was used as an electromagnetic source type in these simulations with frequency range 1MHz to

200MHz. This is the dominant frequency range of the full polarimetric borehole radar system. The electrical permittivity 9 was used for the rock medium.

Figure 5.3 shows the entropy (*H)* and alpha (α) plane distributions for simulation results of these fracture models at 30MHz frequency. We observe that the entropy (*H)* and alpha (α) distributions increase with the fracture surface height increasing. Thus, entropy (*H*) parameter is very sensitive to the randomness of the fracture surface while alpha (α) shows less sensitivity, compared to entropy, and it estimates the electromagnetic scattering mechanism as described in section 5.2. The explanation for these results related to alpha angle (α) can be as the following: the scattering mechanism from the rough fracture has a dominant volume scattering mechanism which is mostly close to forest case in radar remote sensing. The scattering mechanism varies from surface dominant scattering for smooth fracture surface to volume scattering mechanism for the rougher fracture surfaces. This is the reason that we can observe only surface scattering and volume scattering mechanism for such rough fractures. But, no double bounce scattering is observed where the used frequency range is large compare to the fracture roughness for observing this scattering mechanism. Furthermore, for normal incident plane wave double scattering mechanism cannot be produced easily in this case.

The anisotropy parameter (*A)* depends on the ratio between the second and third eigenvalues which has sensitivity for fracture surface randomness that can be compensatory for the entropy parameter. The entropy parameter when it will be more than 0.7(H>0.7). The determination of the surface conditions cannot be maintained with entropy only and in that case the anisotropy parameter helps for describing fracture roughness depending on the variation between the minor eigenvalue parameters (λ_2, λ_3) or we can say it is compensatory parameter for entropy in this case. This condition can be fulfilled in this research work as we deal with the electromagnetic scattering from rough fractures and for very rough fracture surface anisotropy can derive more information about the fracture surface characteristics as integration with entropy parameter.

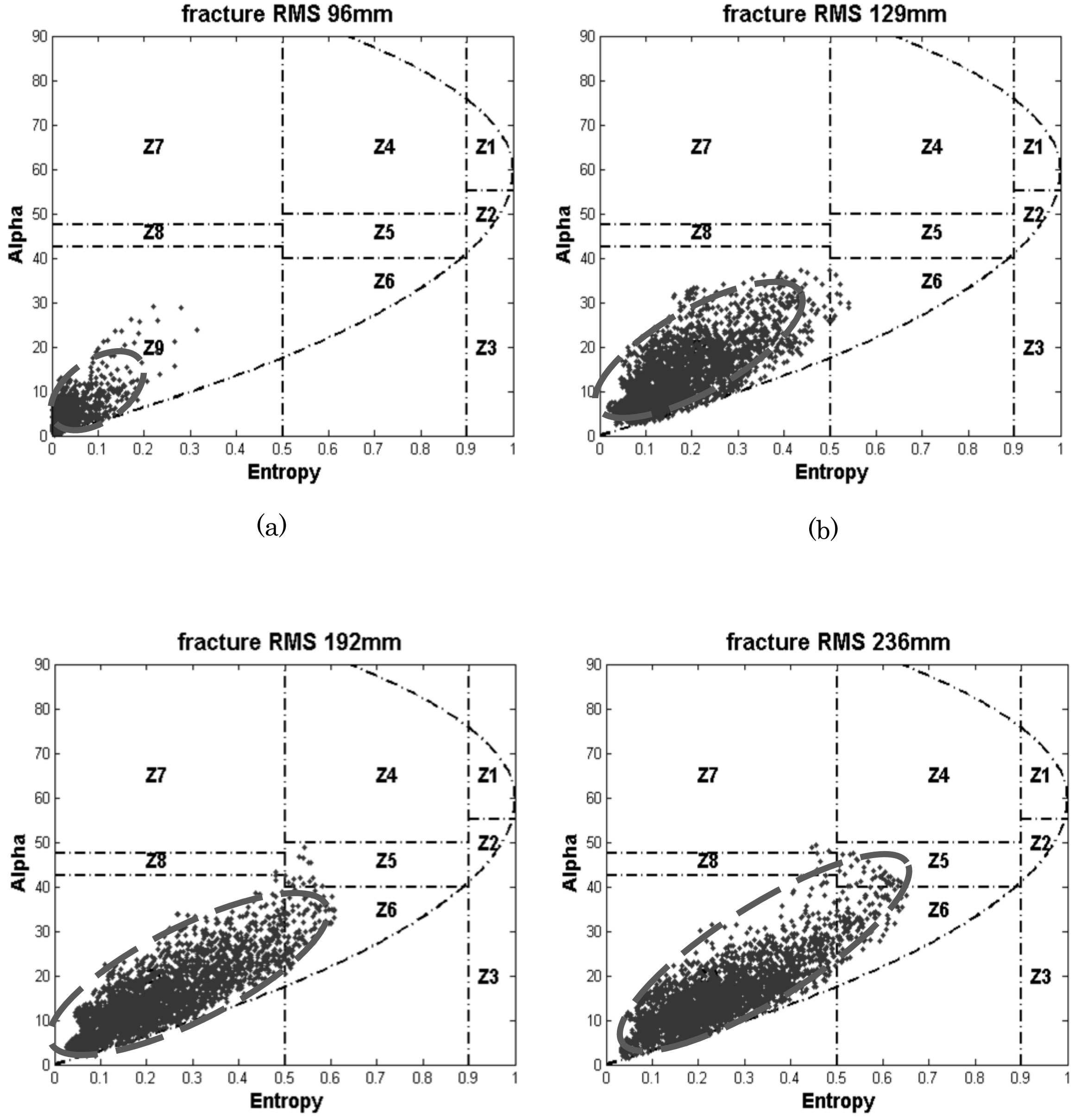

(a) (b)

(c) (d)

Fig.5.3: Entropy-alpha plane distributions for variable fracture fractal models. (a) 9.6 cm RMS height, (b) 12.9 cm RMS height, (c) 19.2 cm RMS height and (d) 23.6 cm RMS height.

The distributions of entropy and anisotropy planes show the changing with different rough fracture models. These results show the reliability of using anisotropy for characterizing the fracture roughness as it showed high value distributions for rougher fractures and low value distributions for smooth fracture models. Thus, introducing the anisotropy parameter revealed more information about the scattering mechanism randomness from fracture roughness as shown in Figure 5.4.

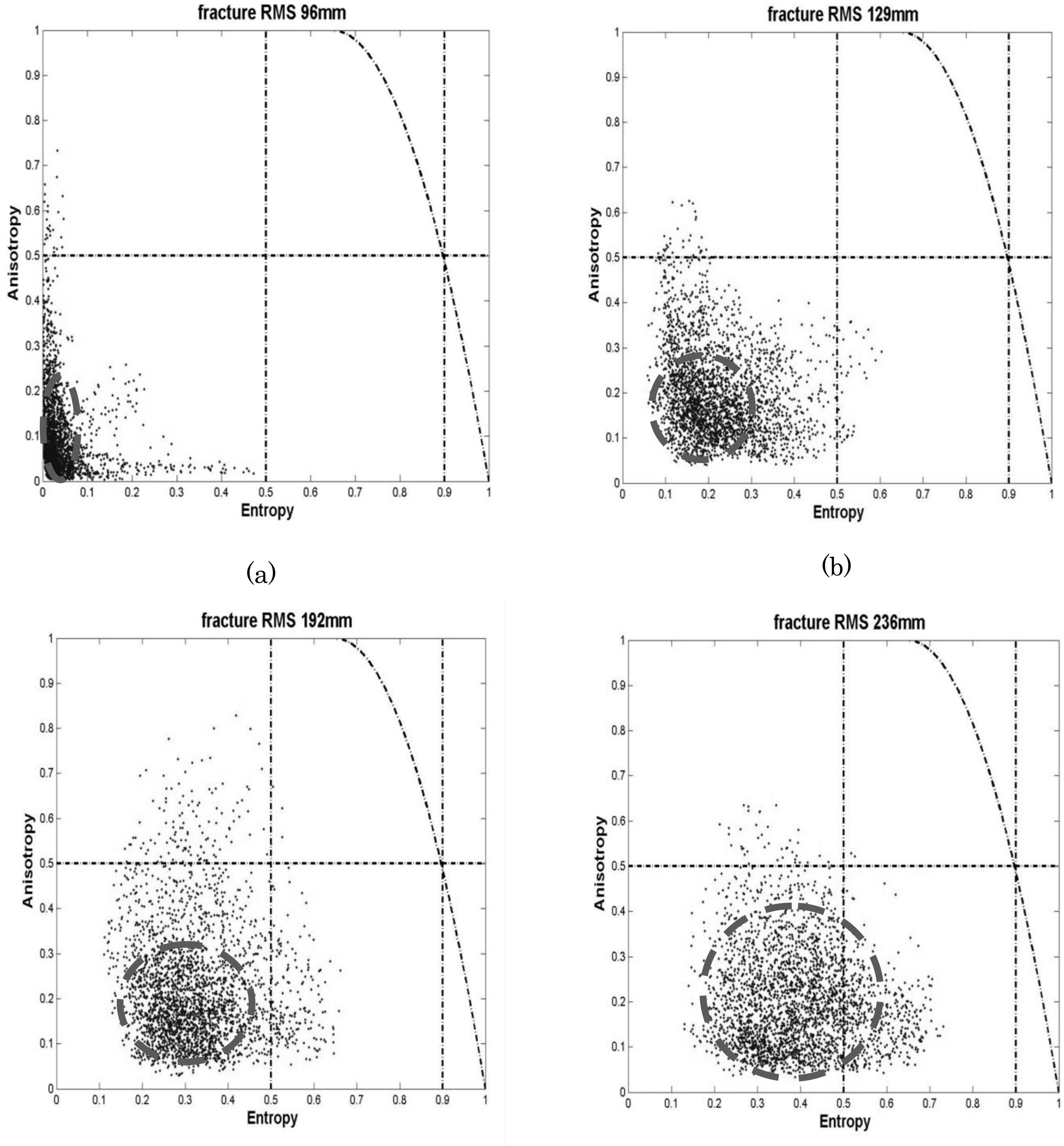

(a)

(b)

(c)

(d)

Fig.5.4: Entropy-anisotropy plane distributions for variable fracture fractal models. (a) 9.6 cm RMS height, (b) 12.9 cm RMS height, (c) 19.2 cm RMS height and (d) 23.6 cm RMS height.

Figure 5.5 shows anisotropy-alpha results after the polarimetric analysis based on eigenvector decomposition for the simulation data and their distributions, the same simulated rough fracture models as the case of entropy–alpha. The distributions of anisotropy-alpha angle vary with fracture roughness model increasing. Hence, for the smooth fracture (9.6cm rms) both of them have very low distributions, surface scattering and low scattering randomness. On the other hand, the anisotropy distributions are increasing but the alpha parameter is slightly changed. The explanation of these results can be as the fellow: the surface scattering mechanism occurs due to electromagnetic scattering from smooth roughness model and volume scattering mechanism is tending to be dominant for the rougher fracture models.

Representations of these three polarimetric parameters (*H*-*A*-alpha) by 3D geometry planes provide a complete view about the response of electromagnetic scattering from various rough fracture models. Furthermore, we can judge correctly the relationship between each parameter and the others. Figure 5.6 illustrated the 3D representations for the three eigenvector parameters. For 9.6 cm rms height fracture model (the smoothest fracture surface), entropy and anisotropy showed low distributions (low scattering mechanism randomness) and alpha provided surface scattering mechanism. For 23.6 cm rms height fracture model (the roughest fracture surface), entropy and anisotropy illustrated high distribution values (high scattering mechanism randomness). Furthermore, alpha showed surface to volume scattering mechanisms.

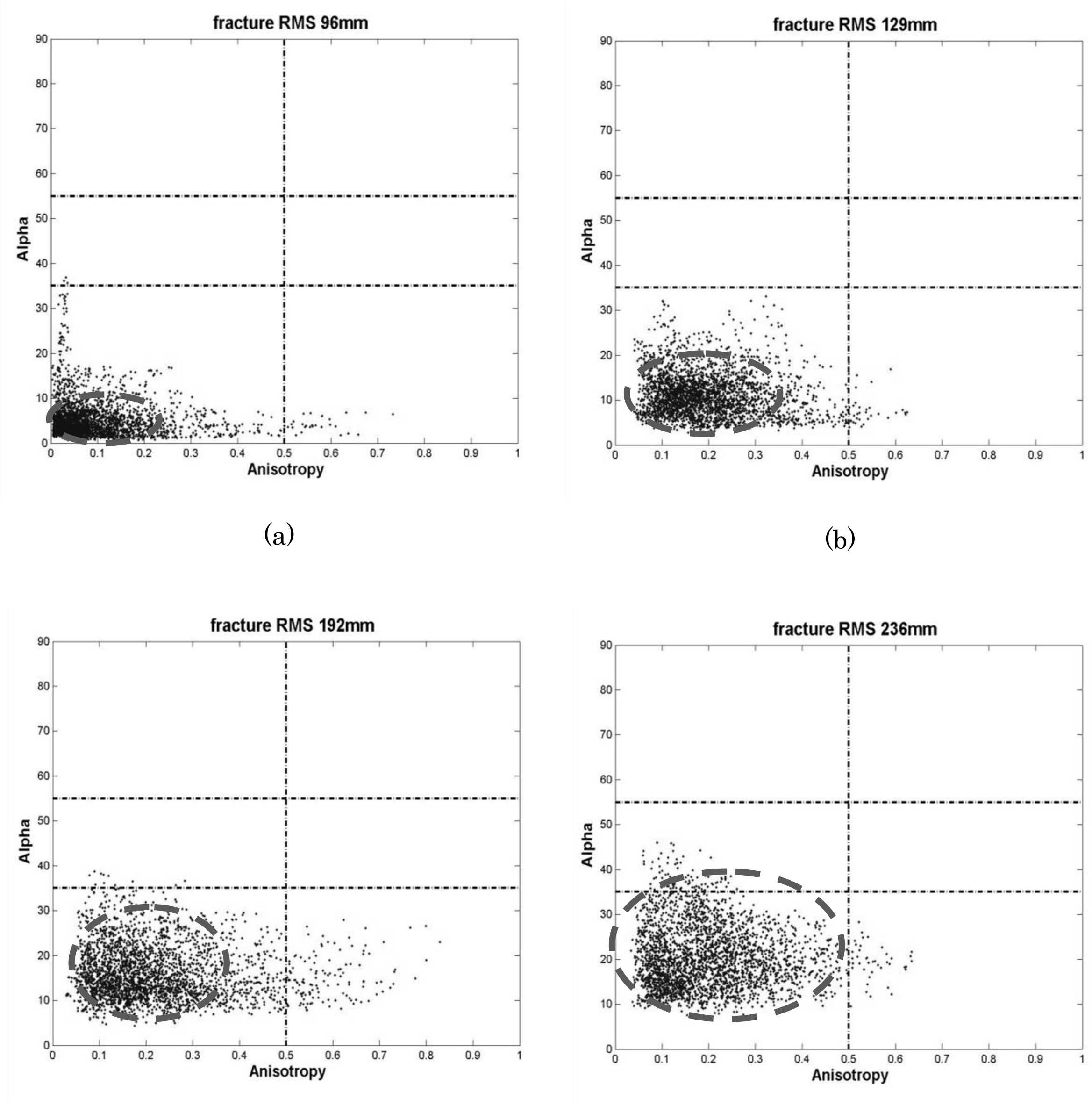

(a) (b)

(c) (d)

Fig.5.5: Anisotropy- alpha plane distributions for variable fracture fractal models. (a) 9.6 cm RMS height, (b) 12.9 cm RMS height, (c) 19.2 cm RMS height and (d) 23.6 cm RMS height.

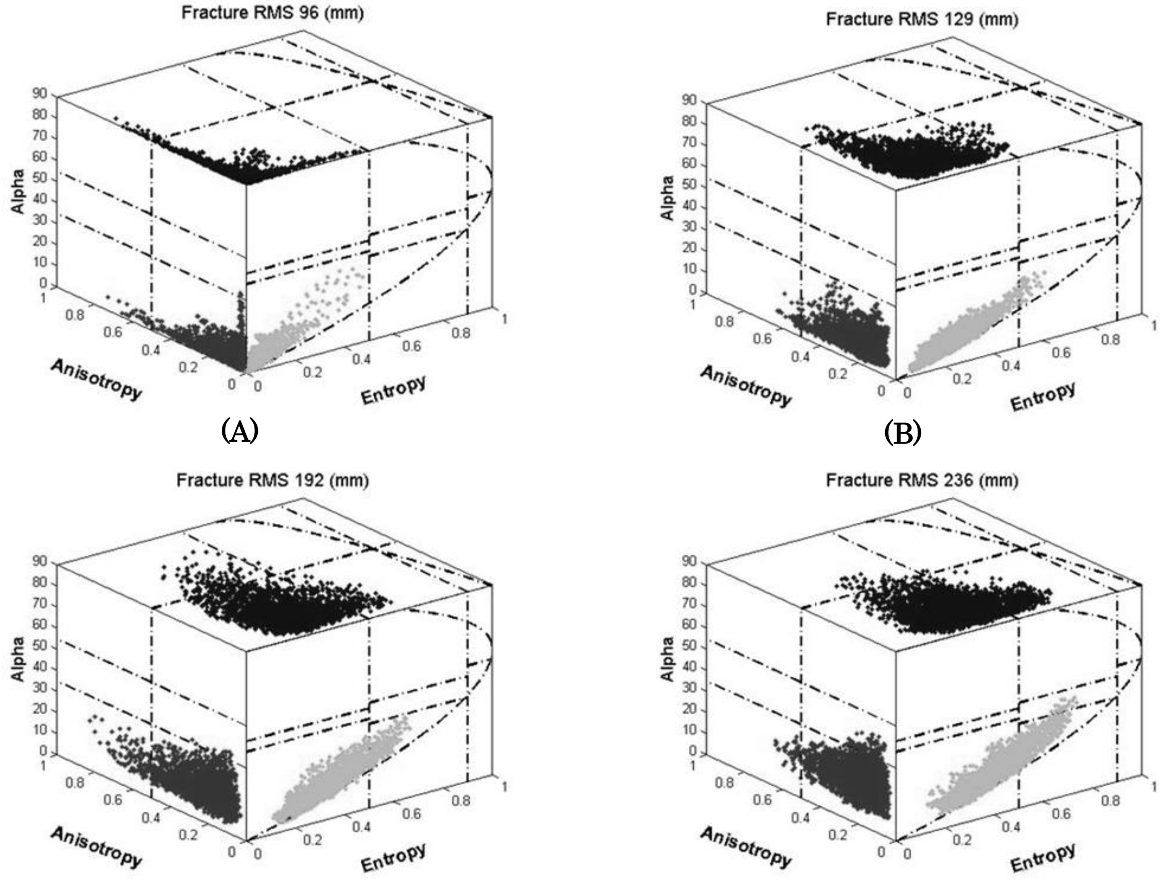

(A) (B)

(C) (D)

Fig.5.6: 3D planes distributions for H-A-alpha for variable fracture fractal models. (A) 9.6 cm , (B) 12.9 cm, (C) 19.2 cm and (D) 23.6 cm fracture roughness heights.

Based on the electromagnetic simulation results and the verification of polarimetric analysis for the eigenvector decomposition, we can confirm the reliability of using the three eigenvectors decomposition for characterizing the fractures depending on its roughness property.

For further research, the variation of the fracture widths is needed to be examined in order to emphasize the concrete reliability of fracture characterization based on the three eigenvector parameters. Different fracture widths have been modeled with the same roughness parameter (12.9 cm). The thickest fracture model was 3 cm width and the thinnest one is a very thin fracture model has various apertures from 0 mm (close aperture) up to 2mm (open aperture), similar to thin fracture model at section 4.6.2 of chapter4. The modelled fractures were also proposed as homogenous and water filled type having electric permittivity 81and rock permittivity of 9. The used frequency range for these simulations was from 1MHz to 200MHz.

3D illustration of the three eigenvector parameters can be seen in Figure 5.7. The variations of the entropy, anisotropy and alpha distributions are observed with the changing of fracture widths. These results reveal that the increasing of fracture aperture produces a changing in scattering mechanism. As, the volume and surface scattering are dominate for the backscattered signals from thick fracture zone. On the other hand, the low surface scattering component can be observed for 5mm and very thin fracture models (>2 mm) as shown in Figure 5.7A and Figure 5.7B. The increasing of the fracture width results in multiple scattering mechanisms. The scattering mechanism randomness increases and the entropy and the anisotropy parameters are getting large due to the fracture zone width increasing. The backscattering from the fracture is consisting of superimposed reflections from the upper and lower fracture surfaces and for the case of thick fractures, the scattering mechanism is getting complex compare to very thin fracture. The multiple reflections from rough surfaces alter the surface scattering into volume scattering case. This can be the explanation for appearing of volume scattering as well as high randomness scattering mechanism for the thick fracture apertures and it cannot be observed for thin and very thin fracture models.

A heterogeneous fracture zone has a complicated EM reflectivity process and probably the EM signals cannot propagate through it, and as a consequence the electromagnetic scattering from upper surface of a fracture zone occurs dominantly and it can be used as characterization index rather than fracture thickness as explained in section 4.3 for chater4.

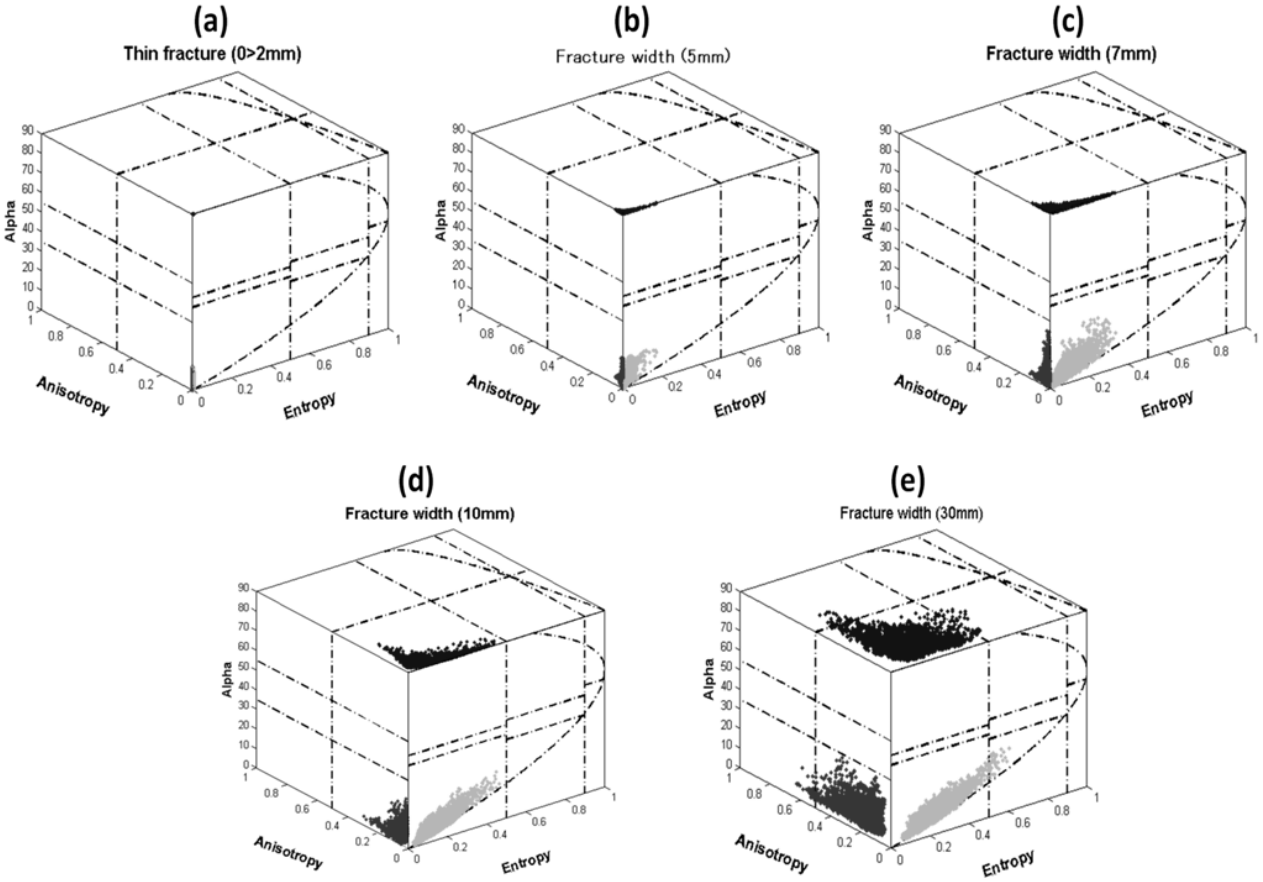

Fig.5.7: 3D planes distributions of H-A-alpha for various fracture widths and the same roughness parameter. (a) thin(0>2mm) mm, (b) 5 mm, (c) 7 mm, (d) 10 mm and (e)30mm fracture widths.

From the EM simulation results and their polarimetric analysis based on eigenvector decomposition, we can confirm the reliability of using the three eigenvectors decomposition for characterizing subsurface fractures. The variation of the fracture roughness and width illustrates a changing in the eigenvector parameters distributions and the scattering mechanisms. The usage of these polarimetric parameters as characterization evidence will be discussed in the next part of this chapter for the measured full polarimertic borehole radar dataset.

5.3 Polarimetric analysis of measured data

5.3.1 Eigenvector based decomposition

The preliminary study for characterizing subsurface fractures based on entropy - alpha decomposition, for the full polarimetric borehole dataset, showed good results and revealed their effectiveness [5]. On the other hand, the third eigenvector parameter (anisotropy) was not examined at this study. The anisotropy as a polarimetric parameter can introduce further information related to the characteristics of subsurface fractures as shown for electromagnetic numerical simulation of different fracture models in the previous section.

The full polarimetric borehole radar system detected the same fractures determined by a directional borehole radar system in USGS research project [6], [7], [8]. In this study, nine fractures were selected as research subjects for evaluating the suitability of applying the entropy-anisotropy-alpha decompositions to fracture characterization. We calculated entropy, anisotropy and alpha distributions for the full polarimetric borehole radar dataset. To, understand the properties of different fractures. We performed a local analysis of the entropy-anisotropy-alpha distributions for every fracture zone of these nine fractures. A local area is chosen for estimating entropy-anisotropy-alpha distributions for every fracture zone of these nine fractures. The explanation of how this local area can be determined from the measure dataset is described in the following part.

The entropy-anisotropy-alpha decomposition was estimated at a single frequency for the polarimetric dataset. The polarimetric borehole radar system is used to make a measurement by scanning along a borehole and each fracture zone interested the borehole axis can be observed. The wavefield separation technique was used based on F-K filtering [9] to determine the borehole intersection depths for fractures intersecting with the borehole axis and simultaneously a migrated image through the F-K migration processing can be obtained from the radar profile.

With using, the frequency-wavenumber (F-K) filter, we can separate the upper-part and the lower-part of the V-shaped train of a reflected signal corresponding to a certain specific fracture zone. Figure 5.8 shows the sketch for the separation steps of subsurface fractures response in the radar profile. The full polarimetric datasets are measured using a borehole radar scan configuration as shown in chapter two and the full polarimetric borehole radar profiles are obtained after direct antenna coupling removal and antenna characteristic compensation. By implementing the wavefield separation technique and rearranging the downward wavefield along the negative time axis [9] we can determine the borehole intersection depths for the main fractures and the radar profiles look like Figure 5.8 (d). From these, we can obtain a power scattering matrix for a specific fracture by integrating the energy inside a slant window, which is a representation of the continuous reflected signal. According to the power scattering matrices for the studied fractures, we are able to carry out a qualitative fracture characterization and classification as shown in the chapter4.

The first process for deriving the radar polarimetric analysis, in order to characterize subsurface fractures for the observed nine fracture zones, is obtained by implementing F-K migration for radar profile as shown in Figure 5.8 (e). Then after, the time-frequency analysis based on Short time Fourier transform is applied to the profile shown for a single frequency dataset reconstruction and the implementation of the entropy-anisotropy-alpha decomposition will be based on the reconstructed single frequency dataset. To clarify the scattering mechanisms from different fractures, a rectangle window around a fracture with size 2.0mx1.5m is chosen as a local area for localizing the entropy-anisotropy-alpha distributions and it can be seen as a dashed rectangle red window in Figure (5.8e). The entropy-anisotropy-alpha features included in the rectangle are predicated to represent all responses from the fracture in question.

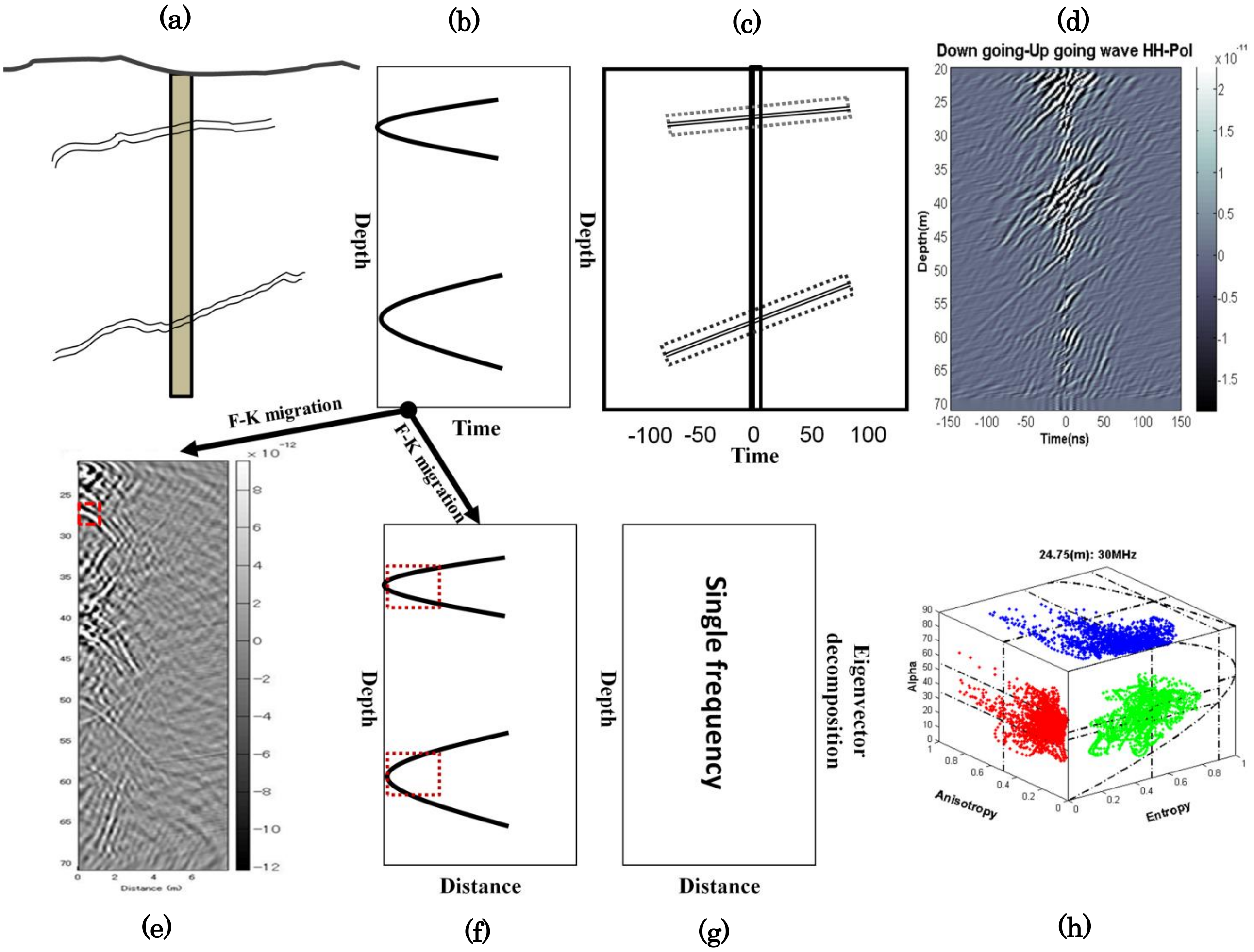

Fig.5.8: The estimation of the three Eigenvector parameters (entropy- anisotropy –Alpha) from the full polarimertic borehole radar dataset.

Referred to the initial study of using entropy-alpha decomposition [10], subsurface fracture zones was classified into three groups depend on entropy-alpha decomposition only: the first group of fractures at 28.5 m, 36.15 m, 44.8 m and 60 m depths, the second group of fracture zones at 42 and 47.8 m depths, and the third group of fracture zones at 40.25 m besides two fractures at 24.75 and 55.2 m depths. I estimated the polarimetric analysis of the three eigenvector parameters (entropy, anisotropy and alpha) of the full polarimetric borehole radar dataset of FSE1 borehole. As was expected, the classification of subsurface fracture was improved with implementing the third eigenvector parameters (anisotropy).

Figure 5.9 shows the anisotropy- alpha distributions for the nine fracture sets at 30MHz single frequency. These nine fractures can be classified into four fracture groups according to their scattering properties. The first fracture group will be defined related to the distribution of 24.7m fracture zone. Those involve fracture sets at 47.8m and 55.2m depths. This characterized group shows electromagnetic volume mechanism and high randomness scattering which resulted of a high rough fracture as well as a large fracture zone width. These conclusions have been observed and confirmed for simulated fracture models. The second category fractures that have similar anisotropy-alpha distribution are at 28.5m and 36.15m depths. This group shows low randomness scattering mechanism as appearing in anisotropy distribution. In addition, surface scattering mechanism from alpha values. Based on that results this group is characterized by a smooth fracture roughness and small fracture zone widths compare to the fracture group of 24.7m. The fracture zones at 40.25m and 42m depths have the resemble anisotropy-alpha decomposition and it can be defined as the third fracture group. The fourth characterized group of fractures is for the fracture zones at 44.8m and 60m depths.

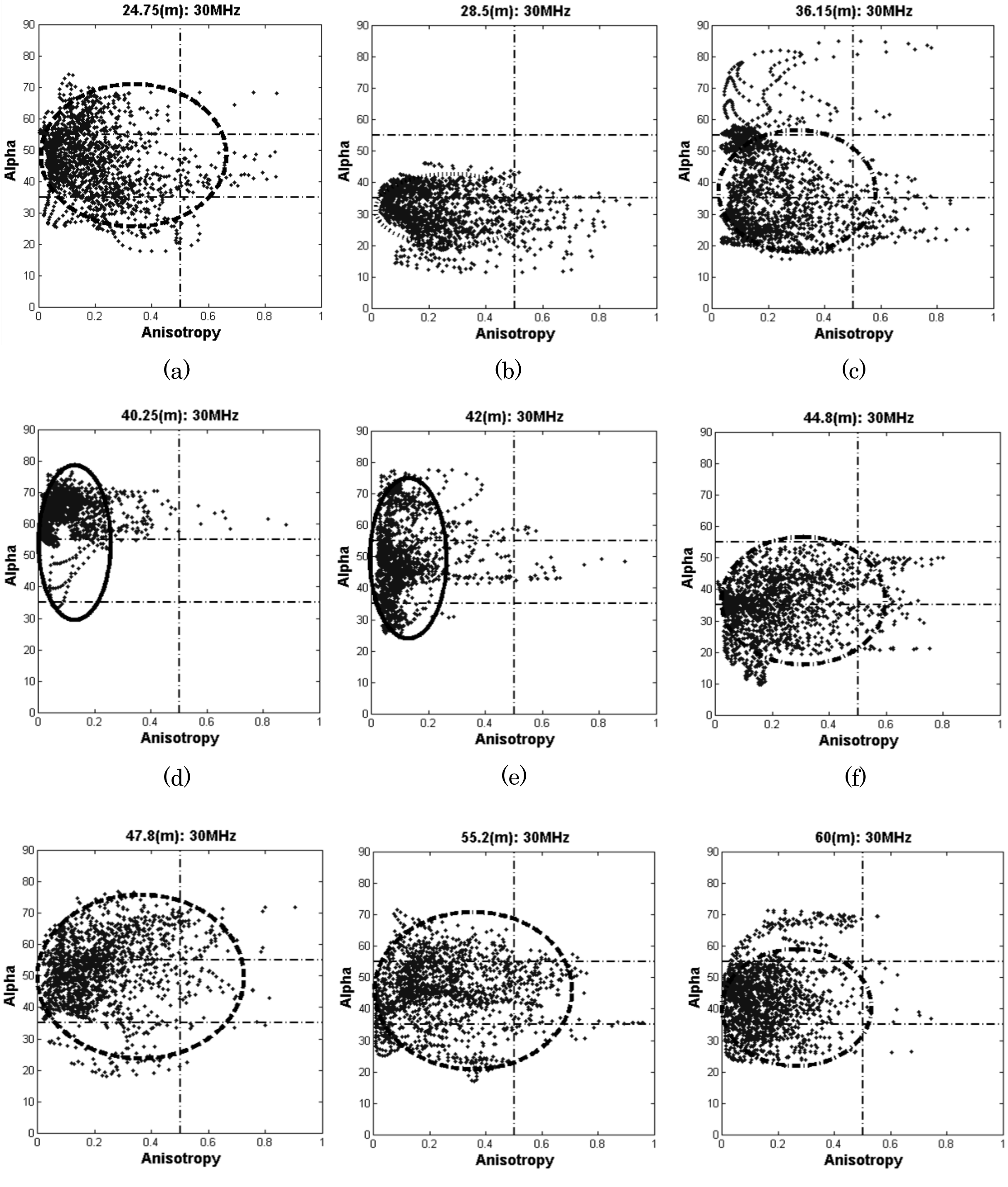

(a) (b) (c)

(d) (e) (f)

(g) (h) (i)

Fig.5.9: Anisotropy- alpha distributions for nine fracture sets at 30 MHz. from the upper left side the fracture set at (a) 24.75 m depth (b) 28.5 m, (c) 36.15 m, (d) 40.25 m, (e) 42 m, (f) 44.8 m, (g) 47.8 m, (h) 55.2 m and (i) 60 m. respectively.

Figure 5.10 illustrates the entropy- anisotropy parameter distributions of the nine fracture zones at 30MHz single frequency. The distributions of these two parameters are

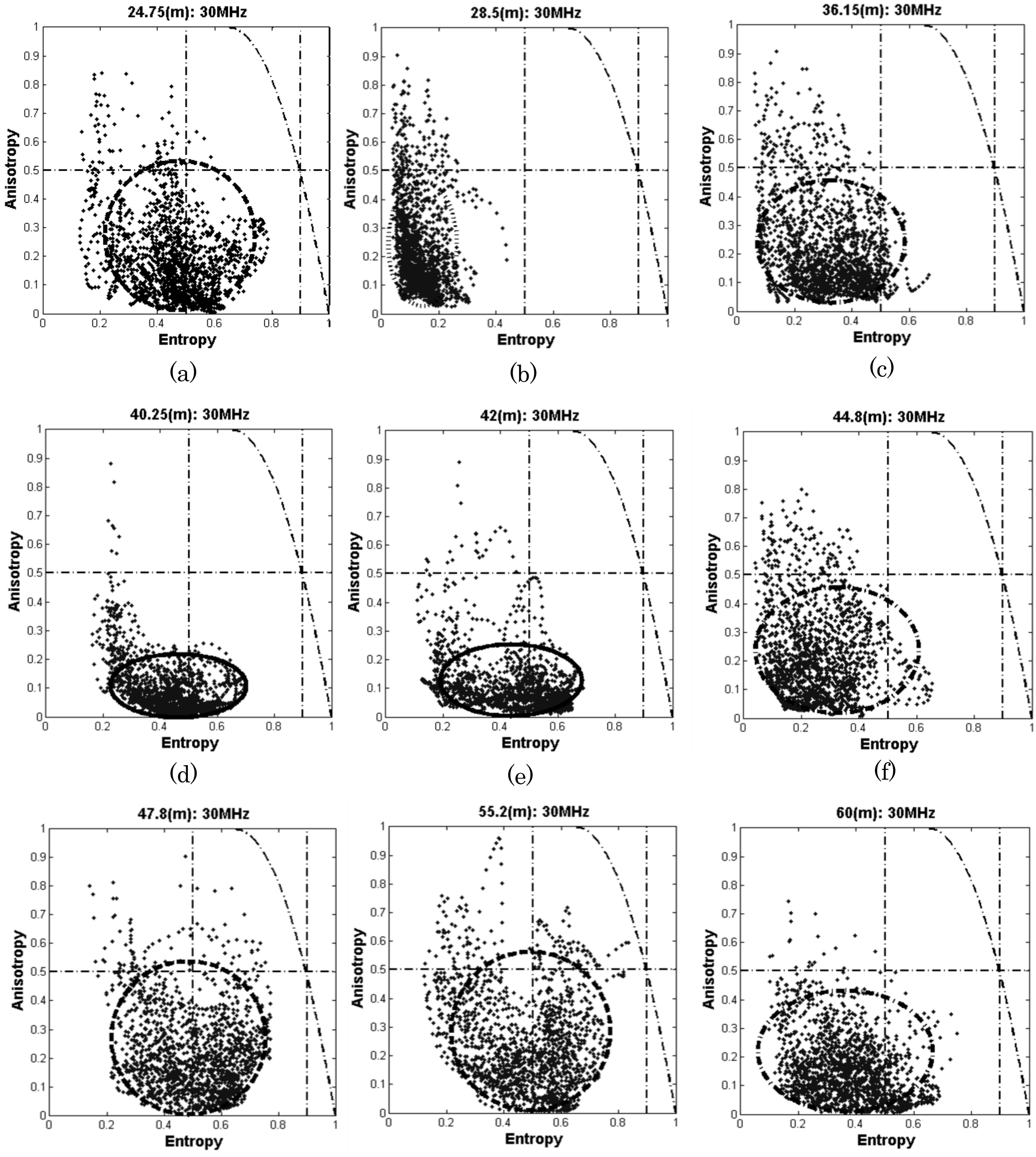

(a) (b) (c) (d) (e) (f) (g) (h) (i)

Fig.5.10: Entropy-anisotropy distributions for nine fracture sets at 30 MHz. from the upper left side the fracture set at (a) 24.75 m depth (b) 28.5 m, (c) 36.15 m, (d) 40.25 m, (e) 42 m, (f) 44.8 m, (g) 47.8 m, (h) 55.2 m and (i) 60 m. respectively.

considered the most reliably eigenvector parameters for classifying the subsurface fractures. Where, the entropy-anisotropy decomposition can differentiate the electromagnetic scattering randomness of various fractures roughness and aperture widths. The classification of these nine fracture zones based on entropy-anisotropy parameters clarified the same conclusion as anisotropy- alpha decomposition revealed. Each classified group of fracture zones shows almost the similar scattering mechanism and distribution pattern. The fracture zones of depths 24.75m, 47.8m and 55.2m have the highest fracture roughness and aperture size according to the entropy-anisotropy distributions and they represent one group as a similar scattering properties can be observed for these fracture zones. On the other hands, the lowest rough fracture zones and the smallest width based on entropy-anisotropy distributions are at 28.5m and 36.15m depths. As, these fracture zones have the lowest random scattering mechanisms. The third characterized fracture zones are at 40.25m and 42m depths. Besides, the fourth classified group at 44.8m and 60m fracture depths.

The polarimetric analysis based on the three eigenvector parameters of the measured polarimetric borehole dataset at 30MHz has been determined and displayed in Figure 5.11. The 3D representation of the three eigenvector parameters provides the possibility to discriminate new classes using the anisotropy value [11]. For example, when the entropy is high and the anisotropy is also high it is corresponding to the presence of two scattering mechanism with the same probability as the fracture group at 24.75 m depths. On the other hands, when the entropy is high and the anisotropy is low it is corresponding to random scattering as for the fracture group at 40.25 m depth and it is expected to be less roughness property and fracture zone width. This electromagnetic scattering property can be interpreted to hydraulic feature. Therefore, we expected that the fracture group of 40.25m depths have less hydraulic transmissivity compare to 24.75m fracture group.

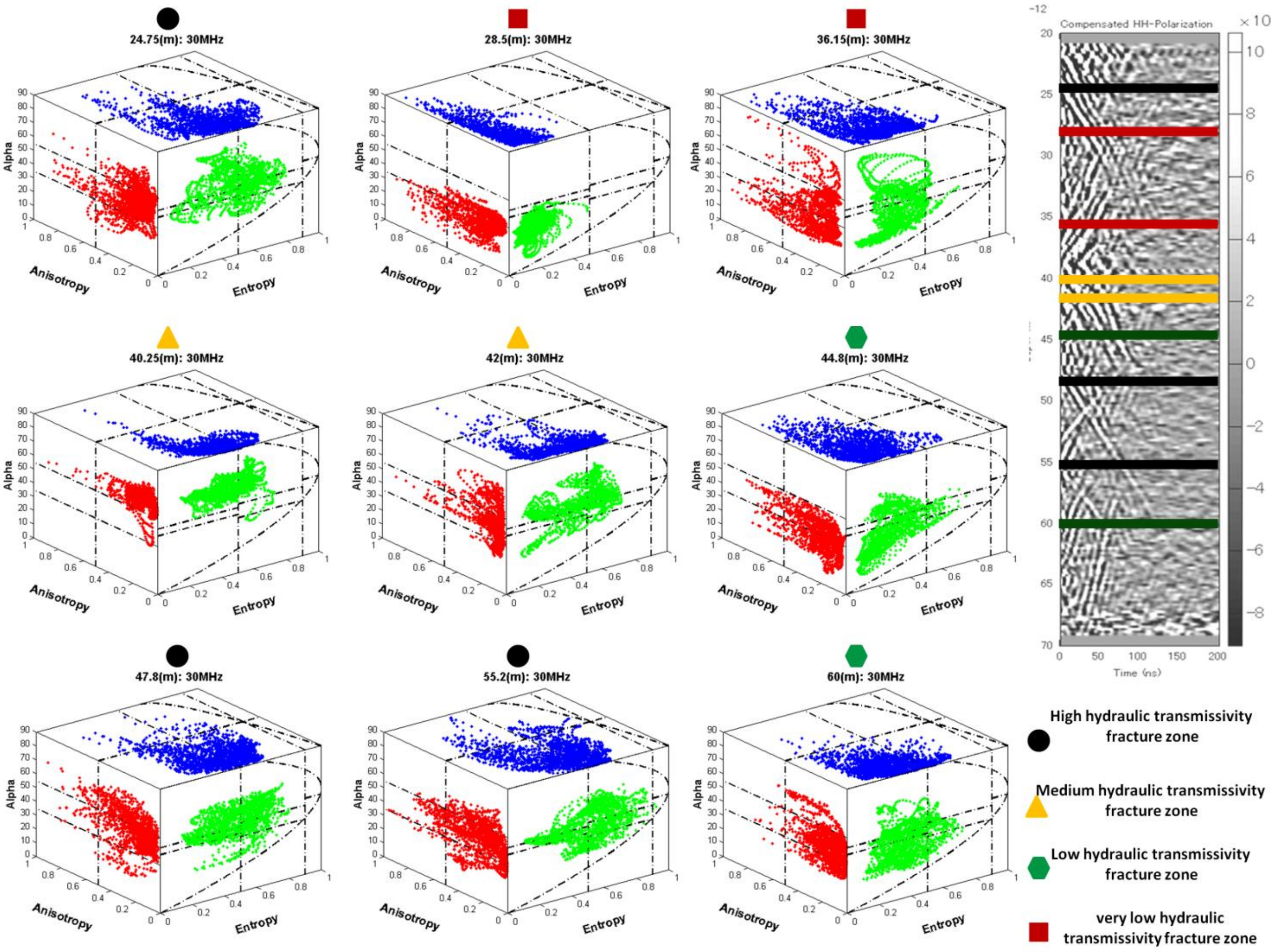

Fig.5.11: Entropy-anisotropy-alpha distributions for nine fracture sets at 30 MHz. from the upper left side the fracture set at 24.75 m depth, 28.5 m depth, 36.15 m depth, 40.25 m depth, 42 m depth, 44.8 m depth, 47.8 m depth, 55.2 m depth and 60 m depth, respectively.

The entropy-alpha, entropy-anisotropy and anisotropy-alpha distributions have been estimated for the different frequencies (30MHz, 40MHz, 50MHz, 60MHz, 70MHz, 80MHz, 90MHz and 100MHz). Where, a local region of each eigenvector parameter was chosen to be a 2 m by 1.5 m rectangle around each fracture and the borehole and fractures intersect precisely at the midpoint of the long side of the rectangle as described in section 5.3.1. Figure 5.12 shows the 3D distributions of the three eigenvector parameters at 100MHz frequency. If we observe carefully the difference of distributions of the three eigenvector parameters for 30MHz and 100MHz case, we can see that the resolution of the three eigenvector parameters to characterize subsurface fractures is becoming weak with increasing frequency. The explanation of this phenomenon is that high frequency components are much more sensitive to small structures so that the depolarization effects become stronger compared to those of low frequency components and the distributions of eigenvector parameters are getting wider such as the case for 28.5m, 40.25m and 60m fracture zones.

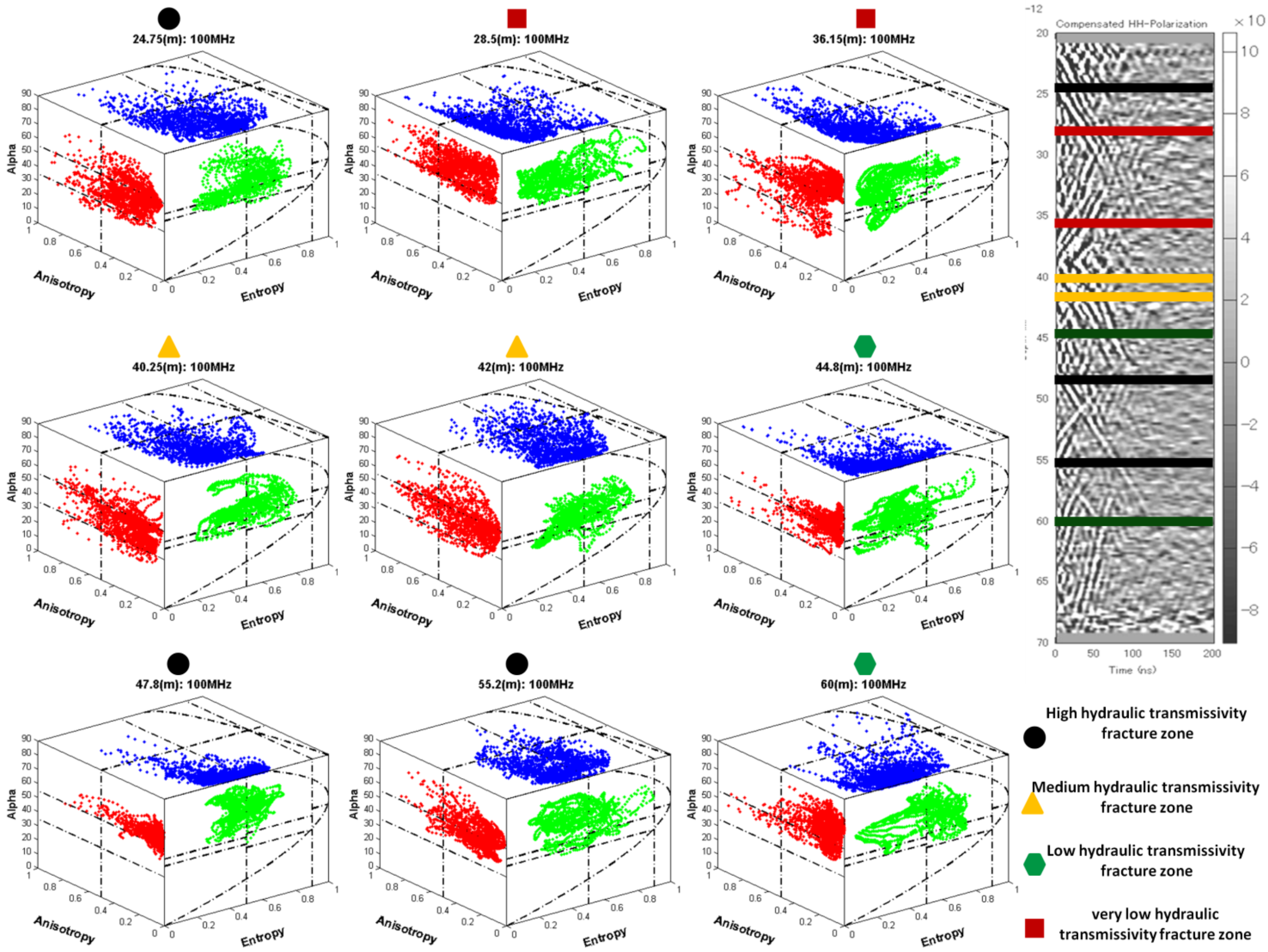

Fig.5.12: Entropy-anisotropy-alpha distributions for nine fracture sets at 100 MHz. from the upper left side the fracture set at 24.75 m depth, 28.5 m depth, 36.15 m depth, 40.25 m depth, 42 m depth, 44.8 m depth, 47.8 m depth, 55.2 m depth and 60 m depth, respectively.

5.4 Validation and description of results

The polarimetirc analysis at 30MHz single frequency of the three eigenvector parameters were performed for nine fracture zones as shown in Figure 5.11. Based on this analysis for the nine fractures, they can be classified into four characterized groups. The fractures at 28.5 m and 24.75 m depths apparently have different distributions property of entropy, anisotropy and alpha. While, the fractures at 47.8 m and 55.2 m have almost consistent scattering mechanisms and distribution patterns with 24.75 m fracture as their scattering properties are similar. This conclusion can be validated by comparing the estimated three eigenvector parameters of the simulation fracture models. These three polarimetric parameters showed a change in their distribution patterns of various fracture roughness as well as the fracture widths as pointed out in Figures 5.6 and 5.7.

The correlation of the derived polarimetric analysis based on the three eigenvector parameters and the hydraulic tracer test results, that was measure by USGS, showed the fracture zones at depths 24.75m and 47.8 have the highest hydraulic transmissivity ($2.5\text{x}10^{-6}$ m^2/s and $5.6\text{x}10^{-5}$ m^2/s, respectively) which is strongly consistence with polarimertic analysis results based on the three eigenvector parameters. Furthermore, the fracture zone at 55.2m depth can be classified also as a high hydraulic transmissive fracture zone depends on its polarimetirc analysis result, Hence, its hydraulic property was not supplied by USGS in this tracer test.

The fractures at 40.25m and 42m depths have the similar type of electromagnetic scattering and the eigenvector parameters distributions. For that, they are considered as one characterized group. Furthermore, the hydraulic property of these two fracture zones showed high fluid transmissivity characteristic ($1.1\text{x}10^{-7}$ m^2/s). But, in the same time have less transmissivity than the first fracture group (24.75m). According to the hydraulic tracer test results the fracture at 36.15m depth is considered the lowest transmissive fracture ($3.4\text{x}10^{-9}$ m^2/s). Furthermore, the polarimetric analysis of this fracture zone showed also the lowest eigenvector parameter distributions which have a close configuration of distributions and scattering mechanisms of fracture zone at 28.5m depth. These two fracture zones have low entropy and anisotropy values compare to other fractures and low alpha distribution as well. These fractures are expected to have a small fracture width and smooth surface roughness as verified from the simulated fracture models. In addition to that, they are having a low water transmissiviy zones. At 44.8m and 60m fractures the entropy and anisotropy parameters show low to moderated scattering mechanism randomness. Furthermore, the mean alpha angles present surface to volume scattering mechanism distributions. These two fractures were proposed as one group category with low hydraulic transmissivity property. On the other hand, they have more water conductivity compare to fracture zone at 28.8m.

Summarization of the expected hydraulic transmissivity of every fracture depends on their polarimetric analysis is included in Table 5.1. These conclusions figure out the fracture characterization based on the eigenvector decomposition for these nine fractures. The comparison of the actual measured hydraulic transmissivity for each fracture zone and the derived polarimetric analysis can be seen also.

The results and the analysis that were achieved in this research work are considered one of the pioneer outcomes for characterizing subsurface fracture systems. For two reasons: the first one, fracture characterization is a difficult goal to be maintained and the second one, there is no other geophysical technique can provide such results and propose the hydraulic property of subsurface fractures. The full polarimetric borehole radar system and the polarimertic analysis of its data can provide that aim. I believe strongly that more applications such as exploring new groundwater resources in arid regions and countries such as Egypt, Saudi Arabia, Kuwait and Libya can utilize this technology. As, a lot of groundwater accumulations are found in crystalline and limestone rock types. In next chapter, I will clear out more details for the expected role of the polarimetric borehole radar system to be applied for a case study in Egypt related to resolve the recharge process for groundwater aquifers via subsurface fracture systems.

In addition, the importance of characterizing different oriented fractures sets and their hydraulic impacts.

Table 5.1: Subsurface fracture characterization based on polarimetric analysis of entropy -anisotropy- alpha parameters at Mirror Lake FSE1 borehole.

Fracture depth	**Fracture property**	**Transmissivity**	**Estimated hydraulic value (m^2/s)**
24.78m-47.80m-55.20m	Very rough	Highest	2×10^{-6} 5×10^{-5}
40.25m-42.00m	Rough	High	1×10^{-7}
44.80m-60.00m	Slight rough	Low	
28.50m-36.15m	Smooth zones	Lowest	3×10^{-9}

5.5 Summary

In this chapter, I introduced the concept of the polarimetric analysis based on the three eigenvector parameters, entropy, anisotropy and alpha, and their physical meaning which is mostly used in the field of SAR remote sensing. I tend to use it for full polarimetric borehole radar data. The verification of using the three polarimetirc parameters for fracture characterization has been shown by using electromagnetic forward modeling of different synthesized fractal models and various fracture widths. The three polarimertic parameters revealed various distribution patterns as well as scattering mechanism complexity with changing of the fracture roughness and fracture widths. Electromagnetic simulation results emphasized, the anisotropy parameter provides complementary information to the entropy and facilitates the interpretation of the scattering from rough fracture surfaces as shown in Figures 5.6.

Subsurface fracture characterization of the measured polarimetric borehole radar dataset has been shown based on the polarimetric analysis of the three eigenvector parameters. The polarimetirc analysis was estimated based on the single frequency datasets constructed at 30MHz, 40MHz, 50MHz, 60MHz, 70MHz, 80MHz, 90MHz and 100MHz. In addition to, it was shown that the employment of lower single frequency polarimetric datasets is more reliable to understand the scattering mechanisms from different fractures as seen for the difference between 30MHz and 100MHz polarimetric distributions.

The correlation between our conclusion of subsurface fractures characterization and hydraulic tracer test results that was measured by USGS showed good consistency. The characterized fracture categories and their hydraulic properties are summarized in Table 5.1. Full polarimetric borehole radar system can share for providing information related to the flow of water and its hydraulic property in fractured rocks.

Chapter 6

The Hydrological Effect of Subsurface Fractures Southwest Aswan and the Polarimertic Approach

6.1 Introduction

The population of Egypt is, indeed, a rapidly increasing one, which is concentrated in less than 6% of the country’s entire land mass. As a consequence, food, water and urbanization demands are also rapidly increasing. Such challenging conditions necessitate the development of the unused desert areas fringing the Nile delta and valley.

A new urban agriculture project was initiated in 1997 in order to relocate the population of Egypt from the old valley. It was referred to as the “Tushka” project. The target area of the project is the south-west Aswan city, as demonstrated in Figure 6.1. The reclamation of the land in that project will depend on two types of water resources, namely the surface water, and the groundwater resources in Lake Nasser area. In other words, the studies of the hydrological conditions of the surface water in Lake Nasser along with the groundwater resources formulate the core of this project. As a consequence, the connection between the surface water and groundwater affects the water balance in Lake Nasser. The storage of surface water in this lake is considered to be the safest and principal water repository in Egypt. The fluctuation in groundwater levels in the wells located in this area has demonstrated a direct relationship with the surface water variation in Lake Nasser [1]. The estimated amount of the infiltrated surface water from Lake Nasser into the adjacent Nubian aquifers was determined to be approximately 2.588 523 m^3 yr^{-1} based on the transient electromagnetic method [2]. It was found that the seepage of the fresh surface water of the lake into the adjacent groundwater aquifers constituted such a significant volume that cannot occur only with normal infiltration mechanisms. Therefore, this occurrence should be related to fault systems and its associated fractures.

The expected role of the fault systems and the tectonics for recharging the Nubian sandstone aquifers in the southwest Aswan from Lake Nasser was investigated by Taha [3]. It was revealed that the subsurface structures controlling the water recharging to the Nubian aquifer and the northeast fault trends are responsible for conduction to and recharging of Nubian aquifers. It can be observed, based upon the previous studies, that the Nubian sandstone aquifer (located to the south of Aswan city) is, mainly, a fractured aquifer due to the tectonic activity, especially around Lake Nasser. From our understanding of the hydraulic properties of the fracture zones in the sedimentary cover or the basement rocks around Lake Nasser, it is important to have an insight, through a new research in hydrology, into the interaction of the surface water and groundwater resources in that location.

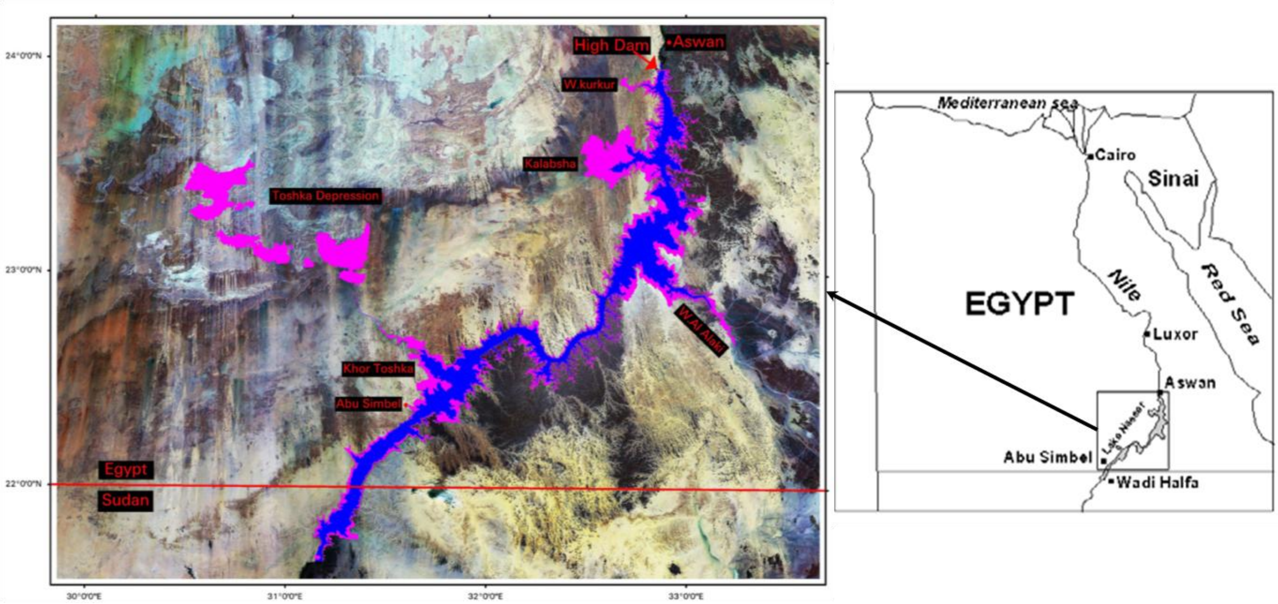

Fig.6.1: The location map of west and south Aswan areas.

The hydrological case, for the seepage of the surface water to groundwater aquifers or the connections of a groundwater bearing formation to other bearing formation(s) through fracture zones, has attracted the attention of several researchers. For instance, Power et al [4] used the surface direct current (dc) resistivity and very low frequency electromagnetic (VLF) methods to determine the location of fracture zones and the fluid migration in the fracture zones located at Mirror Lake, Grafton Country, USA. Monterio Santos et al [5] investigated the aquifer contamination by seawater by using the VLF method, and examined the tectonic structure correlated to seawater infiltration.

The hydrological studies of the fracture zones effect on the recharging of the groundwater aquifers as well as the mechanism of the surface water infiltrated to subsurface through them has not been accurately done to date. Mostly, the surface geophysical methods are not so accurate for defining the hydrological properties of fracture zones, and their results are rough estimates, as they provide the presence of these fracture zones without obtaining their hydraulic properties. The role of the polarimetric borehole radar and its polarimetric analysis for the measured data are expected to enrich the results pertaining to the characteristics of subsurface fracture zones as it was seen in chapter 5 for the case at the Mirror Lake test site. The full polarimetric simulation results for the fracture zones in chapter 3 can be the key for extending this technique in Egypt. The reason behind this hypothesis is the fact that these results exhibit that the polarimetric borehole radar is capable of distinguishing different fractures based on their roughness and fracture widths properties. Those results can indirectly determine the hydraulic properties of certain subsurface fracture trends with referring to Mirror Lake results.

6.2 Fracture trends and occurrences

Most of the structural elements of Egypt originated from compressive stress, which originated primarily from N10^0 W and S10^0 E during the Precambrian period [6] and the fractures cut through different rock units. The trends of the fractures differ greatly owing to different geological conditions and tectonic forces. The interpretation of the detected surface lineaments from Landsat images at the area in south latitude N 29^0 of the Western desert demonstrated that they have the main trends of the fractures in NNW, E-W, N-S and NW. Furthermore, these surface lineaments (fractures) can be classified according to their dimension and spacing into two orders: one with large extension and wide spacing and the second one with small extension and narrow spacing that located close to Aswan and Lake Nasser [7]. These results can help in interpolating the semi regional structures which were observed from the Landsat images to the local geological structures that were derived from field observations and surface geophysical measurements related to subsurface fractures. In addition, it may help researchers to extrapolate subsurface fracture properties which can be derived from the polarimetric borehole radar system applied to this local trends as well as semi regional trends.

The identification of the local geological settings in the southwest Aswan, especially around Lake Nasser, will help in the determination of the fracture distributions in subsurface of that area where the fracture systems are sharing the recharge of the main groundwater aquifers via surface water of Lake Nasser. This lake lies in the extreme southern part of Egypt occupying a considerable area behind the Aswan High Dam. Nasser Lake mainly constitutes Precambrian granitic terrain and extends southward towards the Egyptian-Sudanese border. It was evident through previous geological and geophysical studies that Nasser Lake affected the tectonic stability of the Aswan region, since water penetration through open fractures and other tectonically weak zones in the submerged land has significantly contributed to further fracturing and reactivation of some pre-existing faults [8]. Structurally, the area is highly affected by NW-SE, NE-SW and ENE-WSW faults and fractures, where the Wadies and its tributaries run over these structural lineaments. It has been approved that the surface lineaments are associated to subsurface discontinuity structures such as faults and joints as well as its accompanied fractures zones [9]. The examination of fracture trends, related to the basement rocks, was carried out using the aeromagnetic method. This study delivered the structure map and fracture trends in basement rocks as shown in Figure 6.2. The results reveal that this part of the lake is affected by four sets of deep-seated and near-surface structural lineaments oriented in the NW-SE, E-W, N-S and NE-SW directions. The NW-SE (Red Sea) trend is more strongly developed than the other identified trends. It represents the prevailing tectonic trend in the area, and is considered to have played an important role in the formation of its tectonic framework. It was noticed that this trend is significantly responsible for the formation of the major basin, which trends in the same direction, and occupies the western and southwestern parts of the area. Kamel *et al* [8] stated that the NW and N-S trends represent the prevalent directional orientations of the surface structural lineaments in the north Nasser lake area.

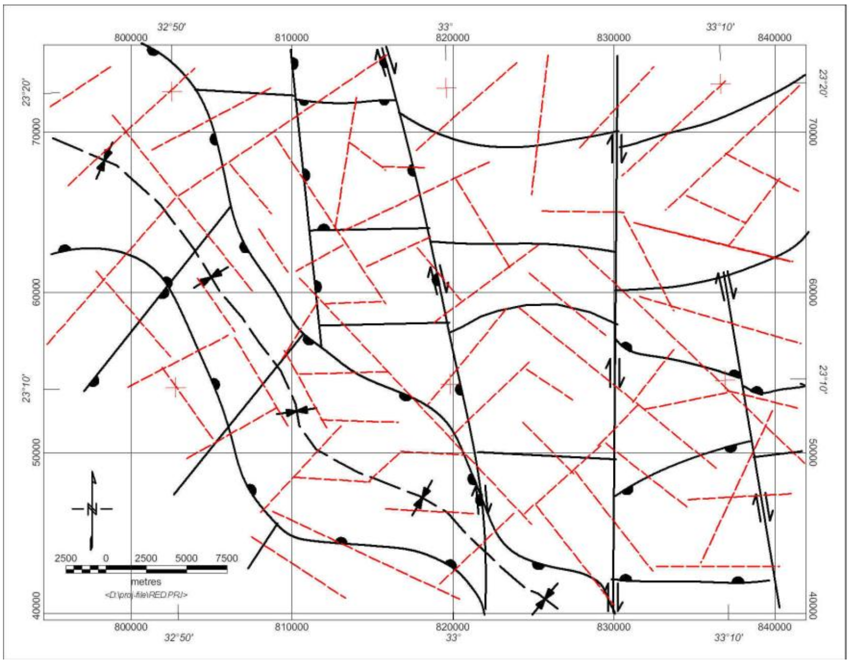

Fig.6.2: Interpreted deep-seated (solid black lines) and near-surface (dashed red lines) structural map and fracture trends.

Detailed geophysical survey methods combined with composite borehole data have revealed the geological and tectonic setting of the southwest Aswan region, and allowed a first insight into the geometry of the aquifers near the Lake Nasser. These studies have indicated that the aquifer system is not homogenous. The studies rather demonstrate that it consists of several horizontal layers, which are crisscrossed by deep seated structures (i.e., reactivated basement structures) causing, in some cases, uplifting or subsistence of aquifer sections. Some of these structures are also responsible for seepage from Lake Nasser into the aquifers as well as across aquifer layers separated by aquaclude horizons. The predominant fracture orientations are NW-SE, N-S, and NE-SW, the latter one being primarily responsible for recharging the aquifers located on the west of Lake Nasser [3].

6.3 Hydrological effects of fracture zones

The hydrological setting around Lake Nasser and its western margin showed that it is affecting strongly the recharge of the adjacent Nubian aquifers via the faulting systems and the accompanying fracture zones. For that reason, I highlighted the hydrological effects of subsurface fractures at that area as a case study where the water flow mechanism (surface water to groundwater aquifer and the internal water flow between the Nubian aquifers) through the fracture systems is not known. It is also worth mentioning that nobody knows, thus far, until when this recharging mechanism takes place. I believe the contribution of the polarimetric borehole radar, in revealing the relationship of subsurface fracture zones for supplying the groundwater aquifers, can be significantly effective in future.

Generally speaking, the hydrogeological data are obtained based upon the hydrological cross sections from the drilled water wells around Lake Nasser as shown in Figure 6.3. It was found that the Nubian sandstone aquifer is consists of two connected water bearing formations in this area, namely Sabaya and Abu Simbel. The Abu Simbel water bearing formation represents the main aquifer around Lake Nasser (i.e., the southwest Aswan) and these aquifers are hydraulically connected with each other as a result of faulting displacement [1]. The Abu Simbel formation is connected to the surface water of Lake Nasser directly according to the hydrological section AA′ as shown in Figure 6.4, and the Sabaya aquifer has its water content recharged from the fault plane and its accompanied fracture zones from Abu Simble formation. However, the role of these fracture zones as a transmissive pass in addition to the direction of water flowing has not evolved yet. Providing these results and outputs can help us estimate the future development in this area and explore the possibility for drilling more water wells relevant to the Sabaya aquifer.

The variations of the water tables in the borehole around Lake Nasser have shown the gradient decrease in the water tables far away from the lake shore which was reversed in the past (before the presence of Lake Nasser and construction of the High Dam). Furthermore, these changes in the water tables are not symmetrical as some close boreholes to the lake indicated lower water tables than farer boreholes.

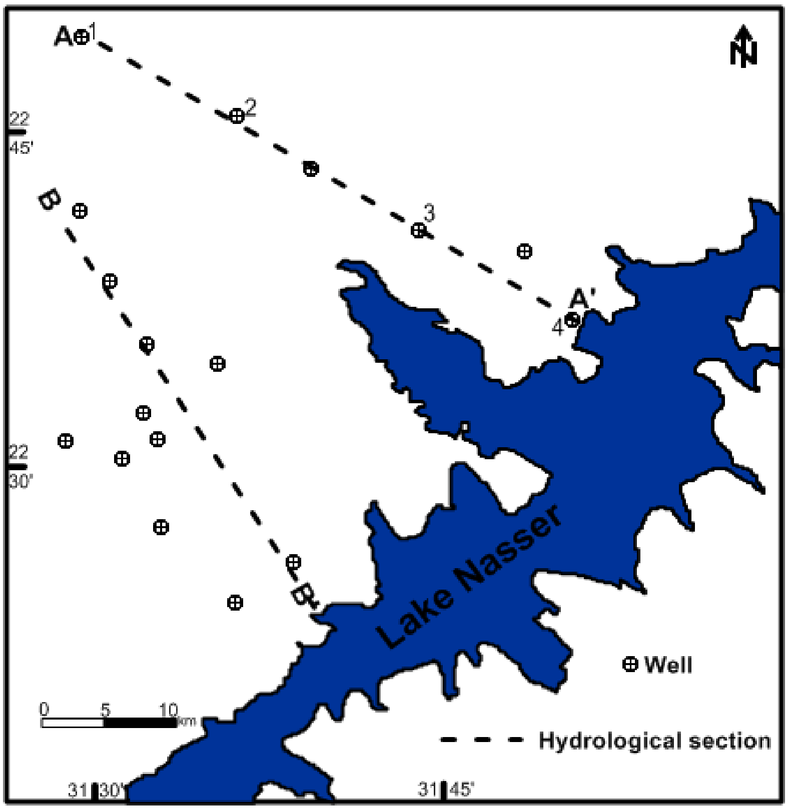

Fig.6.3: The locations of the hydrological sections.

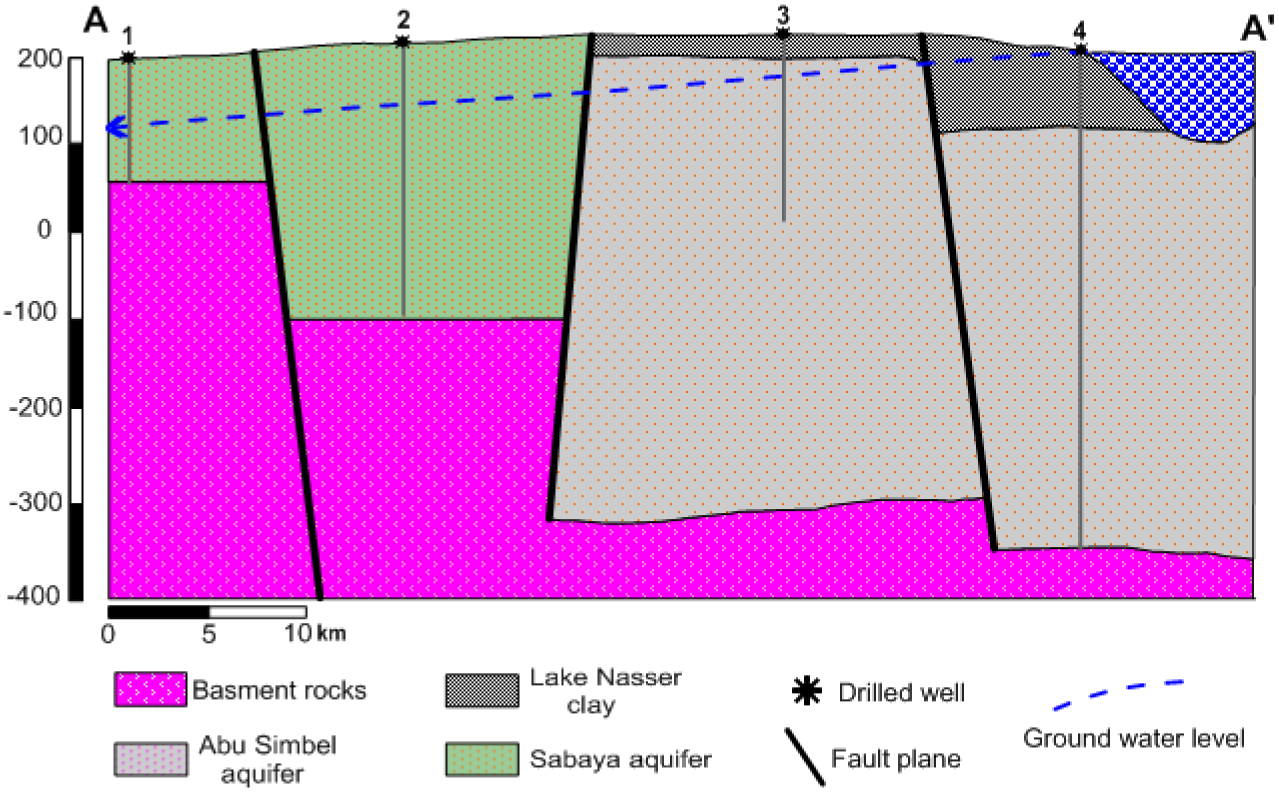

Fig.6.4: The hydrogeological section A-A′.

The afore-mentioned observation emphasized that these far boreholes have much water supply from the Lake Nasser through faulting and fracture systems that have not occurred for some near boreholes. The contribution of subsurface fractures as a hydrological transmissive object has been studied by Khalil et al [10]. The studies noted seepage of water through the fracture zones using the VL F method. However, the studies are not able to provide information related to the hydraulic property of those fracture zones.

6.4 The properties of subsurface fractures and the borehole radar

The hydraulic connectivity in subsurface fracture systems is depending on the fracture geometry, fracture orientation and fracture distribution. For electromagnetic waves, the back reflection of radar signal inside the borehole from subsurface fractures depends on different factors, one of them being the fracture distributions controlled by the rock type and the tectonic setting. Johnson [11] made a comparison of fracturing in the crystalline rock type and his work indicates that the fractures are controlled by the geological settings. In addition, his research revealed that the granitoids are more intensely fractured than the schist and gneissic, pegmatite and basalt rocks, and the quartzite are relatively un-fractured. The count of fractures with respect to the lithology indicates that approximately 72 percent of the total numbers of fractures were in granitoids, whereas 23 percent were in schist. Only 5 percent of the total numbers of fractures were in pegmatite and basalt. These results indicate that in crystalline or metamorphic rocks, for the single borehole radar measurements, the reflection from fractures in the granitoids rock type can be stronger compared to other rock types such as schist and pegmatite. On the other hand, for the cross-hole radar measurements, the delineation of fractures in schist and pegmatite is easier than that in the granitoids. These results might help us to expect (and possibly estimate) the fracture distributions effect on radar signal inside the basement complex around Lake Nasser with prior information about the rock type. Furthermore, the integration of data about the litology identification and the expected fracture characterization, which can be determined with polarimetric borehole radar system, can assist in determining the fracturing distribution in Nubian sandstone aquifer around Lake Nasser. Also, the connection of Nubian sandstone aquifers and the basement complex could be observed through the fractures. Generally, the implementation of the polarimetric borehole radar as subsurface sensing technique will assist in revealing the mechanism of infiltration of groundwater between the Nubian aquifers and basement complex. This is also expected to aid us in discovering the mechanism of the surface water seepage from Lake Nasser into Nubian sandstone aquifers.

6.5 The characteristics of the fractures at southwest Aswan area

The structural geologists have developed a picture of the immensely thick rock foundation of Egypt by examining rock exposed at the surface or in the walls of the escarpments along the Nile valley as well as by studying material brought up from deep boreholes drilled to locate groundwater or oil.

6.5.1 Fractures in the basement complex

The presence of fracture zones in the basement complex around Nasser Lake are formed by chloritic slip surfaces grading into cataclastic parts containing breccia and fault gouge. The cataclastic zones have widths of 9 mm to 89 mm and show evidence of shear displacements of several meters. It has been observed from geotechnical studies of the core samples during the construction of the Tushka project pumping station that fracture in the basement rock consist of approximately planer fractures arranged in a single subparalled and dipping steeply to the east direction. Furthermore, these fractures zones are filled with mineral precipitates, dominantly epidote and chlorite and small quantities of zeolites. Narrow zone of altered granodiorite are seen with many joints and fractures. The altered zones, which appear lighter in color than the surrounding rock, are commonly 3 to 4 cm in width [12].

The results of the observed fractures in the basement rock at southwest Aswan area can be used as an index for defining the fracture property which can be implemented into the FDTD simulation. The hydraulic role and the effect of these fractures can be deuced with referring to the obtained polarimetric analysis, as shown in chapter4 and 5, from practical fracture sets and the effect of them for the groundwater flow in this area as well as the relation of water recharging between the basement rock and the Nubian aquifer.

6.5.2 Fractures in the Nubian Sandstone

The Nubian sandstone aquifer consists of clastic sediment of sandstone, sandy clay intercalated with shale and clay beds, ranging from Cambrian to upper Cretaceous in age. The Nubian Sandstone basin is tectonically affected by regional faulted structures and is separated into different sub-basins or hydrogeologic blocks. The tectonic actions affected the Nubian aquifer strongly as well as the basement rocks hence the thickness of the Nubian sandstone is not large.

Petrophysical studies at this area revealed that the fractures which associated with the NE fault trend at southwest Aswan area (near Nasser Lake) are situated mainly in sandstone rocks and it is expected to be extended to the basement complex. It is steeply dipping with 15mm- 43 mm in width, and has been traced over distance of about 50 m from the surface. During field investigation at Tushka area three cored boreholes were drilled and they intersected a fracture zone at various depths. It was found that up to 27% of the zone remained unsampled by the drilling due to poor core recovery (losses and crushed material) [13]. The effect of the tectonic stress due to water weight at Lake Nasser and water geochemical reaction with rocks deform the fracture sets and increase the fracture widths as well as generate further fractures into sedimentary and basement rocks. This process causes the presence of many micro seismic activities around Nasser Lake.

An interesting feature that shows how the Nubian sandstone aquifer can be highly fractured is the occurrences of sandstone Karst. This phenomenon has been seen at the Aswan area and it provides that the fracturing in the Nubian sandstone can be also due to physical erosion and geochemical process and fractures and joints have large spacing [14]. For Nubian sandstone, Ulf [15] stated that “the groundwater of the Nubian aquifer was formed mainly by local infiltration”, this may help to understand the water flow within Nubian sandstones. In addition, the consensus that occur during the Holocene optimum, the Sahara was much greener than today. The drainage basins on both eastern and western side of the Nile drained from basement mountains to the Nubian sandstone plateau. Moreover, the Karstic process occurs due to many factors including vertical joints, bedding plane in horizontal succession, and high permeability. Consequently, this hydraulic system ensures the Karst potential in Nubian sandstone. Overall the Karst in sandstone which is assessed in consideration to the water rains in Middle Holocene age. This observed structures in Egypt may give a way for further studies support the potentially of groundwater flow within Nubian sandstone and may have new aquifer findings.

The Karst landforms present in Nubian sandstone including caves, columnar in different sizes. There are caves at the end of the vertical joints that is the rain water passage. Other caves not found along the fracture plain but it seen excavation inside the sandstone blocks. In southeastern desert, the caves in Nubian sandstone, has width 2 m and height 1m and width 1 m and height 1.5 m and width 0.6 m and height 0.5 m. Sandstone towers in quartzose Nubian sandstone to the northeast of Aswan is interaction processes leading to Karst development. Sandstone column in southern Egypt exhibit drainage net similar in many ways to limestone. In Western Desert, there is Karst in width 75 cm and height 45 cm and width 1 m and height 1.5 m and width 0.6 m and height 0.5 m. Kurkur area in Western Desert, the Karst at the lower end of joints in width 70 cm and height 40 cm and width 1 m and height 1.5 m and width 0.6 m and height 0.5 m. These witnesses of the Karst into Nubian sandstone pay attention for us about the role of these structures for controlling the groundwater flow of the Nubian aquifer and their recharging process.

The presence of Karst structures into Nubian sandstone explained two things: the first one is these structures are can be found in subsurface within the Nubian sandstone and they produce seepage for recharging the groundwater aquifer through the surface water of Nasser Lake. The Karst as a hydraulic structure can be modeled and its polarimetric scattering property can be used for defining it hydraulic flow properties referring to the results in chapter5.

The implementation of the polarimetric approach for southwest Aswan area can be initially used based on the simulation for obtained fracture properties from surface exposeur and core samples. I correlate the geological conditions as well as fracture system of Mirror Lake, Kamaishi and southwest Aswan locations and summarization for the comparison of the subsurface fracture conditions at Mirror Lake, Kamaishi and southwest Aswan sites is presented in Table 6.1.

Table 6.1: Comparison of subsurface fracture systems for Mirror Lake, Kamaishi and southwest Aswan sites.

	USA **Mirror lake site**	**Japan** **Kamaishi site**	**Egypt** **Southwest Aswan**
Rock type	sillimanite- grade schist intruded by granite, pegmatite, and lesser amounts of lamprophyre	Sedimentary rocks and two igneouse complex (Kurihashi and Ganidake granodiorite)	Nubian sandstone overlain basement complex
Rock fracture properties	Fracture zones- surrounded by less fractured sets	Water filled fractures- host rock invaded by multiple veins	Fracture sets associated with structure tends – joints and seepages
Tectonic trends	N25E to 45E dips predominantly 60 to 67NW and 40 to 80SE	Several trends due to high seismicity effect	NW-SE, E-W, N-S and NE-SW

6.6 The detectability of subsurface fractures with surface geophysical methods

The integration of the polarimetric borehole radar and the surface geophysical measurements can assist in understanding the configuration of subsurface fracture network and its expected hydraulic water flow properties. In this part, I will demonstrate the contribution of surface geophysical methods for detecting subsurface geological structures such as fault planes and its associated fracture zones at southwest Aswan area and the expected share for implementing the polarimertic borehole radar and its polarimertic analysis in proposing hydraulic property of unknown subsurface fracture trends.

The tectonic settings of the south Egypt cases constitute a lot of deformation in subsurface rocks, especially to the south of Aswan area (as explained earlier). The subsurface geological structures can be extended to the ground surface such as fault planes or lineaments and usually they are hidden by sand or surface soils due to the weather effect. Thus, these fault systems and their accompanied fracture zones do not appear on the surface, and they can only be detected with sensing techniques such as geoelectric or geomagnetic methods. Geophysical measurements have been acquired at Tushka area (southwest Aswan) and it showed the presence of subsurface structures (fault systems) that contribute for recharging the groundwater aquifers from the water surface of Lake Nasser [3]. The reason that these subsurface structures (faults and fracture zones) influence the hydrological system in this area is the sedimentary cover not being so thick and the main groundwater aquifer (Fractured sandstone) being connected to Lake Nasser. The geological structure could be obtained from the interpreted results of Vertical Electrical Sounding (VES’s). These results provide an insight to the primary connection between the water recharge from Lake Nasser to the groundwater aquifer and the role of subsurface fractures in this process.

The geoelectric section A-A′, as shown in Figure.6.5, parallel to Khor Tushka and extending in a SE to NW direction, demonstrates that the main aquifer is represented by the saturated Nubian sandstone. This is considered as the lowest resistivity layer, resistivity of which ranges from 70 ohm-m in the southeastern part (near Lake Nasser) to about 180 ohm-m in the northwest areas. This later variation of the resistivity values for the main groundwater aquifer indicates that the water saturation of that aquifer is high near the Lake Nasser and confirms the occurrence of recharging mechanism from Nasser Lake into Nubian aquifer. It shows also that the basement rock surface is affected by four fault lines. This is indicated by the sudden appearance of a high resistivity layer. The resistivity of this layer can reach more than 7,000 ohm-m. Note that these are the faults, which affected the upper Nubian aquifer to be fractured sandstone type. However, these fractures occurrences cannot be determined by VES's measurements due to the high saturation of the aquifer. These fracture zones presence can be determine with the full polarimetric borehole radar and their expected hydraulic property can be evaluated using the polarimetric approach for the simulated fracture models with implementing their parameters (fracture width, fracture materials and fracture orientation) referring to the obtained results of fracture characterization for Mirror Lake test site.

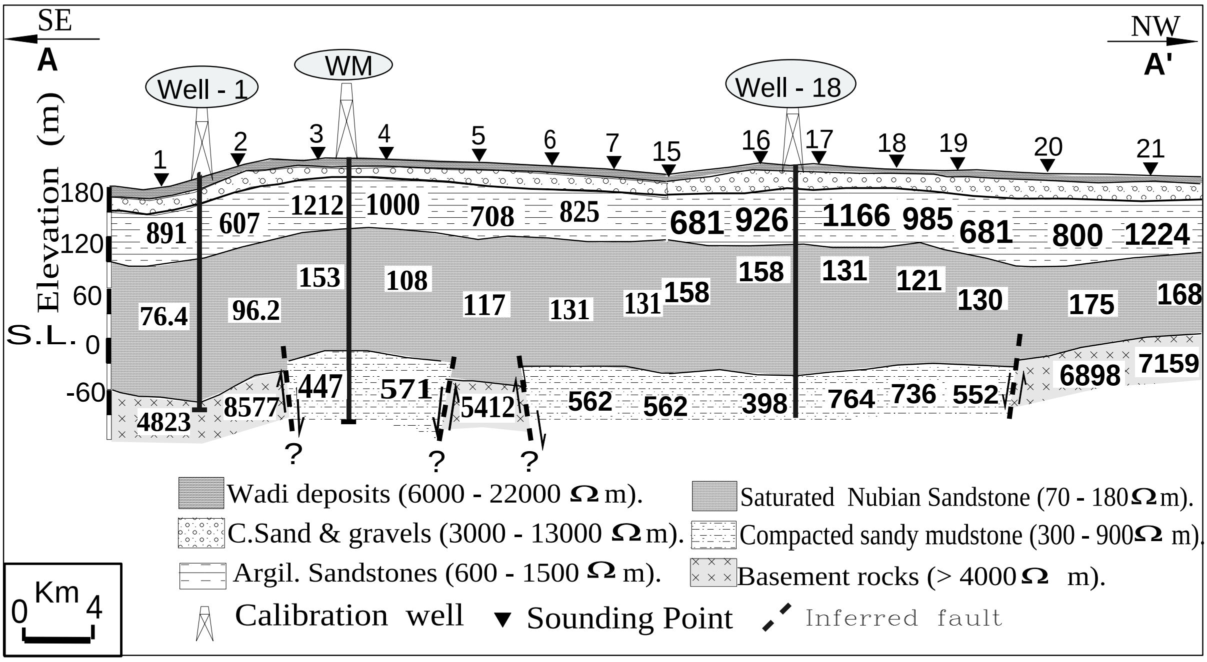

Fig.6.5: Geoelectric section A-A′ demonstrates the lithology sequence.

A land magnetic survey was undertaken in that area to estimate the structure in the basement rock as well as the extension of these structures to the upper sedimentary covers. The geomagnetic results in Figure.6.6 indicate that the most predominant tectonic trends are the N45–65E, N35–45W and NNE–SSW ones. The least predominant trend is the E–W tectonic one; these structure trends are possible due to local tectonic effects. From the correlation of the interpreted fault locations and water resources, it appears that the faults having a NE trend are primarily responsible for conduction and recharging of the water aquifers. Furthermore, a correlation exists between the locations of the faults inferred along the geoelectric cross sections and their locations from the magnetic trend analysis. The results indicate that these faults are caused by the basement tectonics.

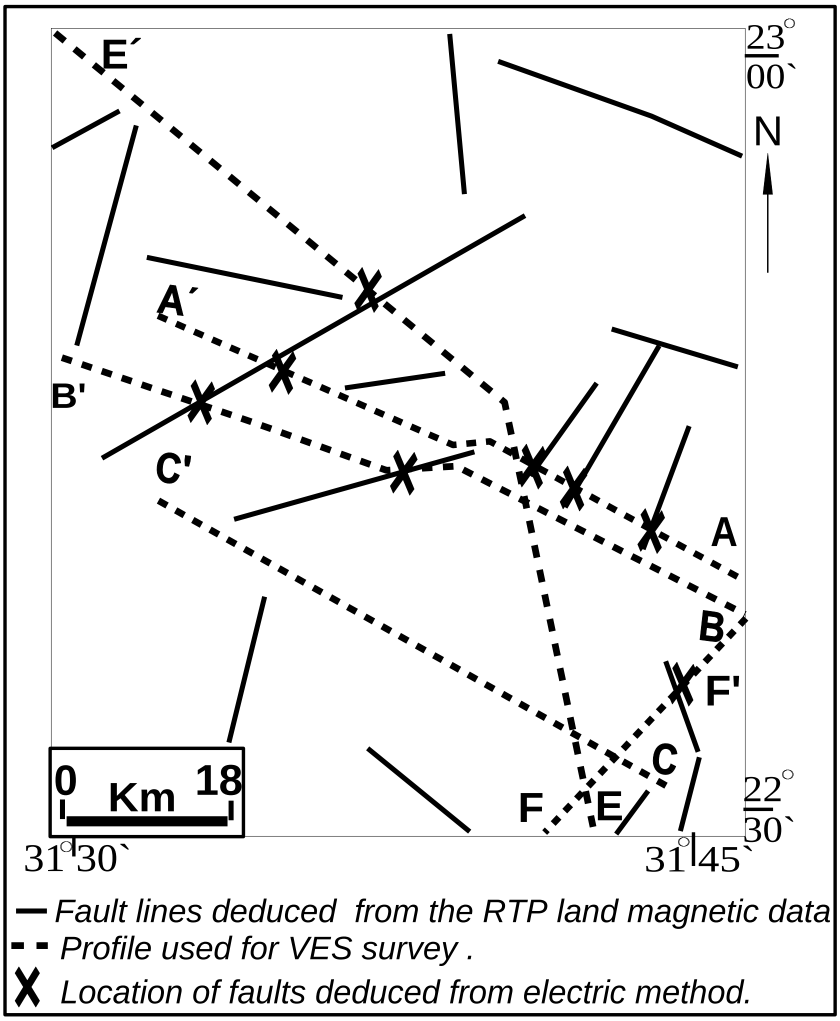

Fig.6.6: Structure map deduced from land geomagnetic survey.

Another surface geophysical study using EM method around the shore line of Lake Nasser provides the 2D resistivity cross sections, which demonstrate a characterized low resistivity zones corresponding to a valley depression, saturated by water from Nasser Lake. This study reveals also the interaction of surface water for recharging the groundwater aquifer from the lake.

In this area, as a case study, I zoomed out the contribution of using the surface geophysical methods for detection of subsurface structures and its relevant fracture zones. However, the determination of the expected hydraulic properties of the fracture zones with respect to certain fracture direction set cannot be obtained with surface methods. On the contrary, the polarimetirc analysis of the measured borehole radar dataset can realize these conclusions and it will increase our understanding about the hydrological properties of the Nubian aquifers as well as accurately design future plans for managing water resources in these aquifers.

6.7 The prospective proposal and summary

The contribution of subsurface facture zones in hydrological situation of the groundwater aquifers in Egypt has been described in this chapter at southwest Aswan area. The fracture zones, accompanied with fault systems, contribute toward recharging of the groundwater aquifers either from the surface water (such as Lake Nasser) or internal water flow between the Nubian bearing formations. These results previewed in this chapter initiated a further investigation of how far the water of the Nile River is recharging the aquifers adjacent to its sides, especially for near zones from the River Nile course, and up to which extent this takes place. The proposed research has two important aspects in the context for Egypt. First, the extension of cities and villages around the river Nile is toward the west and east sides of the Nile banks and it will mostly depend on the groundwater resource for irrigation and drinking. Second, we can monitor the amount of infiltrated water from the Lake Nasser into subsurface aquifers and forecast the amount that annually can recharge into the Nubian aquifer that may affect the quality of groundwater. This also determines the expected development based on the usage of groundwater in these locations.

The fracture properties of the basement rock and the overlain Nubian sandstone at southwest Aswan area have been described based on the surface exposed rock units and the cored samples. The fractures have formed in that region due to tectonic actions, the weight pressure of water of Lake Nasser and physical erosion due to so heavy rain in the Holocene age. It was found at southwest Aswan area that fracture zones have different widths as in some cases it be 3 to 4 cm in the basement complex and up to 30cm for the Nubian Karst sandstone feature. The implementation of FDTD modeling for the observed fracture parameters at Aswan area can be used for defining their hydraulic characteristic related to the polarimertic analysis and the obtained results of Mirror Lake fracture test site.

The full polarimetric borehole radar system in this research, with integration of surface geophysical measurements (geoelectric, electromagnetic, geomagnetic and seismic), can differentiate the fracture zones in subsurface for several characterized fracture sets as in crystalline, limestone and sandstone rock types. Thus, the similar fracture zones or sets can be formed due to the same tectonic process and they may end up having similar hydraulic property. The advantage of the polarimetric borehole radar system as subsurface sensing tool is that it characterizes the whole fracture sets within the measured depths inside the borehole while it cannot be obtained from surface geophysical measurements and also may not be easily determined with other well logging methods. Finally, it is a cost effective method in contrast with other hydraulic borehole tests. In addition, it can be an alternative technique for obtaining subsurface fracture hydraulic characteristics indirectly.

Chapter 7

Conclusions

7.1 Conclusions

The polarimetric borehole radar system was described in this thesis and its results have been analyzed intensively based on the three eigenvector parameters entropy, anisotropy and alpha. These results provide the information about the physical properties of subsurface fractures and their electromagnetic scattering. For the validation and the reliability of this polarimetric approach and its analysis for subsurface characterization, the forward electromagnetic modelings of determined fracture models have been simulated with FDTD technique. The fractal fracture was used as a model in this research work as the closest representation of the fractures in nature. The fracture zone was assumed to be a homogenous and water filled type. The obtained polarimetric analysis for the simulation results provided the reliability of the same analysis of the measured polarimetric borehole radar data. According to these conclusions, the full polarimetric borehole radar system based on a polarimetric analysis has the potentiality to provide physical quantities related to subsurface fractures, which generally cannot be obtained by other geophysical tools. In addition, determination of rock fracture hydraulic property using hydraulic tracer testing is an expensive technique. The polarimetric borehole radar system proves to be a promising tool for fracture characterization and as a consequence to identify transmissive flow paths within fractured rocks.

In Chapter 2, three kinds of borehole radar systems have been introduced and shown. The structure of the full polarimetric has been explained and its antenna configurations. The polarization properties of dipole antenna and slot antennas have been figured out and it was shown how these two antennas combinations can acquire a full polarimetric radar dataset. Thus, this polarization property of these two antennas enabled us to measure the scattering properties of the measured objects, especially which have irregular shape such as subsurface fractures. Two field studies of the measurement of the polarimetric borehole radar system have been clarified for subsurface fracture examination. The first one was for fracture test site in Mirror Lake, USA and the other one was briefly shown for Kamaishi site, Japan. The measurements in Mirror Lake field has an important role for the evolution of our polarimetric borehole radar system because the hydraulic tracer fracture tests have been acquired for that site which can be used for correlating our polarimetric borehole radar analysis while it is not available for Kamaishi test field.

In chapter3, it was shown that the information of the rock fracture surfaces can be obtained with the scanning profilometer apparatus. Thus, a precise data for the fracture surface is derived by the laser profilometer. The power spectral method has been implemented for the modeling of the fracture surface. The fracture model roughness property can be controlled depending on three factors. These are the fractal dimension, fracture surface spatial frequency contents and the proportional constant parameter (C). The fracture aperture was created from fracture surfaces (lower and upper) that the upper and lower fracture surfaces have the same amplitude components and different random phase numbers. Some fracture models that I simulate in this research work are representing fracture zone, in reality it contains inhomogeneous filled materials such as rock fragments, rock matrix, water and air. For simplification, I assumed that the fracture zone is a homogeneous with water filled. The fracture roughness was adjusted by the proportional constant parameter (C). The variation of this parameter generates varied rough fracture models with different RMS heights but in the same time keeping the correlation length to be the same. This is an important property we want to preserve for the FDTD fracture simulation as in this research we concern with fracture roughness parameter and its width variations.

In chapter4, the rough fracture models as target in FDTD simulator have been done. The backscattered electromagnetic waves of the fracture were examined and the difference of reflection for the rough and flat fractures case have been shown. The electromagnetic scatterings due to fracture (zone) material contents were showed when it contains water or air or oil. Thus, in each case I observed the behavior of the back reflected signals and how far the fracture content varies the electromagnetic scattering. The full polarimetric FDTD simulation data have been calculated for different rough fracture models. The polarimetric information of the simulated rough fractures has revealed the ability of the mean power scattering matrix for characterizing subsurface fractures qualitatively. Thus, full polarimetric electromagnetic simulations for varied rough fracture models have been measured and their mean power scattering matrixes have been determined. The full polarimetric backscattered electromagnetic wave shows proportional sensitivity change of cross polarization (VH and HV) components depending on the fracture roughness. These FDTD results and its polarimetric analysis of the mean power scattering matrix validated the initial polarimetric analysis of the measured polarimetric borehole radar data at Mirror Lake field. In addition, emphasizing the reliability of the mean power scattering matrix approach for subsurface fracture characterization has been confirmed with simulating various fracture aperture models and I determined the same analysis for these increase fracture apertures. The mean power scattering matrix of fracture aperture cases showed the variation of the cross polarization with varied rough as well as aperture fractures. From this chapter it can be concluded that full polarimetric borehole radar dataset can be used for subsurface fracture characterization qualitatively based on the mean power scattering matrix polarimetric analysis.

In chapter5, more concrete polarimetric analysis based on the three eigenvector parameters, entropy, anisotropy and alpha has been introduced. These three eigenvector parameters provide meaningful information related to characteristics of the ground surface as they are mostly used for the polarimetric analysis of the obtained SAR remote sensing data. Entropy, anisotropy and alpha were used for deriving the polarimetric analysis of the full polarimetric borehole radar dataset. In addition, the verification of utilizing the three polarimetirc parameters for fracture characterization has been shown by using electromagnetic forward modeling of different synthesized fracture models. The three polarimertic parameters revealed various distribution patterns with changing fracture roughness property. Electromagnetic numerical simulation results emphasized that the anisotropy parameter provides complementary information to the entropy and facilitates the interpretation of the scattering from rough fracture surfaces. Subsurface fracture characterization of the measured polarimetric borehole radar dataset has been shown based on the polarimetric analysis of the three eigenvector parameters. Thus, the polarimetirc analysis were estimated based on the single frequency datasets constructed at 30MHz, 40MHz, 50MHz, 60MHz, 70MHz, 80MHz, 90MHz and 100MHz. Furthermore, the comparison of the polarimertic analysis of different single frequencies has showed that the employment of lower single frequency polarimetric datasets is more reliable to understand the scattering mechanisms of different fractures as seen in the difference between 30MHz and 100MHz distributions.

The correlation of subsurface fracture characterization based on polarimetric analysis with hydraulic tracer test results that were measured by USGS showed a good consistency. The full polarimetric borehole radar system can share with an essential role for providing information related to the flow of water and its hydraulic property in fractured rocks. As in some cases, it can be an alternative tool to classify the groundwater flow in fractured rocks without using other geophysical methods.

Chapter 6 addresses the contribution of subsurface facture zones in hydrological situation of the groundwater aquifers in Egypt at Aswan area. The fracture zones, accompanied with fault systems, contribute toward recharging of the groundwater aquifers either from the surface water (such as Lake Nasser) or internal water flow between the Nubian bearing formations. These results previewed in this chapter initiated a further investigation of how far the water of the Nile River is recharging the aquifers adjacent to its sides, especially for near zones from the River Nile course, and up to which extent this takes place. The proposed research has two important aspects in the context for Egypt. First, the extension of cities and villages around the river Nile is toward the west and east sides of the Nile banks and it will mostly depend on the groundwater resource for irrigation and drinking. Second, we can monitor the amount of infiltrated water from the Lake Nasser into subsurface aquifers and forecast the amount that annually can recharge into the Nubian aquifer. As, this process affects the quality of groundwater as well as we may determine the expected horizontal development of a new urban societies depending on the usage of groundwater in these locations.

The fracture properties of the basement rock and the overlain Nubian sandstone at southwest Aswan area have been shown based on the surface exposed rock units and the cored samples. The fractures have formed in that region due to tectonic actions, the weight pressure of water of Lake Nasser and physical erosion due to so heavy rain in the Holocene age. It was found at southwest Aswan area that fracture zones have different widths as in some cases it be 3 to 4 cm in the basement complex and up to 30cm for the Nubian Karst sandstone feature. The implementation of FDTD modeling for the observed fracture parameters at Aswan area can be used for defining their hydraulic characteristic related to the polarimertic analysis with referring to the obtained results of Mirror Lake fracture test site.

The full polarimetric borehole radar system in this research, with integration of surface geophysical measurements (geoelectric, electromagnetic, geomagnetic and seismic), can differentiate the fracture zones in subsurface for several characterized fracture sets as in crystalline, limestone and sandstone rock types. Thus, the similar fracture zones or sets can be formed due to the same tectonic process and they may end up having similar hydraulic property. The advantage of the polarimetric borehole radar system as subsurface sensing tool is that it characterizes the whole fracture sets within the measured depths inside the borehole while it cannot be obtained from surface geophysical measurements and also may not be easily determined with other well logging methods. Finally, it is a cost effective method in contrast with other hydraulic borehole tests. In addition, it can be an alternative technique for obtaining different subsurface fracture hydraulic characteristics.

7.2 Further recommendations

The full polarimetric borehole radar system with the polarimetric analysis of its data represents an efficient technique for charactering subsurface fractures. In addition, electromagnetic forward simulation of determined fracture models has emphasized this conclusion. Further applications of the polarimetric borehole radar system of different fracture rock types are still needed in the future. For example, the fractures in limestone rock are complicated targets to be characterized and in the same time they control the presence and the flow of water inside it for many aquifers (western desert in Egypt). Applying the polarimetric borehole radar of that fractured rock type can be used for showing an advanced ability of that system for providing characteristics of these kinds of fractures in limestone rocks. Before that, the forward FDTD simulation can be used as guidance for examining the limitation and the reliability of using the full polarimetric borehole radar for characterizing fractures in different rock types.

Appendix A

EM reflectivity of flat fracture by ABCD matrix

The multiply reflection concept is a known term in seismic exploration. It can be observed also for electromagnetic waves. Especially if we have a large rectangular geometry object with a thick aperture width compare to the operating frequency range. Fault plane, geological cross bedding layers and sometime fracture zones can be the reason for this phenomenon to appear for the received GPR signals. Here, I focused on deriving the analytical solution for estimating the reflectivity of EM from such geometry targets (thick fracture planes or fracture zones) with using the ABCD (Cascade) matrix.

The calculation of total reflection for flat fracture geometry can be determined by using transmission line theory as shown in the model of Figure A.1.

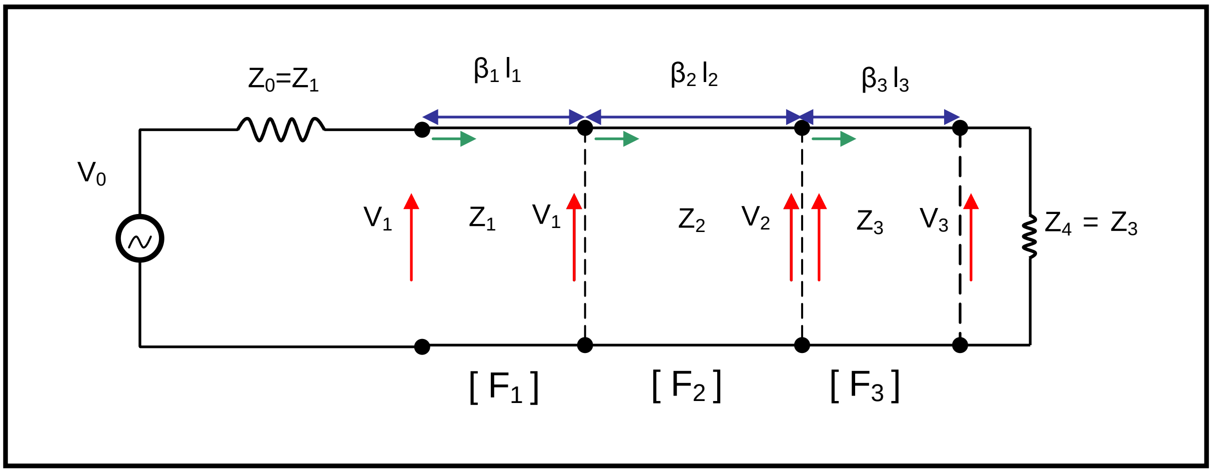

Fig. A.1: Transmission line model of flat fracture.

The formula for Cascade (ABCD) matrix F1, F2, F3 is

$$\begin{pmatrix} V_1 \\ I_1 \end{pmatrix} = F_1\ F_2\, F_3 \begin{pmatrix} V_4 \\ I_4 \end{pmatrix} \qquad (A.1)$$

Where $F = F_1 * F_2 * F_3$

So the previous equation can be rewrite as

$$\begin{pmatrix} V_1 \\ I_1 \end{pmatrix} = F \begin{pmatrix} V_4 \\ I_4 \end{pmatrix} \qquad (A.2)$$

Hence $F = \begin{pmatrix} A & B \\ C & D \end{pmatrix}$

By manipulating the transmission line equivalent circuits we can modify the model in Figure A.1 to one in Figure A.2.

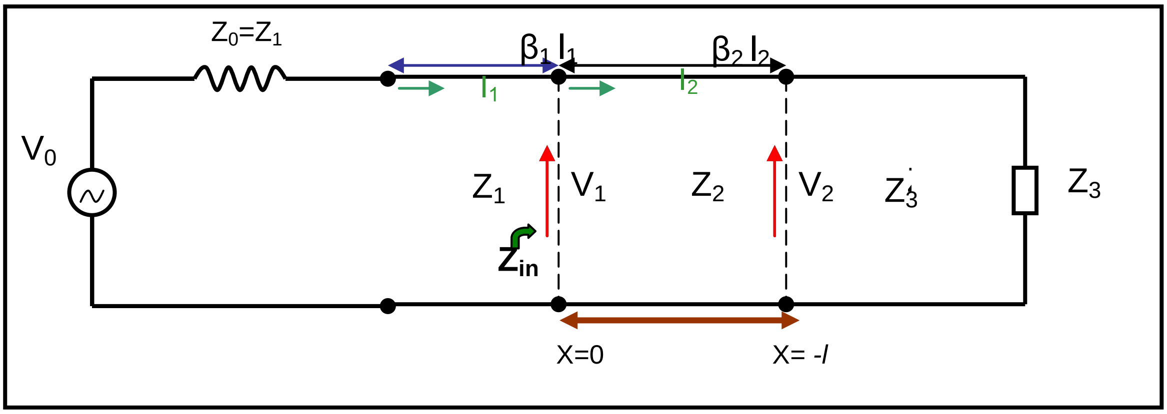

Fig.A.2: Transmission line model of flat fracture after modification.

From the model of Figure A.2, We can get the total characteristics impedance of this model as in Equation A.3.

$$\begin{pmatrix} V_0 - Z_1 I_1 \\ I_1 \end{pmatrix} = \begin{pmatrix} \cos(\beta_1 l_1) & jZ_1 \sin(\beta_1 l_1) \\ j/Z_1 \sin(\beta_1 l_1) & \cos(\beta_1 l_1) \end{pmatrix} \begin{pmatrix} I_2 Z_{in} \\ I_2 \end{pmatrix} \qquad (A.3)$$

Hence the characteristics impedance Z_{in} has the form in Equation A.3.

$$Z_{in} = Z_2 \left(\frac{Z_3 + jZ_2 \tan(\beta_2 l_2)}{Z_2 + jZ_3 \tan(\beta_2 l_2)} \right) \qquad (A.4)$$

Thus, the formula for cascade (ABCD) matrix F1, F2, F3 is

$$\begin{pmatrix} V_1 \\ I_1 \end{pmatrix} = F_1 \; F_2 \, F_3 \begin{pmatrix} V_4 \\ I_4 \end{pmatrix}$$

Where $F = F_1 * F_2 * F_3$

So the previous equation can be rewrite as

$$\begin{pmatrix} V_1 \\ I_1 \end{pmatrix} = F \begin{pmatrix} V_4 \\ I_4 \end{pmatrix}$$

Hence $F = \begin{pmatrix} A & B \\ C & D \end{pmatrix}$

From Equation A.3 we can derive

$$V_0 - Z_1 I_1 = I_2 Z_{in} \cos\left(\beta_1 l_1\right) + jZ_1 I_2 \sin\left(\beta_1 l_1\right) \qquad (A.5)$$

And

$$I_1 = I_2 \left(\frac{jZ_{in}}{Z_1} \sin\left(\beta_1 l_1\right) + \cos\left(\beta_1 l_1\right) \right) \qquad (A.6)$$

From Equation A.6

$$I_2 = \frac{I_1}{\frac{jZ_{in}}{Z_1} \sin\left(\beta_1 l_1\right) + \cos\left(\beta_1 l_1\right)} \qquad (A.7)$$

By substituting of Equation A.7 in Equation A.5 we get

$$V_0 - Z_1 I_1 = I_1 \left(\frac{Z_{in} \cos(\beta_1 l_1) + jZ_1 \sin(\beta_1 l_1)}{j \frac{Z_{in}}{Z_1} \sin(\beta_1 l_1) + \cos(\beta_1 l_1)} \right) \qquad (A.8)$$

$$V_0 = I_1 \left[Z_1 + \left(\frac{Z_{in} \cos(\beta_1 l_1) + jZ_1 \sin(\beta_1 l_1)}{j \frac{Z_{in}}{Z_1} \sin(\beta_1 l_1) + \cos(\beta_1 l_1)} \right) \right] \qquad (A.9)$$

$$I_1 = \frac{V_0}{Z_1 + \left(\frac{Z_{in} \cos(\beta_1 l_1) + jZ_1 \sin(\beta_1 l_1)}{j \frac{Z_{in}}{Z_1} \sin(\beta_1 l_1) + \cos(\beta_1 l_1)} \right)} \qquad (A.10)$$

$$= \frac{V_0}{\left(\frac{Z_{in} \cos(\beta_1 l_1) + jZ_1 \sin(\beta_1 l_1) + jZ_{in} \sin(\beta_1 l_1) + Z_1 \cos(\beta_1 l_1)}{j \frac{Z_{in}}{Z_1} \sin(\beta_1 l_1) + \cos(\beta_1 l_1)} \right)} \qquad (A.11)$$

$$= \frac{V_0 \left(j \, {}^{Z_{in}}\!/_{Z_1} \sin(\beta_1 l_1) + \cos(\beta_1 l_1) \right)}{\left(Z_{in} \cos(\beta_1 l_1) + jZ_1 \sin(\beta_1 l_1)) + (jZ_{in} \sin(\beta_1 l_1) + Z_1 \cos(\beta_1 l_1) \right)} \qquad (A.12)$$

By using the nominator of Equation A.12 as Δ

$$\Delta = \left((Z_{in}\cos(\beta_1 l_1) + jZ_1 \sin(\beta_1 l_1)) + (jZ_{in}\sin(\beta_1 l_1) + Z_1 \cos(\beta_1 l_1))\right)$$

$$= \left(Z_{in}(\cos(\beta_1 l_1) + j\sin(\beta_1 l_1)) + Z_1(\cos(\beta_1 l_1) + j\sin(\beta_1 l_1))\right)$$

$$= Z_{in}\exp^{+j\beta_1 l_1} + Z_1 \exp^{+j\beta_1 l_1}$$

$$= (Z_{in} + Z_1)\exp^{+j\beta_1 l_1}$$

$$\frac{1}{\Delta} = \frac{1}{(Z_{in} + Z_1)\exp^{+j\beta_1 l_1}} = \frac{\exp^{-j\beta_1 l_1}}{(Z_{in} + Z_1)}$$

By using the dominator of Equation A.12 as Ω

$$\Omega = V_0\left(j\frac{Z_{in}}{Z_1}\sin(\beta_1 l_1) + \cos(\beta_1 l_1)\right)$$

Using Euler's formula we get

$$\Omega = V_0\left(\frac{jZ_{in}}{Z_1}\left(\frac{\exp^{j\beta_1 l_1} - \exp^{-j\beta_1 l_1}}{2j}\right) + \left(\frac{\exp^{j\beta_1 l_1} + \exp^{-j\beta_1 l_1}}{2}\right)\right)$$

$$= \frac{V_0}{2Z_1}\left(Z_{in}\left(\exp^{j\beta_1 l_1} - \exp^{-j\beta_1 l_1}\right) + Z_1\left(\exp^{j\beta_1 l_1} + \exp^{-j\beta_1 l_1}\right)\right)$$

$$= \frac{V_0}{2Z_1}((Z_1 + Z_{in})\exp^{j\beta_1 l_1} + (Z_1 - Z_{in})\exp^{-j\beta_1 l_1})$$

From Δ and Ω we can get I_1

$$I_1 = \frac{\Omega}{\Delta} = \frac{\frac{V_0}{2Z_1}\left((Z_1 + Z_{in})\exp^{j\beta_1 l_1} + (Z_1 - Z_{in})\exp^{-j\beta_1 l_1}\right)}{(Z_{in} + Z_1)\exp^{+j\beta_1 l_1}}$$

$$I_1 = \frac{V_0}{2Z_1}\left(1 - \Gamma\exp^{-2j\beta_1 l_1}\right) \qquad (A.13)$$

By replacing the voltage instead of current in last Equation A.13 we obtain

$$V_1 = V_0 - Z_1 \frac{V_0}{2Z_1}\left(1 - \Gamma \exp^{-2j\beta_1 l_1}\right)$$

As we have $V_1 = V_0 - Z_1 I_1$

So further we can get

$$= V_0 - \frac{V_0}{2}\left(1 - \Gamma \exp^{-2j\beta_1 l_1}\right)$$

$$V_1 = \frac{V_0}{2}\left(1 + \Gamma \exp^{-2j\beta_1 l_1}\right) \qquad (A.14)$$

Where

$$\Gamma = \frac{Z_{in} - Z_1}{Z_{in} + Z_1} \qquad \Gamma_1 = \frac{Z_2 - Z_1}{Z_2 + Z_1} \qquad \Gamma_2 = \frac{Z_3 - Z_2}{Z_3 + Z_2} \quad (A.15)$$

From relations in (A.15) we can have

$$\Gamma = \frac{Z_{in} - Z_1}{Z_{in} + Z_1} = \frac{Z_2\left(1 + \Gamma_2 \exp^{-2j\beta_2 l_2}\right) - Z_1\left(1 - \Gamma_2 \exp^{-2j\beta_2 l_2}\right)}{Z_2\left(1 + \Gamma_2 \exp^{-2j\beta_2 l_2}\right) + Z_1\left(1 - \Gamma_2 \exp^{-2j\beta_2 l_2}\right)}$$

$$= \frac{Z_2 - Z_1 + (Z_2 + Z_1)\left(\Gamma_2 \exp^{-2j\beta_2 l_2}\right)}{Z_2 + Z_1 + (Z_2 - Z_1)\left(\Gamma_2 \exp^{-2j\beta_2 l_2}\right)}$$

$$\Gamma = \frac{\Gamma_1 + \Gamma_2 \exp^{-2j\beta_2 l_2}}{1 + \Gamma_1 \Gamma_2 \exp^{-2j\beta_2 l_2}} \qquad (A.16)$$

By adding $-\Gamma_1^2 \Gamma_2 \exp^{-2j\beta_2 l_2} + \Gamma_1^2 \Gamma_2 \exp^{-2j\beta_2 l_2}$ to the nominator of Equation A.16 we can get

$$\Gamma = \frac{\Gamma_1 - \Gamma_1^2 \Gamma_2 \exp^{-2j\beta_2 l_2} + \Gamma_1^2 \Gamma_2 \exp^{-2j\beta_2 l_2} + \Gamma_2 \exp^{-2j\beta_2 l_2}}{1 + \Gamma_1 \Gamma_2 \exp^{-2j\beta_2 l_2}}$$

$$\Gamma = \Gamma_1 + \left(1 + \Gamma_1\right) \frac{\Gamma_2 \exp^{-2j\beta_2 l_2}}{1 + \Gamma_1 \Gamma_2 \exp^{-2j\beta_2 l_2}} \left(1 - \Gamma_1\right) \qquad (A.17)$$

Where we can modify this part $\frac{\Gamma_2 \exp^{-2j\beta_2 l_2}}{1+\Gamma_1\Gamma_2 \exp^{-2j\beta_2 l_2}}$ in Equation A.17 to be

$$\frac{\Gamma_2 \exp^{-2j\beta_2 l_2}}{1+\Gamma_1\Gamma_2 \exp^{-2j\beta_2 l_2}} = \Gamma_2 \exp^{-2j\beta_2 l_2} + \left(-\Gamma_1\right)\Gamma_2^2 \exp^{-4j\beta_2 l_2} + \left(-\Gamma_1\right)^2 \Gamma_2^3 \exp^{-6j\beta_2 l_2} + \ldots\ldots\ldots\ldots\ldots\ldots\ldots$$

Where

$$\frac{x}{1+\alpha x} = \sum_{n=1}^{\infty} (-\alpha)^{n-1} x^n = x^1 + (-\alpha)^1 x^2 + (-\alpha)^2 x^+ + \ldots\ldots\ldots\ldots\ldots\ldots$$

Based on this last configuration Equation A.17 can be rewrite as

$$\Gamma = \Gamma_1 + \left(1+\Gamma_1\right)\left(\exp^{-j\beta_2 l_2} \Gamma_2 \exp^{-j\beta_2 l_2} + \exp^{-j\beta_2 l_2} \Gamma_2 \exp^{-j\beta_2 l_2} (-\Gamma_1) \exp^{-j\beta_2 l_2} \Gamma_2 \exp^{-j\beta_2 l_2}\right)\left(1-\Gamma_1\right) + \ldots\ldots \qquad (A.18)$$

By substituting of Equation A.18 into Equation A.14 we obtain

$$V_1 = \frac{V_0}{2}\left(1 + \exp^{-2j\beta_1 l_1} \Gamma_1 + \exp^{-2j\beta_1 l_1} \left(1+\Gamma_1\right)\left(\exp^{-j\beta_2 l_2} \Gamma_2 \exp^{-j\beta_2 l_2} + \exp^{-j\beta_2 l_2} \Gamma_2 \exp^{-j\beta_2 l_2} (-\Gamma_1) \exp^{-j\beta_2 l_2} \Gamma_2 \exp^{-j\beta_2 l_2}\right)\left(1-\Gamma_1\right) + \ldots\ldots\ldots\right)$$

$$V_1 = \frac{V_0}{2}\left(1 + \exp^{-2j\beta_1 l_1} \Gamma_1 + \exp^{-2j\beta_1 l_1} \left(1+\Gamma_1\right)\left(\sum_{n=1}^{\infty} (-\Gamma_1)^{n-1} \left(\Gamma_2 \exp^{-2j\beta_2 l_2}\right)^n\right)\left(1-\Gamma_1\right)\right) \qquad (A.19)$$

Equation A.19 is expressing the total voltage for thin flat fracture V_1 as a function of source voltage V_0 and the reflection coefficient Γ_1 and Γ_2.

The received electromagnetic signal wave form is composed of superposition of multiple reflections due to flat fracture geometry with relatively small aperture compare to the frequency band width of incident pulse. Figure A.3 (a) shows mathematical solution for model with 20 cm width, for the zoomed part we can see different reflected signal that should be superimposed on each other. ***I*** represent the reflection from upper surface, ***II*** is the reflection from the lower surface and ***III*** represents first internal reflection inside flat fracture between upper and lower surfaces. Figure A.3 (b) illustrates the same behavior. But in that case, we use 3cm fracture width which can be close to the case of fracture zone that we sometimes simulated.

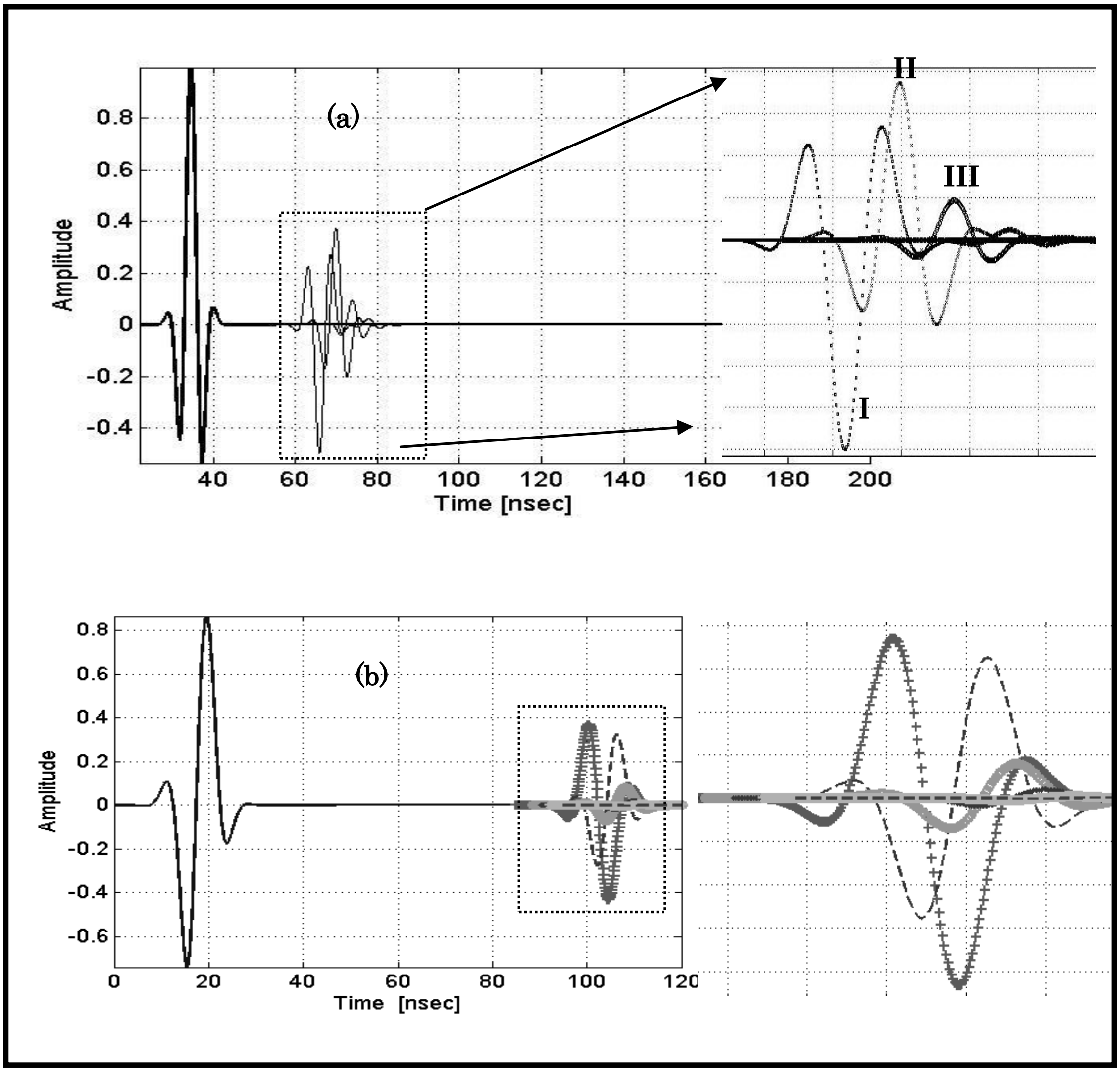

Fig.A.3: Representation for analytical solution of EM multiple reflection from (a) 20 and (b) 3 cm flat aperture.

References

Chapter 1

[1] Kranz, R,L., A.D. Frankel, T. Engelder, and C.H. Scholz, 1979, The permaebailty of whole and jointed Barre granite: Int.J.Rock Mech. Min. Sci. Geomech. Abstr., 16,225-2234.

[2] M. Sato M. Takeshita, T. Miwa, and J. W. Lane, Jr., 1999, Polarimetric borehole radar measurement at the Mirror Lake test site: Proc. SPIE, vol. 3752, pp. 104–112.

[3] K. Mansour and M. Sato, 2010, FDTD simulation of electromagnetic wave scattering from a rough surface synthesized by Fractal theory: in Proceeding of The Formation Evaluation Symposium of Japan, E1-E7.

[4] Mandelbrot B.B. 1982, The Fractal Geometry of Nature: W.H. Freeman.

[5] M. Sato and T. Takeshita, 2000, Estimation of subsurface fracture roughness by polarimetric borehole radar: IEICE Trans. Electron., vol.83, no12.

[6] Daniels, D.J., 2004, Ground Penetrating Radar, 2nd edition, Radar, Sonar, Navigation and Avionics Series15, Institute of Electrical Engineers (IEE), London, UK.

[7] Annan, A.P. and J.L. Davis (1976), Impulse radar sounding in permafrost, Radio Science, 11, 383–394.

[8] Morey, R.M. (1974), Continuous sub-surface profiling by impulse radar, in Proceedings Conference on Subsurface Exploration for Underground Excavation and Heavy Construction', pp. 213–232.

[9] Davis, J.L. and A.P. Annan (1989), 'Ground-penetrating radar for high-resolution mapping of soil and rock', *Geophysical Prospecting* **37**, 531–551.

[10] Leimbach, G. and H. Lowy (1910), *German Patent*, No. 237944.

[11] Rubin, L.A., J.C. Fowler and G.G. Marino (1978), Borehole radar, Technical report, Ensco

[12] Wright, D.L. and R.D. Watts (1982), A single-hole, short-pulse radar system, Technical report, Geophysical investigations in connection with geological disposal of radioactive waste. OECD/NEA, Ottawa, Canada.

[13] Bradley, J.A. and D.L. Wright (1987), Microprocessor-based data-aquisition system for a borehole radar, *IEEE Transactions on Geoscience and Remote Sensing* GE-25, 441–447.

[14] Nickel, H., F. Sender, R. Thierbach and H.Weichart (1983), Exploring the interior of salt domes from boreholes, *Geophysical Prospecting* **31**, 131–148.

[15] Thierbach, R. (1994), Twenty years of ground probing radar in salt and potash mines, *in* Proceedings of 5th International Conference on GPR.

[16] Halleux, L., P. Feller, A. Monjoie and R. Pissart (1992), Ground penetrating and borehole radar surveys in the Borth salt mine (FRG), Proceedings of 4th International Conference on GPR.

[17] Olsson, O., E. Falk, O. Forslund, L. Lundmark and E. Sandberg (1992), Borehole radar applied to the characterization of hydraulically conductive fracture zones in crystalline rock, *Geophysical Prospecting* **40**, 109–142.

[18] Miwa, T., M. Sato and H. Niitsuma (1999), Subsurface Fracture Measurement with Polarimetric Borehole Radar, *IEEE Transactions on Geoscience and Remote Sensing* **37**, 828–837.

[19] Cardarelli, E., C. Marrone and L. Orlando (2003), Evaluation of tunnel stability using integrated geophysical methods, *Journal of Applied Geophysics* **52**, 93–102.

[20] Wanstedt, S., S. Carlsten and S. Tiren (2000), Borehole radar measurements aid structure geological interpretation, *Journal of Applied Geophysics* **43**, 227–237.

[21] Topp, G.C., J.L. Davis and A.P. Annan (1980), Electromagnetic determination of soil water content: Measurements in coaxial transmission lines, *Water Resources Research* **16**, 574–528.

[22] Annan, A.P. (1996), Transmission dispersion and GPR, *Journal of Environmental Engineering and Geophysics* **0**, 125–136.

[23] Galagedara, L.W., G.W. Parkin, J.D. Redman and A.L. Endres (2002), Temporal and spatial variation of soil water content measured by borehole GPR under irrigation and drainage, Proceedings of 9th International Conference on GPR’, pp. 180–185.

[24] Zhao and Sato, (2006), Radar polarimetry alanlysis applied to single-hole fully polarimetric borehole radar, IEEE Trans. Geosciences & Remote Sensing, vol.44, no. 12, pp 3547-3554.

Chapter 2

[1] Sheriff, R.E. and L.P. Geldart, (1982), Exploration Seismology, Cambridge University, Press (New York).

[2] S., Liu, M., Sato and K., Takahashi, (2004), Application of borehole radar for subsurface physical measurement, J., Geophysics Eng., Vol., 1, P 221–227.

[3] R., C., Johnson, (1993), Antenna Engineering Handbook, McGraw-Hill, New York, NY, 2nd Ed., pp.8(6)-8(9).

[4] T., Takayama, (2009), Radar applications to temporal change monitoring of environment, PhD thesis, Tohoku University.

[5] M. Sato and T. Miwa, (2000), Polarimetric Borehole Radar System for Fracture Measurement," *Subsurface Sensing Technologies and Applications*, vol. 1, no. 1, pp. 161-175.

[6] K. lizuka, and A. Freundorfer, (1983), Detection of nonmetallic buried objects by a step frequency radar, in *Proc. IEEE*, vol. 71, no. 2, pp. 276-279.

[7] J. A. Bradley and D. L. Wright, (1987), Microprocessor-based data acquisition system for a borehole radar, *IEEE Trans. on Geosci. and Remote Sensing*, vol. GE-25, no. 4, pp. 441-447.

.

[8] D. L. Wright, R. D. Watts and E. Bramsoe, (1984), A short-pulse electromagnetic transponder for hole-to-hole use, IEEE Trans. on Geosci. and Remote Sensing, vol GE-22, no. 6, pp. 720-725.

[9] J. R. Wait, (1959), Electromagnetic Radiation from Cylindrical structure, Pergamon, London, pp. 48-60.

[10] H., Mott, (1992), Antennas for Radar and Communications-A Polarimetric Approach, John Wiley and Sons, New York, NY.

[11] Hsieh, P.A., (1993), Some Experience gained from using packers and transducers in ground-water investigations of crystalline-rock aquifers, in Latkovich, V. J., ed., Proceedings of a pressure transducer-packer workshop, June 25-28, 1991: U.S. Geological Survey Open-File Report 93-71, p. 5-7.

[12] J. W. Lane, Jr, and F. P. Haeni, (1998), Use of a multi-offset borehole-radar reflection method in fractured crystalline bedrock at mirror lake, grafton county, new hampshire, *Proc. of symposium on the Application of Geophysics to Engineering and Environmental Problems*, pp. 359-368.

[13] D. L. Wright, J. W. Lane, Jr, “Mapping hydraulically permeable fractures using directional borehole radar and hole-to-hole tomography with a saline tracer” *Proc. of symposium on the Application of Geophysics to Engineering and Environmental Problems*, pp. 379-388, 1998.

[14] Lyons, J.B., Bothner, W.A., Moench, R.A., and Thompson, J.B., Jr., (1997), Bedrock geologic map of New Hampshire: U.S. Geological Survey State Geologic Map, 2 sheets, scales 1:250,000 and 1:500,000.

[15] Barton, C.B., (1996), Characterizing bedrock fractures in outcrop for studies of groundwater hydrology-An example from Mirror Lake, Grafton County, New Hampshire, *in* Morganwalp, D.W. and Aronson, D.A., eds., U.S. Geological Survey Toxic Substances Hydrology Program-Proceedings of the Technical Meeting, Colorado Springs, Colo., September 20-24, 1993: U.S. Geological Survey Water-Resources Investigations Report 94-4015, v. 1, p. 81 - 88.

[16] H. Zhou and M. Sato, (2004), Subsurface cavity imaging by crosshole borehole radar measurements, *IEEE Trans. on Geosc. and Remote Sensing*, vol. 42, no. 2, pp. 335-341.

[17] J. Peterson, B. Paulsson, and T. Mcevilly, (1985), Applications of algebraic reconstruction techniques to crosshole seismic data, *Geophysics*, vol. 50, no. 10, pp. 1566-1580.

[18] J., Zhao, (2006), Application of polarimetric technique to subsurface fracture characterization by borehole radar, PhD thesis, Tohoku University.

[19] Yoshida, H., Aoki, K., Semba, T., Ota, K., Amano, K., Hama, K., Kawamura, M., Tsubota, K., (2000), Overview of the stability and barrier functions of the granitic geosphere at the Kamaishi Mine: relevance to radioactive waste disposal in Japan, Eng. Geol. 56, 151– 162.

[20] Y. Nishi and T. Ishido, (2012), Characterization of Fractured Reservoirs Using a Combination of Downhole Pressure and Self-Potential Transient Data, Int., Journal of Geophysics, Vol., 2012.

Chapter 3

[1] Atkinson, B. K., (1989), Fracture Mechanics of Rock, Academic Press, pp. 548.

[2] Palmer, I. D. and D. P. Sparks (1991), Measurement of induced fractures by downhole TV camera in Black Warrior Basin coalbeds, *Journal of Petroleum Technology*, 43(3), 270.

[3] Overbey, W. K., L. E. Yost and A. B. Yost (1988) Analysis of natural fractures observed by borehole video camera in a horizontal well, paper SPE 17760 presented at the *1988 SPE Gas Technology Symposium*, Dallas, June 13-15

[4] Brown, A. R., R. L. Kranz and B. P. Bonner (1986), Correlation between the surfaces of natural rock joints, *Geophysical Research Letters*, 13(13), 1430-1433.

[5] Brown, A. R. and C. H. Scholz (1985), Broad bandwidth study of the topography of natural rock surfaces, *Journal of Geophysical Research*, 90(B14), 12575-12582.

[6] National Research Council (1996), Rock fractures and fluid flow: Contemporary understanding and applications, Washington, D.C., National Academy Press, 107-108 p.

.

[7] Brown, S. and C. H. Scholz, (1985), Broad bandwidth study of the topography of natural rock surfaces: Journal of Geophysical Research, 90:575–582.

[8] Power, W. L., T. E. Tullis, S. R. Brown, G. N. Boitnott, and C. H. Scholz (1987), Roughness of natural fault surfaces, Geophysics Research Letters, 14:29–32.

[9] Brown, S., (1995), Simple mathematical model of a rough fracture, Journal of Geophysical Research, 100:5941-52.

[10] Paillet, F. L., Hess, A. E., Cheng, C.H., and Hardin, E., (1987), Characterization of fracture permeability with high- resolution vertical flow measurements during borehole pumping, Ground water. 25, 28-40.

[11] Mandelbrot, B. B., (1982), The Fractal Geometry of Nature, W. H. Freeman, San Francisco.

[12] K., Matsuki, Y., Chida, K., Sakaguchi, P., W., J., Glover, (2006), Size effect on aperture and permeability of a fracture as estimated in large synthetic fractures, Int., Journal of Rock Mechanics and Mining Sciences, 43, 726-755.

Chapter 4

[1] Balanis, C. A., (1989), Advanced Engineering Electromagnetic, JohnWiley &Sons, New York.

[2] Yee, K.S., (1966), Numerical solution of initial boundary value problems involving Maxwell’s equations in isotropic media, IEEE Transactions on Antennas and Propagation. 14, 302–307.

[3] K. Kunz and R. Lubbers, (1993), The Finite Difference Time Domain Method for Electromagnetic, *Baca Raton, FL, CRC.*

[4] CST MICROWAVE STUDIO, (2009), 3D Electromagnetic simulator software, http://www.cst.com/Content/Products/MWS/Overview.aspx

[5] Motoyuki, Sato, Moriyasu Takeshita, Takashi Miwa and John W. Lane, Jr., (1999), Polarimetric borehole radar measurement at the Mirror Lake test site, Proc. SPIE 3752, 104.

[6] Jian-Guo Zhao, (2006), Application of polarimetric technique to subsurface fracture characterization by borehole radar, PhD thesis, Tohoku University, Japan.

[7] M. Sato and M. Takeshita, (1998), Polarimetric borehole radar applied to geophysical exploration, *Korea-Japan AP/EMC/EMT Joint Conference*, pp. 7-12.

[8] M. Sato, M. Takeshita, T. Miwa, and H. Niitsuma, (1998), Polarimetric borehole radar applied to geological exploration, *Proc. 7th Int. Conf. on Ground Penetrating Radar*, Lawrence, Kansas, USA, pp. 7-12.

[9] M. Sato and M. Takeshita, (2000), Polarimetric borehole radar approach to subsurface fracture classification, *Proc. 8th Int. Conf. on Ground Penetrating Radar*, Gold Coast, Australia, pp. 50-54.

[10] F. L. Paillet, A. E. Hess, C. H. Cheng and E. Hardin, (1987), Characterization of fracture permeability with high-resolution vertical flow measurements during borehole pumping, GROUND WATER, Vol., 25, No. 1.

Chapter 5

[1] Cloude, S.R. and E. Pottier, (1996), A review of target decomposition theorems in radar polarimetry, *IEEE Trans. GRS*, vol. 34(2), pp. 498-518.

.

[2] Cloude S.R. and E. Pottier, (1997), An Entropy-Based Classification Scheme for Land Applications of Polarimetric SAR, *IEEE Trans GRS*, vol. 35(1), pp. 68-78.

[3] M. Hellmann and E. Krogager, (2000), Comparison of decompositions for pol-SAR image interpretation, in *Proc. IGARSS*, Honolulu Hawaii, USA, Vol. 3, pp. 1313-1315.

[4] I., Hajnsek, E., Pottier and S., Cloude, (2003), Inversion of surface parameters from polarimetric SAR, *IEEE Trans. GRS*, vol. 41(4), pp. 727-743.

[5] Zhao and Sato, (2006), Radar polarimetry alanlysis applied to single-hole fully polarimetric borehole radar, IEEE Trans. Geosciences & Remote Sensing, vol.44, no. 12, pp 3547-3554.

[6] F. D. Day-Lewis, J. W. Lane, Jr., J. M. Harris, and S. M. Gorelick, (2003), Time-lapse imaging of saline-tracer transport in fractured rock using difference-attenuation radar tomography, *WATER RESOURSES RESEARCH*, vol. 39, no. 10, pp. 1-14.

[7] J. W. Lane, Jr, and F. P. Haeni, (1998), Use of a multi-offset borehole-radar reflection method in fractured crystalline bedrock at mirror lake, Grafton county, new Hampshire, *Proc. of symposium on the Application of Geophysics to Engineering and Environmental Problems*, pp. 359-368.

[8] J. W. Lane, Jr, F. P. Haeni, and G. Placzek, (1996), Use of borehole-radar methods to detect a saline tracer in fractured crystalline bedrock at Mirror lake, Grafton county, New Hampshire, USA, *Proc. 6th Int. Conf. on Ground Penetrating Radar*, Sendai, Japan, pp. 185-190.

[9] M. Suprajitno and S. A. Greenhalgh, (1985), Separation of upgoing and downgoing waves in vertical seismic profiling by contour-slice filtering, *Geophysics*, vol. 50, pp. 950-962.

[10] Jian-Guo Zhao, (2006), Application of polarimetric technique to subsurface fracture characterization by borehole radar, PhD thesis, Tohoku University, Japan.

[11] Jong-Sen Lee and Pottier Eric, (2009), Polarimetric radar imaging: from basics to applications, CRC Press, Taylor and Francis.

Chapter 6

[1] Ghoubashi S., 2010, Impact of Lake Nasser on the groundwater of the Nubia sandstone aquifer system in Tushka area, South Western Desert, Egypt: Journal of King Saud University-science, 24, 101-109.

[2] Metwaly M., Khalil M., Al-Sayed E. and Osman S., 2006, A hydrogeophysial study to estimate water seepage from northwestern Lake Nasser, Egypt: Journal of Geophysics and Engineering, 3, 21-27.

[3] Rabeh T., Beder S., Miranda M., Carvalho J., Khalil A., 2009, Subsurface

structures and hydrogeologic aquifers at the western side of Lake Nasser, Southwestern Desert, Egypt: Journal of Environmental & Engineering Geophysics, Vol. 14 No.2, pp.87-95.

[4] Powers C. J., Singha K and Haeni F., P., 1999, Integration of surface geophysical methods for fracture detection in bedrock at mirror lake, New Hampshire *U. S. Geological Toxic Substances Hydrology Program—Proc: Technical Meeting (Charleston, SC, 8–12 March)* ed D W Morganwalp and H T Buxton vol. 3, pp 757–68 *(USGS Water-Resources Investigations Report 99–4018C).*

[5] Monteiro S., Afonso A. R. and Dupis A., 2007, 2D joint inversion of dc and scalar audio-magnetotelluric data in the evaluation of low enthalpy geothermal fields: *J. Geophys. Eng.* **4** 53–62.

[6] Youssef M. I., 1968, Structural pattern of Egypt and its interpretation: Bull. Amer. Associ. Petroleum Geologists, 52, 5, 60–614.

[7] Kamel A. F., 1994, Regional fracture analysis south latitude 29^o N of Egypt and their influence on earthquakes: Natural Hazards, 9, 235–245.

[8] Kamel A. F. and Elsirafe A. M., 1994, Delineation and analysis of the surface and subsurface structural lineament patterns in the North Lake Nasser area and its surroundings, Aswan, upper Egypt: Int. J. Remote Sensing, 15 (7), 1471-1493.

[9] Gaber A., Koch M., Helmi M. and Sato M., 2011, SAR Remote Sensing of Buried

Faults: Implications for Groundwater Exploration in the Western Desert of Egypt: Sensing and Imaging: An International Journal. Vol. 12. No. ¾, pp. 133-151.

[10] Khalil M., Santos F., Moustafa S. and Saad U., 2009, Mapping water seepage from Lake Nasser, Egypt, using the VLF-EM method: a case study: Journal of Geophysics and Engineering, Vol. 6, pp. 101-110.

[11] Johnson C. D., 2006, Effects of Lithology and Fracture Characteristics on Hydraulic Properties in Crystalline Rock: Mirror Lake Research Site, Grafton County, New Hampshire: U.S. Geological Survey Water-Resources Investigations Report.

[12] Research Institute for Groundwater (RIGW), 1998, Hydrogeological Characteristics of Tushka area, Egypt.

[13] Bassem S. N., Pierre R., Yves G., 2009, Petrophysical and magnetic pore network anisotropy of some cretaceous sandstone from Tushka basin, Egypt: Geophys. J. Int., 177, 43-61.

[14] El Gammal E. S., 2010, New findings on the karst in Nubia sandstone southern Egypt: Natural and science, Vol., 8, 125-129.

[15] Ulf Thorweihe, 1990, Nubian aquifer system from The Geology of Egypt: Balkema Rotterdam Brookfield.

Acknowledgement

I would like to extend deepest gratitude to my supervisor, Prof. Motoyuki Sato, for all his support and guidance, persistence, patience, and suggestions throughout the time of my doctoral program.

I also thank my dissertation committee members Prof. Dr. Kunio Sawaya, Prof. Dr. Noriyoshi Tsuchiya and Prof. Dr. Tomochika Tokunaga for their instructive suggestion and encouragement to complete the thesis.

I am also grateful to Dr. M. Watanabe and Dr. T. Kido whom helped me so much and gave me a lot of my guidance during their being in Satolab. A lot of gratitude to Naoko Nakei who gave me so much helps to solve my administrative problems while I was in Satolab. I want to thank the stuff of Satolab: Dr Kazunori Takahashi and Dr Yuya Yokota for their help to me to finish this PhD. I would like to thank my pervious and recent colleagues of Satolab: Dr T. Takayama, Dr M. Gaballah, Dr Naoko Hayashi, Dr Tseedulam Khuut, Dong-Hun Kim, M.Matsumoto, A.Gaber, Chen Siwei, K.Kusano, Liu Hai, Riafeni Karlina, Zhu Shiping, N.Muratani, T.Kitajyo, Iee Li, K.Muramatsu, O.Saika and T. Nakada for your comments, ideas and presentations you made every week. Thanks to you all for sharing this PhD life with me and your wonderful friendship.

I want to express my great thanks for the Egyptian government that is represented in the mission sector for providing me the change to study my PhD in Japan.

Finally, and most of all, I am extremely grateful to my wife; Ebtesam Bekheet and my son Moataz Khamis in addition to my big family Hagag, Ghareeb, Safy, Safia and Hala for their patient, support and pray for me during my PhD life in Japan.

Publications by the author

Conferences

- K. Mansour and M. Sato, "Characterization of fractures by borehole radar," Japan-Egypt Geosciences forum, Cairo, Egypt, December, 2008.
- K. Mansour and M. Sato, "Comparison of electromagnetic scattering from flat and rough single rock fracture models," in *Proceeding of the 123rd SEGJ Conference*, Sendai, Japan, September,2010.
- K. Mansour and M. Sato, "FDTD simulation of electromagnetic wave scattering from a rough surface synthesized by Fractal theory," in *Proceeding of The Formation Evaluation Symposium of Japan*, Chiba, Japan, October, 2010.
- K. Mansour and M. Sato, "Subsurface fractures Characterization by analyzing Anisotropy & Entropy and Alpha decompositions of full polarimetric borehole radar data," 8th International Workshop on WATER DYNAMICS, Tohoku University, Sendai, March, 2011.
- K. Mansour and M. Sato, "Characterizing subsurface fractures based on forward molding of EM scattering from synthesized fractal fractures," JpGU International Symposium, Chiba, Tokyo, May, 2011.

Journals

- K. Mansour and M. Sato, "Subsurface fractures characterization using full polarimetric borehole radar data analysis with numerical simulation validation," Journal of Exploration Geophysics, Vol.43, No.2, pp.125-135, June, 2012.

- K. Mansour T. Rabeh A. Basheer and M. Sato, "Polarimetric borehole radar application for characterizing subsurface fractures zones: Implication for fracture systems around Lake Nasser area-Egypt," Journal of Exploration Geophysics (Submitted).

- K. Mansour and M. Sato, " Polarimetirc approach implementation for fracture models based on Finite Difference Time Domain simulations," in preparation for submission to International Journal of Geosciences.